The impact of zooplankton calcifiers on the marine carbon cycle

Nielja S. Knecht[1], Fabio Benedetti[2], Urs Hofmann[1], nina Bednaršek[3], Sonia Chaabane[4], Catharina de Weerd[5], Katja Peijnenburg[5], Ralf Schiebel[6], and Meike Vogt[7]

[1]ETH Zurich
[2]Environmental Physics, Institute of Biogeochemistry and Pollutant Dynamics, ETH Zürich, 8092, Zürich, Switzerland.
[3]National Institute of Biology
[4]CEREGE
[5]Naturalis Biodiversity Center
[6]Max Planck Institute for Chemistry
[7]ETH Zuerich

January 4, 2023

Abstract

Shelled pteropods and planktic foraminifers are calcifying zooplankton that contribute to the biological carbon pump, but their importance for regional and global plankton biomass and carbon fluxes is not well understood. Here, we modelled global annual patterns of pteropod and foraminifer total carbon (TC) biomass and total inorganic carbon (TIC) export fluxes over the top 200m using an ensemble of five species distribution models (SDMs). An exhaustive newly assembled dataset of zooplankton abundance observations was used to estimate the biomass of both plankton groups. With the SDM ensemble we modeled global TC biomass depending on multiple environmental parameters. We found hotspots of mean annual pteropod biomass in the high Northern latitudes and the global upwelling systems, and in the high latitudes of both hemispheres and the tropics for foraminifers. This largely agrees with previously observed distributions. For the biomass of both groups, surface temperature is the strongest environmental correlate, followed by chlorophyll-a. We found mean annual standing stocks of 52 (48-57) Tg TC and 0.9 (0.6-1.1) Tg TC for pteropods and foraminifers, respectively. This translates to mean annual TIC fluxes of 14 (9-22) Tg TIC yr-1 for pteropod shells and 11 (3-27) Tg TIC yr-1 for foraminifer tests. These results are similar to previous estimates for foraminifers standing stocks and fluxes but approximately a factor of ten lower for pteropods. The two zooplankton calcifiers contribute approximately 1.5% each to global surface carbonate fluxes, leaving 40%-60% of the global carbonate fluxes unaccounted for. We make suggestions how to close this gap.

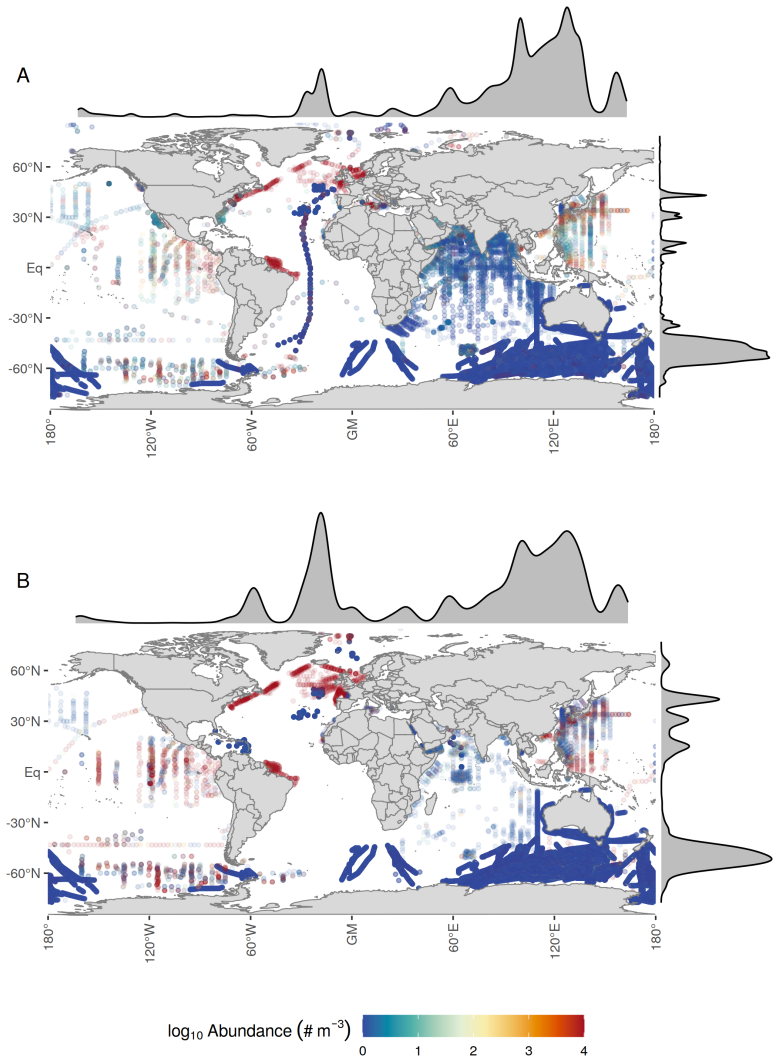

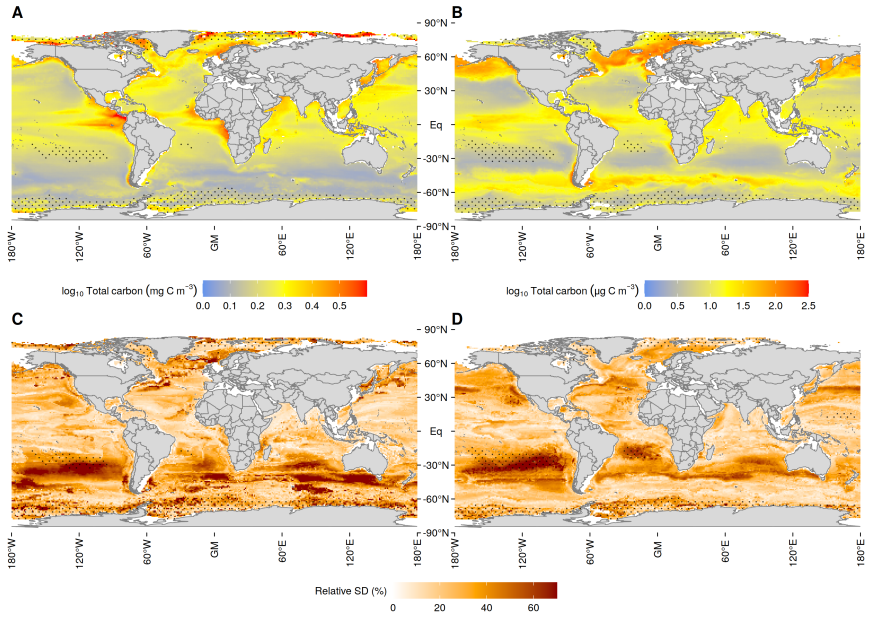

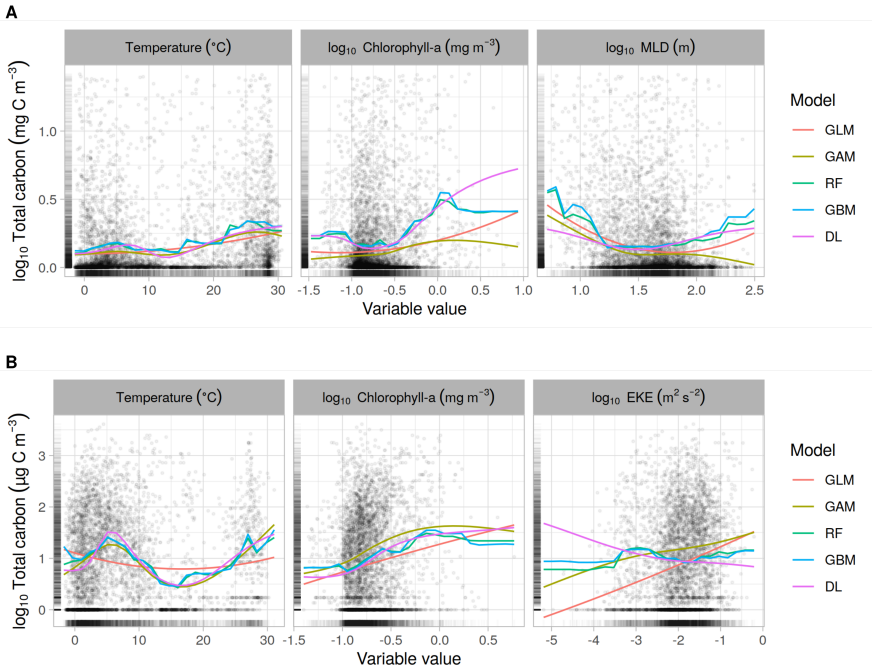

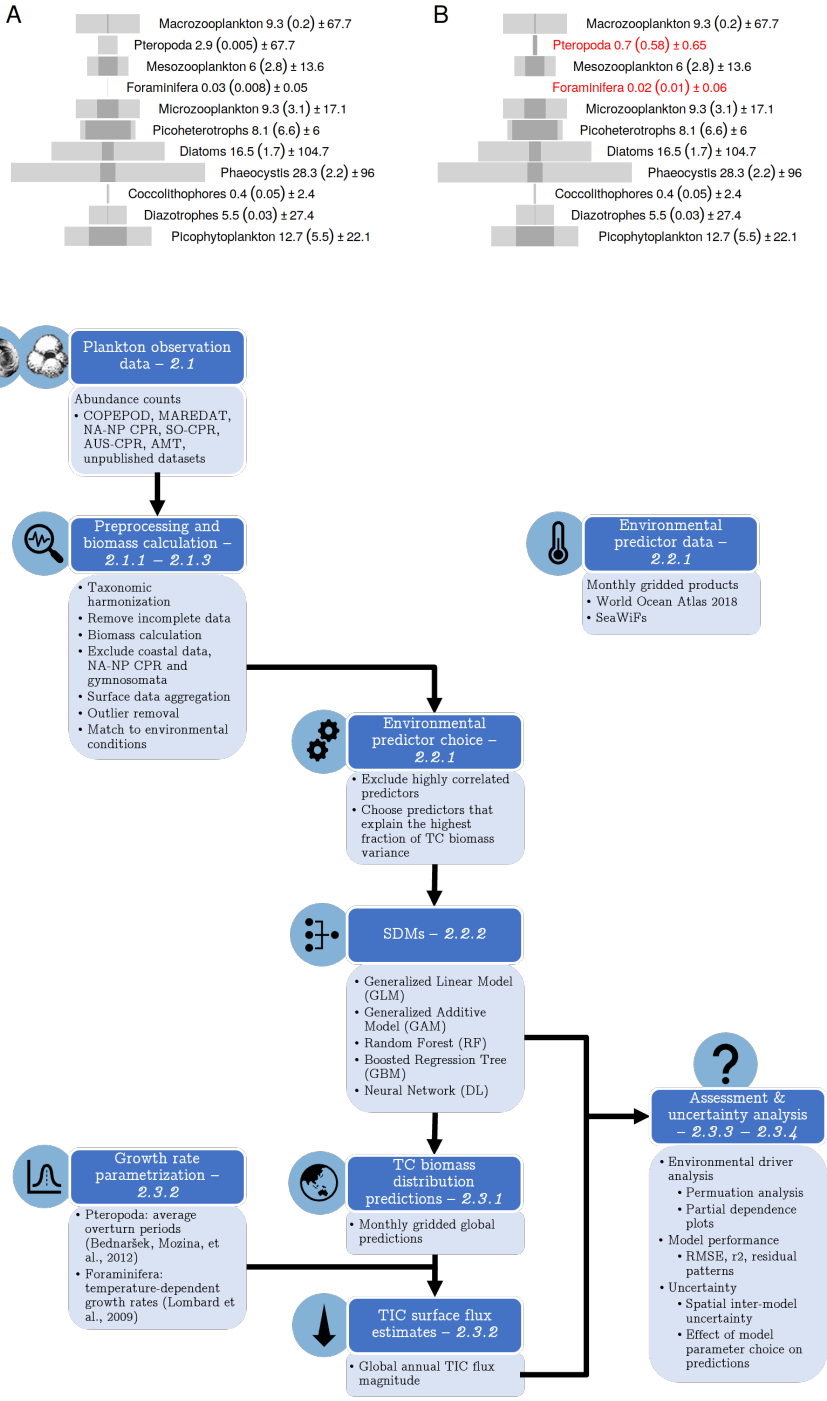

The impact of zooplankton calcifiers on the marine carbon cycle

[1]Nielja S. Knecht, [1]Fabio Benedetti, [1]Urs Hofmann Elizondo, [2,3]Nina Bednaršek, [4,5,6]Sonia Chaabane, [7]Catharina de Weerd, [7,8]Katja T. C. A. Peijnenburg, [6]Ralf Schiebel, [1]Meike Vogt

[1]Environmental Physics, Institute of Biogeochemistry and Pollutant Dynamics, ETH Zurich, Zurich, Switzerland
[2]National Institute of Biology, Marine Biological Station, Piran, Slovenia
[3]Cooperative Institute for Marine Resources Studies, Oregon State University, Oregon, USA
[4]Aix-Marseille Université, CNRS, IRD, INRAE, CEREGE, Aix-en-Provence, France
[5]French Foundation for Research on Biodiversity (FRB-CESAB), Paris, France
[6]Department of Climate Geochemistry, Max-Planck-Institute for Chemistry, Mainz, Germany
[7]Plankton Diversity and Evolution, Naturalis Biodiversity Center, Leiden, The Netherlands
[8]Institute for Biodiversity and Ecosystem Dynamics, University of Amsterdam, Amsterdam, The Netherlands

Key Points:

- Calcifying zooplankton
- Species distribution models
- Carbonate fluxes

Corresponding author: Nielja S. Knecht, `nknecht@ethz.ch`

Abstract

Shelled pteropods and planktic foraminifers are calcifying zooplankton that contribute to the biological carbon pump, but their importance for regional and global plankton biomass and carbon fluxes is not well understood. Here, we modelled global annual patterns of pteropod and foraminifer total carbon (TC) biomass and total inorganic carbon (TIC) export fluxes over the top 200 m using an ensemble of five species distribution models (SDMs). An exhaustive newly assembled dataset of zooplankton abundance observations was used to estimate the biomass of both plankton groups. With the SDM ensemble we modeled global TC biomass depending on multiple environmental parameters. We found hotspots of mean annual pteropod biomass in the high Northern latitudes and the global upwelling systems, and in the high latitudes of both hemispheres and the tropics for foraminifers. This largely agrees with previously observed distributions. For the biomass of both groups, surface temperature is the strongest environmental correlate, followed by chlorophyll-a. We found mean annual standing stocks of 52 Tg TC (48 Tg TC to 57 Tg TC) and 0.9 Tg TC (0.6 Tg TC to 1.1 Tg TC) for pteropods and foraminifers, respectively. This translates to mean annual TIC fluxes of 14 Tg TIC yr^{-1} (9 Tg TIC yr^{-1} to 22 Tg TIC yr^{-1}) for pteropod shells and 11 Tg TIC yr^{-1} (3 Tg TIC yr^{-1} to 27 Tg TIC yr^{-1}) for foraminifer tests. These results are similar to previous estimates for foraminifers standing stocks and fluxes but approximately a factor of ten lower for pteropods. The two zooplankton calcifiers contribute approximately 1.5% each to global surface carbonate fluxes, leaving 40%–60% of the global carbonate fluxes unaccounted for. We make suggestions how to close this gap.

1 Introduction

Marine calcifying plankton play a key role in the ocean's carbon cycle, particularly through the formation, sinking, and dissolution of their $CaCO_3$ shells (J. L. Sarmiento & Gruber, 2006). These processes impact the carbonate system throughout the water column and thus also affect the oceanic CO_2 uptake (Takahashi & Bé, 1984; J. Sarmiento & Gruber, 2006). Annually, the inorganic carbon export flux from the surface ocean amounts to 0.6 Pg C yr^{-1} to 1.4 Pg C yr^{-1} (Iglesias-Rodriguez et al., 2002; Lee, 2001; Berelson et al., 2007; Jin. et al., 2006; Schiebel, 2002). However, there are significant uncertainties regarding the spatial and seasonal carbon flux patterns and the relative contribution of the different plankton groups to global calcification rates.

The major groups of calcifying plankton are coccolithophores, shelled pteropods and planktic foraminifers (Schiebel & Hemleben, 2017; Stepien, 1980; Lalli & Gilmer, 1989; Schiebel, 2002; Bednaršek, Mozina, et al., 2012). Shelled pteropods from the suborder Thecosomata (in the following referred to as pteropods) build shells of aragonite, a metastable form of calcium carbonate (Lalli & Gilmer, 1989) with adults ranging from 1 mm to 30 mm in size (Bednaršek, Mozina, et al., 2012; Bednaršek, Tarling, et al., 2012). Aragonite is 50% more soluble than calcite (Mucci, 1983), which makes pteropods more sensitive to ocean acidification than calcite-shelled organisms (Fabry et al., 2008; Bednaršek et al., 2016; Manno et al., 2016). Pteropods are flux feeders, i.e., they secrete a floating mucus web to trap sinking organic particles (Gilmer & Harbison, 1986). They are active swimmers and some species perform diel vertical migration (DVM), feeding at night at the surface and spending the day at depths between 100 m and in some cases up to 1000 m (Bé & Gilmer, 1977; Bednaršek, Tarling, et al., 2012) to avoid predation. Foraminifers build calcareous tests that can reach diameters ranging between 100 µm and 1 mm (Frerichs et al., 1972; Schiebel & Hemleben, 2017). They are generally omnivorous and can capture prey actively, but feeding preferences differ between species (Rhumbler, 1911; Caron & Bé, 1984; Spindler et al., 1984; Anderson et al., 1979) with some species also harboring facultative photosymbionts (Hemleben et al., 1989). The global abundances and habitat suitability of pteropods and foraminifers are known to be controlled by a range of environmental parameters, including temperature (Beaugrand et al., 2010; Helaouët

& Beaugrand, 2009; Hofmann Elizondo et al., 2021; Jonkers et al., 2019; Bednaršek et al., 2022), chlorophyll-a as a proxy for food availability (Vereshchaka et al., 2022; Pinkerton et al., 2020; Thibodeau et al., 2019), and parameters related to physical mixing that influence and phytoplankton growth through light availability and particle sinking rates (Longhurst, 2007; Rothschild & Osborn, 1988; Boyce et al., 2010; Seuront et al., 2001; Govoni et al., 2010; Mackas et al., 2005; Bednaršek et al., 2022).

The relative importance of the different calcifying plankton groups for global carbonate fluxes remains uncertain. Coccolithophores were long thought to dominate the inorganic carbon export (Rost & Riebesell, 2004; Rembauville et al., 2016; Anglada-Ortiz et al., 2021; Iglesias-Rodriguez et al., 2002; Schiebel, 2002). However, in global observation-based estimates, they only accounted for 26%–52% of global carbonate fluxes, which leaves a significant fraction of the carbonate fluxes unattributed (Buitenhuis, Vogt, et al., 2013; C. J. O'Brien, 2015). This discrepancy shifted the attention towards the contribution of the two calcifying zooplankton groups, pteropods and foraminifers. Recent observational studies estimated pteropods to contribute more than previously thought to global surface carbonate fluxes with a fraction of 20% to 42% (Bednaršek, Mozina, et al., 2012). Foraminifer carbon flux estimates vary by a factor of 100 (Schiebel & Movellan, 2012; Schiebel, 2002; Buitenhuis et al., 2019; Buitenhuis, Vogt, et al., 2013). However, recent studies based on newly available observations find significantly lower fluxes. Finally, a recent mechanistic modelling study found pteropods to dominate upper subsurface $CaCO_3$ export, with contributions ranging between 33% - 89% (Buitenhuis et al., 2019). These results further suggest the key role of pteropods and foraminifers for the oceanic inorganic carbon cycle.

To derive the magnitude of carbon export mediated by zooplankton calcifiers, we first need to quantify the global biomass standing stocks and characterize the global distribution patterns of these groups. Earlier descriptions of the global patterns based on global plankton sampling data were made by the MARine Ecosystem DATa (MAREDAT) project (Buitenhuis, Vogt, et al., 2013). Additionally, large-scale observational datasets have been collected by the Continuous Plankton Recorder (CPR) survey (Richardson et al., 2006). However, the existing observations are usually confined to specific ocean regions and have an overall low data coverage in the central oceanic basins (Bednaršek, Mozina, et al., 2012; Schiebel & Movellan, 2012; de Garidel-Thoron et al., 2022). Furthermore, plankton distributions are generally patchy in space and time (Boltovskoy, 1971; Beckmann et al., 1987; Siccha et al., 2012; Buitenhuis, Vogt, et al., 2013), which causes high variability in the observed abundances. Different sampling techniques and varying sampling depths and mesh sizes introduce additional variation (Wells, 1973). The derivation of continuous global biomass maps and standing stock estimates for zooplankton calcifiers hence requires us to account for these data gaps and biases by employing statistical methods.

As statistical techniques, species distribution models (SDMs) empirically learn the relation between the target variable and a range of environmental predictors through response curves and can then extrapolate said target variable to un-sampled regions by projecting these response curves on predictor values (Guisan & Zimmermann, 2000; Elith & Leathwick, 2009; Merow et al., 2014). They have been successfully used in marine macroecology to model plankton species distributions based on occurrence data (presence/absence) (Righetti et al., 2019; Benedetti et al., 2021; Brun et al., 2016; Barton et al., 2016; Brun et al., 2015; Bednaršek et al., 2022) and are increasingly being used to model continuous abundance values (Waldock et al., 2022; Pinkerton et al., 2010; De Broyer et al., 2014). In the present work, we apply an SDM framework to estimate global biomasses for calcifying zooplankton.

To this end, we use newly compiled global data compilation of pteropod and foraminifer abundances and species-specific biomass conversion methods to calculate biomass concentrations over the top 200 m. We combine the global gridded biomass data with an en-

semble of SDMs to address the following questions: (1) What are the biogeographic patterns and main environmental covariates of global total carbon (TC) biomass for pteropods and foraminifers (on a monthly, 1×1° gridded scale of the upper open ocean)? (2) What is the magnitude and range of uncertainty of the associated annual total inorganic carbon (TIC) fluxes from pteropods and foraminifers?

2 Methods

We model the biomass patterns and associated carbon fluxes of pteropods and foraminifers at a global scale using SDMs and updated abundance datasets for the two groups. To this end, we use a multi-step modelling pipeline as shown in figure 1.

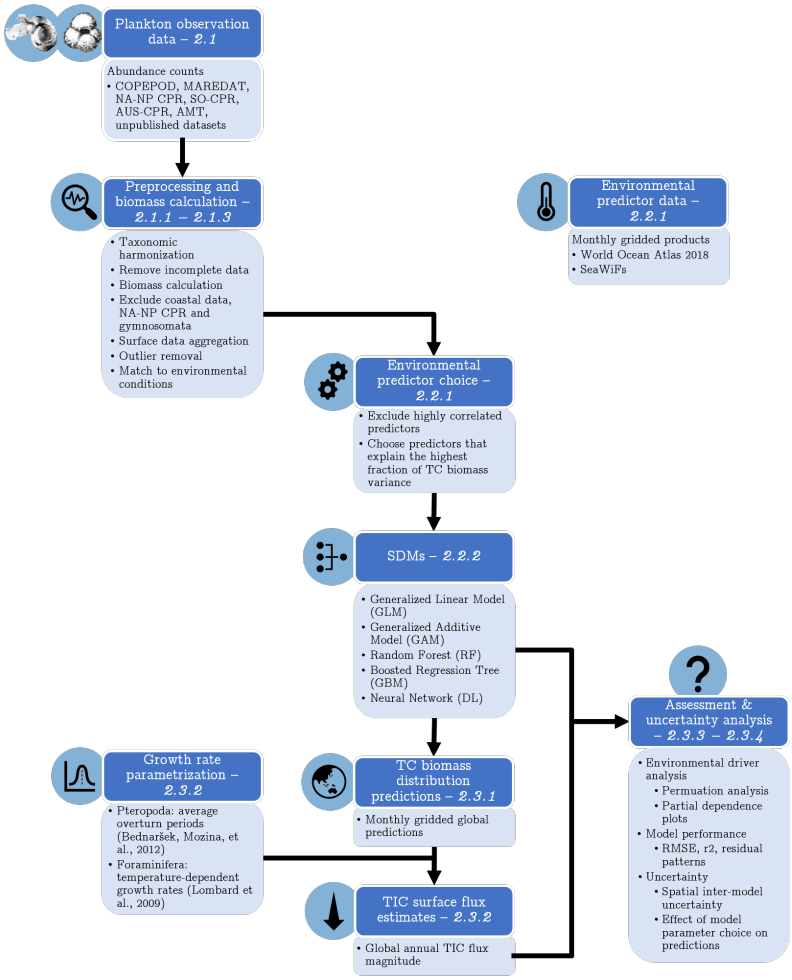

Figure 1. Flow diagram illustrating the pipeline of numerical analyses implemented for the present study. The various steps taken from the raw data to the final total carbon (TC) biomass distributions and total inorganic carbon (TIC) flux estimates using species distribution models (SDMs) are shown. The numbers in italics indicate the subsection of the Methods where the corresponding step is described.

2.1 Plankton data

2.1.1 Data collection and pre-processing

We updated the original MAREDAT pteropod and foraminifer abundance and biomass datasets of Schiebel and Movellan (2012) and Bednaršek, Mozina, et al. (2012) by aggregating abundance concentration data from large scale sampling campaigns, existing data compilation efforts, and unpublished sampling data (figure 1). The main data sources (figure S1) for both plankton groups included the Southern Ocean Continuous Plankton Recorder (SO-CPR) (Hosie, 2021), the Australian CPR (Aus-CPR) (IMOS, 2022), the North Atlantic and North Pacific CPR (NA-NP CPR) (Johns, 2021), and the Coastal and Oceanic Plankton Ecology, Production and Observation Database (COPEPOD) (T. D. O'Brien, 2010). For pteropods, we added data from the Tara Oceans expeditions (Brandão et al., 2021), the Atlantic Meridional Transect (AMT24) (Burridge et al., 2017) and AMT27 (Peijnenburg, 2021), as well as unpublished sampling data from the North Atlantic (Schiebel, 2021). For foraminifers, we also gathered data from various individual sampling campaigns (Schiebel et al., 1995; Schiebel & Hemleben, 2000; Schiebel et al., 2001; Schiebel, 2002; Schiebel et al., 2002, 2004; Jentzen et al., 2018).

We took several pre-processing steps to ensure the quality of the biological observations. To harmonize all classifications across datasets and correct for potential deprecated scientific species names, we matched all taxonomic information against the list of accepted taxon names of the World Register of Marine Species (WoRMS) (Horton et al., 2017). Observations lacking complete sampling metadata (date, depth, longitude, latitude, and abundance value) and observations of body parts were removed (21303 points for pteropods, mainly due to observations of body parts and larvae, and 522 for foraminifers). Additionally, pteropod abundance values from the Ecosystem Monitoring - Ships Of OPportunity surveys (EcoMon-SOOP) in the Gulf of Maine from the COPEPOD dataset were corrected by dividing them by a factor of 100 as the units in the original dataset had been erroneously reported. We did not standardize the abundance estimates between the various mesh sizes used in the different sampling cruises as there were not yet any published correction factors that we were aware of for these two specific plankton groups .

The final, quality-controlled pteropod abundance dataset (figure S2) contains 841239 data points at 309921 individual locations, collected at a mean sampling depth (± sd) of 38.15 ± 190.89 m over the 1938–2021 period (2001.25 ± 15.23). Abundances range between 0 ind /m^3 and 1066.67 ind /m^3, with a mean of 4.38 ± 79.86 ind /m^3. The median abundance (0.00 ind /m^3) is low due to the CPR datasets which make up 91.15% of the data, and contain 92.06% absence observations. 50.19% of the data is resolved only to the order-level, whereas 24.03% of the observations are species-resolved and 22.41% resolved to the genus level (see table S2). The dataset contains observations on 33 species out of 165 currently recognized pteropod species (Peijnenburg et al., 2020) (see table S2). The largest contributions to total abundance summed over all observations stem from *Limacina helicina* sensu lato (47.7% of the total species-resolved abundance), *Heliconoides inflatus* (26.7%), and *L. retroversa* s.l. (10.0%).

The final, quality-controlled foraminifer abundance dataset (figure S2) consists of 1021283 points at 308641 unique locations, with a mean sampling depth of 108.06±340.49 m and collected during the 1939-2021 period (mean 2000.36 ± 13.30). Foraminifer abundances range between 0 ind /m^3 and 152170.00 ind /m^3, with a mean abundance of 3.63± 163.08 ind /m^3. There is a high prevalence of CPR data (74.35% of the total data) with 89.72% zero abundance observations, which causes a low median abundance value of 0.00 ind /m^3. 59.79% of the data are species resolved, followed by 33.07% of the observations on a phylum level (see table S4). This dataset contains observations on 42 of the 47 extant foraminifer species (Schiebel & Hemleben, 2017). Most of the total abundance is composed of *Glo-*

bigerina bulloides (25.6% of the total species-resolved abundance), *Neogloboquadrina incompta* (23.7%), *Turborotalita quinqueloba* (13.3%), and *Globigerinita glutinata* (11.3%).

For model training, we performed additional data quality controls to ensure sensible relations between environmental predictors and biomass values could be derived. The NA-NP CPR dataset was flagged and discarded for modelling as it contained discrete medians of abundance bins instead of continuous values (removal of 340250 points for pteropods and 250620 points for foraminifers). Additionally, we excluded data from neritic sampling locations associated with a climatological salinity < 30 PSU from the analysis to avoid observations influenced by terrestrial freshwater and nutrient inputs (Brun et al., 2015) (removal of 18725 data points for pteropods and 17207 points for foraminifers). Lastly, observations for pteropods from the clades Gymnosomata and Pseudothecosomata were removed for modelling, as only some of the latter are calcifiers (Lalli & Gilmer, 1989), and there is very little literature on their role in the carbon cycle (removal of 106929 points). The final datasets used for modelling contain 375336 points for pteropoda and 770663 points for foraminifers as shown in figure 2.

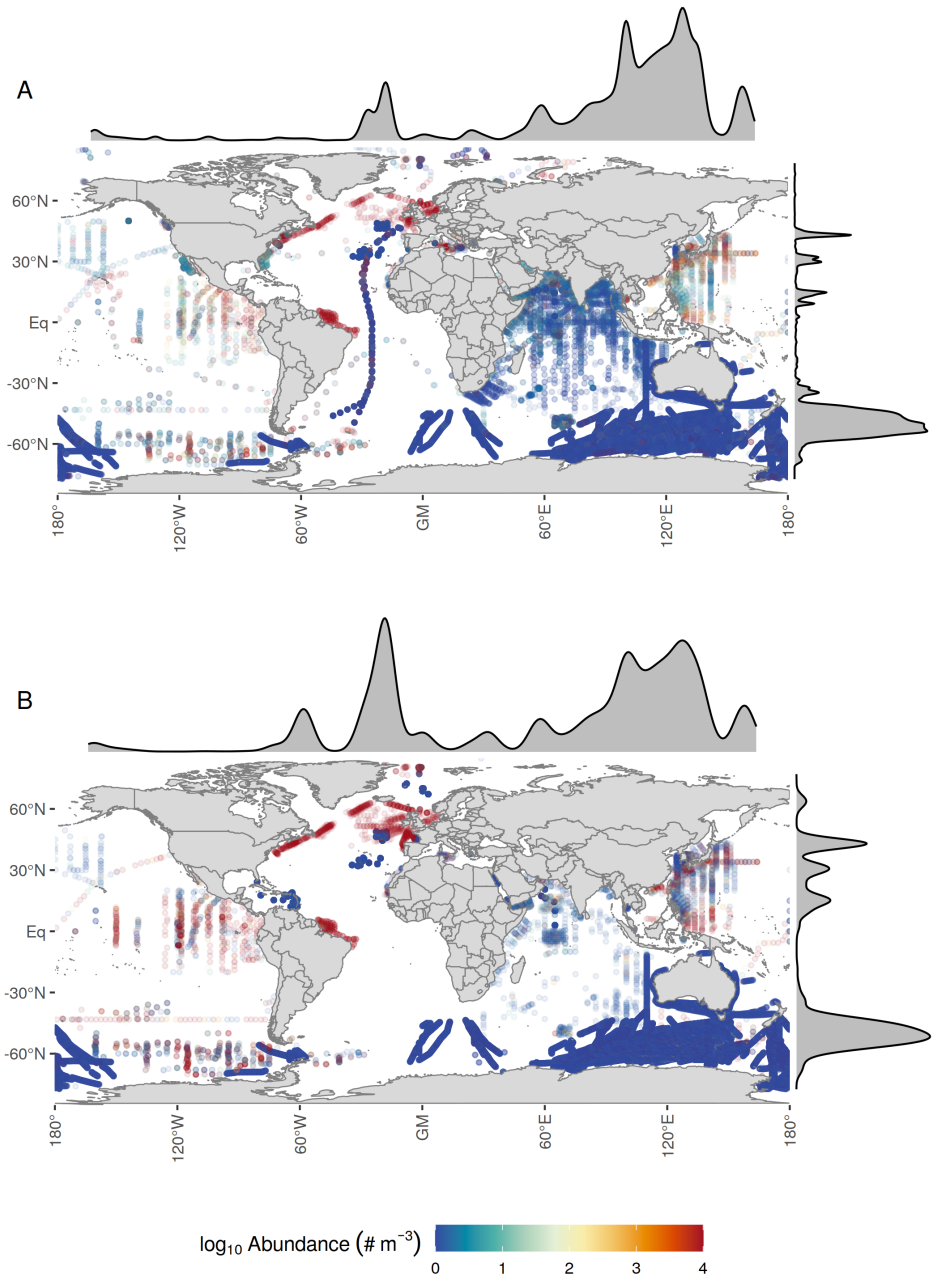

Figure 2. Global distribution of the final quality-controlled observations of pteropod (**A**) and foraminifer (**B**) abundance used for modelling. The marginal plots show the density of observations and highlight the dominant role of the Southern Ocean Continuous Plankton Recorder (SO-CPR) survey as well as a spatially confined, highly resolved dataset in the North Atlantic. This plot shows the dataset used for modelling, i.e., the dataset after removing the North Atlantic and North Pacific CPR data, coastal observations with surface salinity $\leq$ 30, and observations of naked pteropods (Gymnosomata) as described above. For the full collected dataset, see figure S2.

2.1.2 Biomass calculations

To estimate calcifying zooplankton biomass and subsequent carbon fluxes, we converted the abundances to biomass data based on morphology-based conversion factors (cf. figure 1). To this end, we grouped species of similar morphology into shape groups and derive biomass as a function of average body size (maximum elongation) based on shape-specific conversion equations. Generally, we applied all conversions on the lowest taxonomic level available and only used shape-group or phylum-wise averages where the species identification was not available.

Biomass calculation for pteropods To convert pteropod abundance into carbon biomass, we used corrected species-specific biomass conversion equations from Bednaršek, Mozina, et al. (2012) to calculate wet weight (WW) as shown in table S1. These equations are based on six different morphological shape groups and relate an individual species' body length in millimeters to its biomass. For observations without morphometric data (99.8%), we used the species-average lengths from (Bednaršek, Mozina, et al., 2012). We used pteropod shell length whenever given in Bednaršek, Mozina, et al. (2012), otherwise we used the body length values from the same source. Table S2 shows the average length value used for each species, their respective shape group, and the number of observations for each species. WW was then transformed to dry weight (DW) as per Davis and Wiebe (1985) (equation 1)

$$DW = WW \cdot 0.28 \tag{1}$$

and subsequently transformed to total carbon (TC) following Larson (1986) (equation 2).

$$TC = DW \cdot 0.25 \tag{2}$$

Finally, total inorganic carbon (TIC) was computed (equation 3) following Bednaršek, Mozina, et al. (2012).

$$TIC = 0.27 \cdot TC \tag{3}$$

This TC-TIC conversion factor is based on data for *L. helicina antarctica* and hence probably not representative for all pteropod species and life stages (Hofmann Elizondo & Vogt, 2022). To account for the lack of species-specific TC-TIC conversion factors in literature, we added an uncertainty range of ±20% to the conversion factor, based on the range of TIC values reported in Bednaršek, Tarling, et al. (2012). The effect of this parameter choice is assessed according to the methodology in section 2.3.4.

Biomass conversion for foraminifers A morphological approach was also carried out for converting foraminifer abundances to TC concentrations. We were not aware of any published shape class definitions for foraminifers. Thus, we defined eight morphological shape groups based on similar adult test shape and structure as shown in table S3.

To derive biovolume-to-biomass conversion equations, we constructed species and group-specific maximum test length to biomass functions from the literature. We collected species-specific test weight measurements per plankton size class from Schiebel and Hemleben (2000) and Takahashi and Bé (1984). We fitted linear functions to calculate biomass as a function of length per species and per shape group, where the biomass of a shape group is calculated as the average of all species within the group (figure S7). To compare the ranges of the conversion factors to published equations for the entire foraminifera phylum, we used the equation provided by Michaels et al. (1995) (figure S7). This function computes foraminifer cytoplasm carbon (i.e., total organic carbon, TOC) as a function of test length. The TC biomass is calculated based on the following conversion fac-

tors (Schiebel & Movellan, 2012):

$$TIC = 0.36 \cdot TOC \tag{4}$$

$$TIC = 0.265 \cdot TC \tag{5}$$

To compute TC from the test weight measurements of Schiebel and Hemleben (2000) and Takahashi and Bé (1984), we used the following molar relationship:

$$m(C) = \frac{m(\mathrm{CaCO_3})}{M(\mathrm{CaCO_3})} \cdot M(C) = \frac{m(\mathrm{CaCO_3})}{100.09\,\mathrm{g\,mol^{-1}}} \cdot 12.01\,\mathrm{g\,mol^{-1}}, \tag{6}$$

where m denotes the mass and M the molar weight.

The biomass conversion factors (BCF) shown in table S5 are the coefficients of the linear relation between foraminifer TC biomass and their biovolume. To apply the conversion factors, the BCF values were substituted into the following equation:

$$TC = a * L^3 * BCF, \tag{7}$$

where TC represents the TC biomass of foraminifers in µg, a denotes foraminifer abundance and L the species' length in µm.

We collected average length values for all species from the images of (Schiebel & Hemleben, 2017). These average length values as well as the number of observations per species can be found in table S4.

2.1.3 Surface ocean aggregation

To reduce spatio-temporal patchiness and noise in the data, we conducted a surface ocean aggregation (C. J. O'Brien, 2015). To this end, we re-gridded all data onto the 1×1° grid of the World Ocean Atlas 2018 (WOA18; Boyer et al. (2018)). For each grid cell, we summed all biomass concentrations from the same sampling event, as different species were sometimes counted as separate measurements. Next, we averaged all biomass and abundance values per grid cell and month of the year over the top 200 m. This depth cutoff was deemed reasonable as 99.1% and 99.4% of the summed abundance of pteropods and foraminifers, respectively, stem from the top 200 m (figure S3).

To better approximate a normal distribution, TC mass values were log-transformed with a $\log_{10}$(TC+1) transformation for further analyses. Lastly, to dampen the effect of plankton patchiness and bloom dynamics, we flagged outliers in the surface aggregated values based on the z-score criterion (Burba & Anderson, 2005). Hence, for modelling, we excluded high biomass observations with a score of $z > 3$, i.e., more than three standard deviations away from the sample mean.

2.2 Modelling

2.2.1 Environmental predictor selection

To identify the set of predictors used for training the biomass-based SDMs, we collected gridded monthly climatologies of meaningful environmental predictors as shown in table 1 and figure 1. Whenever necessary, the fields were averaged and re-gridded to monthly climatologies at a 1x1° resolution. Depth-resolved predictors from the WOA18 were averaged over the climatological mixed layer depth (MLD). As many pteropods actively migrate vertically (on a daily or seasonal basis) and both groups are passively vertically mixed within the water column (Mackas et al., 2005; Lalli & Gilmer, 1989; Schiebel & Hemleben, 2017; Wormuth, 1981; Myers, 1968), the depth-averaged environmental predictors are more representative of the conditions they experience rather than the surface values. However, as sampling devices are often towed vertically or obliquely, the reported water depth interval of each observation is not directly representative of the depth

Table 1. Environmental predictor variables used in the univariate predictor evaluation. WOA18 refers to the 2018 edition of the World Ocean Atlas (Boyer et al., 2018), SeaWiFS denotes the Sea-viewing Wide Field-of-view Sensor satellite data (OB.DAAC, 2018) and SODA describes the Simple Ocean Data Assimilation project (Carton et al., 2018).

Predictor	Source	Reference
Temperature	WOA18	Locarnini et al. (2018)
Chlorophyll-a	SeaWiFs	NASA OB.DAAC (2018a)
Mixed layer depth (MLD)	SODA3.4.2	Carton et al. (2018)
Eddy kinetic energy (EKE)	Copernicus	Copernicus (2021)
Salinity	WOA18	Zweng et al. (2019)
Dissolved oxygen	WOA18	Garcia et al. (2019b)
Nitrate	WOA18	Garcia et al. (2019a)
Phosphate	WOA18	Garcia et al. (2019a)
Depth of the euphotic layer (z_{eu})	SeaWiFS	NASA OB.DAAC (2018c)
Photosynthetically active radiation (PAR)	SeaWiFS	NASA OB.DAAC (2018e)
Particulate backscattering coefficient at 443 nm (BBP_{443})	SeaWiFS	NASA OB.DAAC (2018d)
Diffuse attenuation coefficient for downwelling irradiance at 490 nm (Kd_{490})	SeaWiFS	NASA OB.DAAC (2018b)
Total alkalinity (TA)	OceanSODA-ETHZ	Gregor and Gruber (2021)
Dissolved inorganic carbon (DIC)	OceanSODA-ETHZ	Gregor and Gruber (2021)
Partial pressure of CO2 (pCO_2)	OceanSODA-ETHZ	Gregor and Gruber (2021)
Calcite saturation state (Ω_{Ca})	OceanSODA-ETHZ	Gregor and Gruber (2021)
Aragonite saturation state (Ω_{Ar})	OceanSODA-ETHZ	Gregor and Gruber (2021)

an organism dwells at over the entire day or even through its life span. Hence, we assume that pteropods and foraminifers move within the mixed layer, where the majority of the organic matter is present (Sallée et al., 2021; Soviadan et al., 2022). For all depth-resolved environmental predictors considered, the average over the top 200m, the values at the surface and the MLD-averaged predictor values are each correlated with a Pearson correlation coefficient of $r > 0.99$, so this simplification is deemed reasonable. For dissolved oxygen concentration, we used the value at 200 m depth to avoid the strong collinearity with the sea surface temperature (SST) values. The distribution of chlorophyll-a concentrations, nutrient variables, MLD, and eddy kinetic energy (EKE) were right-skewed (figure S9), therefore we log-transformed those variables so their distribution is closer to a normal one. Then, we collocated the environmental parameters with the gridded monthly pteropod and foraminifer biomass fields.

To select the most meaningful environmental predictors for the final biomass-based SDMs we used a multi-step approach for each zooplankton group. First, we identified clusters of collinear predictors (Pearson correlation coefficient $|r| > 0.7$ calculated from the values matched up with the monthly biomass climatologies, Brun et al. (2020)). Second, we excluded all but one predictor in each cluster, which improves model performance (Dormann et al., 2013; Brun et al., 2020) (figures S10 and S11). Thus, for each cluster we first chose the most normally distributed predictor as assessed by the Shapiro-Wilk test (Shapiro & Wilk, 1965), and second, we chose predictors whose effect are easier to interpret from an ecological point of view (e.g. chlorophyll-a over Kd_{490}, the remotely sensed light attenuation at a wave length of 490 nm, which is an indirect measure of surface productivity and turbidity). This selection procedure resulted in the following seven candidate predictors for both foraminifers and shelled pteropods: surface chlorophyll-a, MLD, temperature averaged over the MLD, surface EKE, oxygen at 200 m depth, salin-

ity averaged over the MLD, partial pressure of CO_2 (pCO_2), photosynthetically active radiation (PAR), and particulate backscattering coefficient at 443 nm (BBP_{443}).

The exclusion of a predictor variable does not mean that it is not ecologically relevant for the organisms modelled. The calcite and aragonite saturation states are known to influence habitat suitability for foraminifers and pteropods, respectively (Lischka et al., 2011; Lischka & Riebesell, 2012; Manno et al., 2016; Bednaršek et al., 2016, 2022). However, the matched saturation states were determined to be highly correlated with water temperature averaged over the MLD (Pearson $r > 0.99$). As previous studies have shown temperature to be more biologically relevant in influencing large-scale biogeographic distribution patterns (Bednaršek et al., 2018; Howes et al., 2015; Beaugrand et al., 2013; MacKas & Galbraith, 2012), we excluded the saturation states as predictors. Exchanging temperature for the aragonite saturation state in the pteropod models does not have a significant effect on the biomass distribution pattern or the annual TC fluxes (figure S22).

To choose the final predictor set, we assessed the variance of the TC biomass explained by each of the seven candidate predictors using univariate regression models (figure S12). For this, we calculated both 1° pixel-wise and latitudinal 10°, 5°, and 1° monthly means of the TC biomass and the environmental predictors to identify the large-scale effects of the environmental predictors. To model variations in the TC biomass as a function of each environmental predictor, we trained two Generalized Linear Models (GLMs) with a Gaussian response function (one with only a linear term and the second with both a linear and a quadratic term) and a Generalized Additive Model (GAM) with a cubic regression spline. Then, we assessed the percentage of deviance explained by each predictor (Hosmer Jr et al., 2013; Nelder & Wedderburn, 1972). We retained all predictors that explained $\geq 5\%$ of variability at any of the spatial aggregation levels. For pteropods, the resulting set of predictors included: MLD-averaged temperature, surface chlorophyll-a, and MLD. For foraminifers, we retained the MLD-averaged temperature, surface chlorophyll-a, and EKE (figure S12 and figure S13 for mean annual maps of the predictors).

To assess the impact of this predictor selection procedure on SDM outputs, we also trained the models for both plankton groups on a Principle Component Analysis (PCA) transformation of the full initial predictor set (table 1). There was no significant difference between the PCA-based global annual TIC fluxes and those calculated based on our final choice of predictors ($p > 0.05$ for both plankton types as assessed with a Kruskal-Wallis test (Kruskal & Wallis, 1952), see figure S23). This shows that the predictor selection procedure did not substantially affect the SDMs estimates.

2.2.2 Multivariate modelling

We used the identified predictors to train an ensemble of five SDMs of increasing complexity: a GLM, a GAM, a Random Forest (RF), a Gradient Boosting Machine (GBM) and a Neural Network/Deep Learning Model (DL) (see figure 1). GLMs, GAMs and RFs have been widely and successfully used in the modelling of global marine plankton distributions (Righetti et al., 2019; Benedetti et al., 2021; Brun et al., 2016). The more complex models have also been used for modelling plankton distributions, though less frequently (GBMs in Pinkerton et al. (2020, 2010), DL models in C. J. O'Brien et al. (2016); Benedetti et al. (2021)). For an extensive description of the more complex model types, we refer to Boehmke and Greenwell (2019e, 2019b, 2019a) and sources within. All modelling was conducted with the `h2o 3.36.0.3` R package (H2O.ai, 2021).

For the GLM, we included both first and second-order dependencies on the predictors and assumed a normal distribution of the target variable with an identity link function (Nelder & Wedderburn, 1972). In the GAM, we fitted smoothing terms for all predictor variables using cubic regression splines, the most common smoothing algorithm

(Hastie & Tibshirani, 1990), and a normal distribution with the identity function as link for the target variable. For the RF, GBM, and DL, the hyperparameters were tuned using a grid search (Boehmke & Greenwell, 2019d). Tables S6, S7, and S8 show the grid of parameters evaluated for each model. The final setup of the RF as determined from the tuning process (table S6) included 830 trees for pteropods and 330 for foraminifers. At each tree node, one and two environmental predictors were evaluated (m_{try}) for pteropods and foraminifers, respectively, and the minimum number of rows at each final node (min_{rows}) was set to three and two. The maximum tree size was constrained to 30 for pteropods and 10 for foraminifers. For each bootstrap replicate of the tree, we chose a fraction (r_{sample}) of 0.8 and 0.632 of the total dataset. For the GBM, we determined a maximum depth ($max_{depth} = 5$) and minimum number of observations per terminal node ($min_{rows} = 1$) for each individual tree for both plankton groups (see also table S7). The learning rate (r_{learn}) was determined to be 0.01 and each individual tree is trained on a fraction of 0.75 and 0.5 of the total dataset for pteropods and foraminifers, respectively, using all of the predictor columns ($r_{samplecolumns}$). The DL (see also table S8) was determined to have a Tanh activation function for both plankton groups. The pteropod model has two hidden layers with 20 neurons each and the foraminifer model has two three hidden layers of 15 neurons each. To avoid overfitting, L_1 and L_2 regularizations were included (Boehmke & Greenwell, 2019a) with weight factors $\lambda_{L_1} = 0$ and $\lambda_{L_2} = 1 * 10^{-3}$ for pteropods, and $\lambda_{L_1} = 1 * 10^{-3}$ and $\lambda_{L_1} = 1 * 10^{-5}$ for foraminifers.

We assessed the effect of the hyperparameter tuning on the global annual TIC fluxes by comparing the fluxes calculated using the tuned models (for the RF, GBM, and DL) to those based on the untuned models with standard hyperpameter set-up (see tables S6–S8). As expected, the tuned models showed a better model performance, but the global annual TIC fluxes did not differ significantly ($p > 0.05$ as assessed with a Kruskal-Wallis test (Kruskal & Wallis, 1952) for each plankton group). Tuning the models hence does not introduce unfounded model complexity or biases.

To train the SDMs and assess their performance, we split the dataset into a training and a testing set (Boehmke & Greenwell, 2019d). For a conservative estimate of model performance, we randomly assigned 75% of the values to the training dataset. On the training dataset, we performed a 5-fold cross validation, where we (i) split the training dataset into five equally-sized, randomly chosen, non-overlapping subsets, (ii) train the SDMs on four of the subsets, and (iii) evaluate the model performance of the trained SDM on the remaining subset based on the average root mean squared error (RMSE). This procedure was repeated until each of the five subsets of the data were used four times for training and once for validation. Finally, we evaluated the trained SDM on the testing set.

2.2.3 Model performance

We assessed model performance using three metrics (figure 1). The root mean squared error (RMSE) is an error metric estimating the deviation between predicted and true values. Pearson's coefficient of correlation, R^2 indicates the magnitude of correspondence between trends in the predicted and observed values. Finally, the Nash-Sutcliffe-efficiency (NSE; Nash and Sutcliffe (1970)) compares the model performance to a null model, i.e., the mean of all observations. Positive NSE values indicate that the assessed model performs better than the null model. Each performance metric was calculated on both the training and the testing set of the data (cf. section 2.2.2).

2.3 Model inference

2.3.1 Global total carbon (TC) biomass patterns

We used the SDMs to project global monthly TC biomass values as a function of the monthly climatological environmental predictors (see figure 1). Projections were made for each grid cell and month where environmental data were available. We flagged and excluded all predictions of negative biomass values, because they correspond to unrealistic predictions (0.33% of all predicted values for pteropods and 0.06% for foraminifers). Many complex SDMs suffer from low transferability into novel environmental conditions due to non-linear response curves (Elith et al., 2010; Qiao et al., 2019; Bell & Schlaepfer, 2016). Thus, for each grid cell we evaluated whether the environmental conditions lie within the range of the training dataset or are considered non-analog using a Multivariate Environmental Similarity Surfaces (MESS) analysis (Elith et al., 2010). The MESS analysis assesses the similarity between the environmental conditions at any given point and the training dataset of each SDM. To avoid including unrealistically high values in the flux calculations and global summaries of calcifying zooplankton biomass, we excluded the biomass values from regions where non-analog environmental conditions were detected by the MESS analysis (3.25% of the values for pteropods and 4.03% for foraminifers). To analyze the spatial biomass patterns, we defined hotspots as unusually high biomass concentrations that lie above the 90th percentile for each plankton group.

2.3.2 Annual total inorganic carbon (TIC) export fluxes

We computed TIC fluxes from the projected global TC biomass values and environmental conditions (see figure 1). To compare our results to those of Buitenhuis et al. (2019), biomass values were calculated for TC, while export fluxes were based only on the inorganic shells, i.e., on TIC. Hence, we assumed that the carbon export flux is dominated by the sinking and empty shells.

TIC export flux calculation for pteropods To compute the annual pteropod TIC flux, we applied a simplified approach based on an average overturn time of one year, following the methodology of Bednaršek, Mozina, et al. (2012). Based on grid cell-wise mean annual biomass concentrations, we computed the global annual mean biomass as the spatially weighted mean of the average concentrations of each grid cell, multiplied by the TIC-TC factor (Bednaršek, Mozina, et al., 2012), the depth of 200 m, and the global open ocean area excluding shelf seas ($362e6\,\mathrm{km}^2$) (Bednaršek, Mozina, et al., 2012; Dietrich et al., 1975). To represent the variability and uncertainty in turnover times between various pteropod species and regions, we added an uncertainty factor of $\pm 20\%$ to the flux conversion equation based on the range of values given in the review study by Wang et al. (2017). The effect of this parameter choice is evaluated according to the uncertainty analysis described in section 2.3.4.

TIC export flux calculation for foraminifers To calculate foraminifer TIC fluxes, we used the phylum-resolved temperature-dependent growth rates from Lombard et al. (2009). To calculate annual TIC fluxes, we multiplied the daily growth rate at each grid cell and month by the current biomass concentration, the TIC-TC factor (equation 4 in section 2.1.2), and the depth of 200 m, and weighted the result by grid-cell area. To represent uncertainty in the growth rate, we calculated the minimum and maximum growth rates by computing all combinations within the parameter uncertainty range. Then, we chose those parameter combinations that would minimize or maximize the integral of the growth rate as a function of temperature from 0 to 30°C, while maintaining ecologically-sensible response shapes (see figure S8 for an illustration of the growth rate options). The effect of this choice was evaluated according to the methodology described in section 2.3.4.

2.3.3 Environmental predictor analysis

To examine how underlying ecological processes were captured by the SDMs (figure 1), we assessed the models' dependence on the predictor variables in two ways. First, we assessed the overall effect of each environmental predictor based on a permutation analysis using the Fisher-Yates algorithm (Fisher & Yates, 1953). Second, we characterized the biological relevance of the response curve learned by each SDM using partial dependence plot (PDP) curves. The PDP curves were calculated by computing biomass prediction at 25 evenly spaced points across each predictor's range while keeping all other predictors constant at their mean value (Boehmke & Greenwell, 2019c).

2.3.4 Uncertainty quantification

We assessed the three main sources of uncertainty underlying our SDMs predictions: SDM choice (Thuiller et al., 2019), TIC-TC factor, and growth rate parametrization (figure 1). First, we identified potential non-normal relationships based on the patterns of the model residuals. Second, we quantified the effect of different model and parameter choices (see sections 2.1.2, 2.2.2 and 2.3.2 for details on the uncertainty setup) on the carbon flux predictions using a multivariate Analysis of Variance (mANOVA; Weinfurt (1995)) whose target variable was the monthly TIC flux values at each grid cell. We used the model type, the growth rate definition, the TIC-TC conversion factor, and the interactions between these three factors as input for the mANOVA.

3 Results

3.1 Global biogeographic total carbon (TC) biomass patterns

The global mean annual TC biomass (±sd) is $0.701 \pm 0.648\,\mathrm{mg\,TC\,m^{-3}}$ for pteropods, and $13.5 \pm 28.7\,\mathrm{\mu g\,TC\,m^{-3}}$ for foraminifers, implying that pteropod biomass is a factor of 50 larger than foraminifer biomass. The projected global mean biomass patterns are shown in figure 3A and 3B for pteropods and foraminifers, respectively. For both plankton groups, high biomass concentrations are found in the tropics and at latitudes $\geq 50°$N. Lower biomass concentrations (mean values of $0.31\,\mathrm{mg\,TC\,m^{-3}}$ and $5\,\mathrm{\mu g\,TC\,m^{-3}}$ are found between 40°S and 50°S for pteropods and between 30° and 40° in both hemispheres for foraminifers. Contrary to pteropods, we find high biomass concentrations of up to $880\,\mathrm{\mu g\,TC\,m^{-3}}$ for foraminifers in the Southern Ocean south of 50°S.

On a regional scale, the North Atlantic Ocean is associated with biomass hotspots (values above the 90th percentile) for both plankton groups, but particularly for foraminifers. A trail of high foraminifer biomasses with a mean value of $150\,\mathrm{\mu g\,TC\,m^{-3}}$ is found across the North Atlantic that is likely associated with the Gulf Stream. Other regions of high biomass are associated with tropical and coastal upwelling systems. Pteropod biomass concentrations are particularly high in the coastal Eastern Boundary Upwelling Systems (EBUS) with an average concentration of $3\,\mathrm{mg\,TC\,m^{-3}}$. For foraminifers, regions of high biomass are associated with the equatorial upwelling region.

On a seasonal scale, biomass hotspots shift towards high latitudes during global summer (figures S16 and S17). The seasonal variation in biomass is stronger in the Northern Hemisphere (NH) than in the Southern Hemisphere (SH) with a difference in variability V ($V_{NH} - V_{SH}$) of $+0.73\,\mathrm{mg\,TC\,m^{-3}}$ for pteropods and of $+45.59\,\mathrm{\mu g\,TC\,m^{-3}}$ for foraminifers ($p < 2{*}10^{-16}$ for both groups; t-test (Student, 1908) where seasonal variability is computed from the maximum difference between the monthly mean surface ocean biomass concentrations at each grid point per model type). Foraminifers display a higher seasonal variation than pteropods ($+0.28$, $p < 2 * 10^{-16}$ when comparing the maximum seasonal variation at each grid point normalized by the mean global biomass between the plankton groups with a t-test).

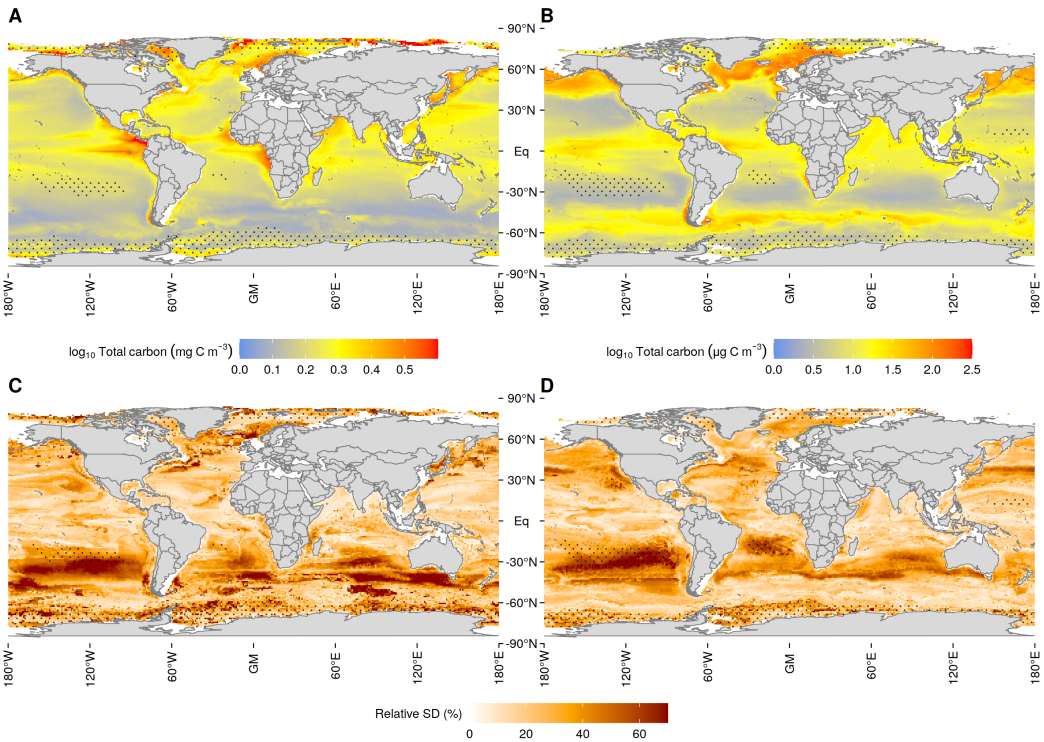

Figure 3. Global mean annual total carbon (TC) biomass concentration for pteropods (left, **A**) and foraminifers (right, **B**), averaged over all months and models. Values are shown as $\log_{10}(TC + 1)$, note also the different color scales for pteropods and foraminifers. Stippled regions in plots **A** - **D** indicate grid points where the environmental conditions were outside the training dataset for more than six months of the year as calculated with the Multivariate Environmental Similarity Surfaces (MESS) analysis. The lower panel plots **C** and **D** show the mean annual relative standard deviation of the model predictions for pteropods (left) and foraminifers (right), normalized with the mean prediction value at each grid point to facilitate comparability.

3.2 Model performance

To assess model performance of the five SDMs, we evaluated each model using the the root mean squared error (RMSE), the R^2 and the Nash-Sutcliffe-Efficiency (NSE) as shown in table 2 for both plankton groups. Compared to the GLM and GAM, the more complex model types (RF, GBM, and DL) have a lower RMSE, a higher R^2, and a higher NSE, i.e., they generally perform better across all three metrics (table 2, see also section 2.2.3 for a description of the metrics). For both pteropods and foraminifers, the RF performs best, followed by the GBM. However, the GBM's R^2 is significantly higher on the training set than on the testing set (2), which indicates model overfitting. The same pattern is visible for RMSE (table 2). In contrast, the RF achieves similar performances on the training an testing set, which indicates a robustly high performance. All model types perform better than using the mean observation value as prediction, which is indicated by the positive NSE values (table 2). Comparing the R^2 values between the plankton groups shows that the pteropod models generally perform better and can explain a higher fraction of the biomass variability (table 2). For the complex non-parametric models (RF, GBM, DL), R^2 is not an optimal metric (Spiess & Neumeyer, 2010). However,

Table 2. Model performance for the pteropod and foraminifer models. Each model metric was calculated on both the training set (X_{train}) and the testing set (X_{test}). R^2 ranges from $-\infty$ to $+1$, with a perfect fit of the model and full variance explained indicated by a value of $+1$. The root mean squared error (RMSE) is an error measure, hence smaller values show higher accuracy. The Nash-Sutcliffe-efficiency (NSE) indicates improvement of the model predictions over using the observation mean, with perfect model performance indicated by a value of $+1$ and a value of 0 indicating that the models perform no better than the observation mean. The models are ranked by their performance over the five metrics.

	Model	R^2_{train}	R^2_{test}	$RMSE_{train}$	$RMSE_{test}$	NSE_{train}	NSE_{test}	**Ranking**
Pteropoda	GLM	0.1113	-0.6427	0.2612	0.3633	0.1113	0.1442	**5**
	GAM	0.1299	0.1678	0.2585	0.2586	0.1299	0.1678	**4**
	RF	0.2332	0.2805	0.2408	0.2404	0.5581	0.2805	**1**
	GBM	0.409	0.2674	0.2114	0.2426	0.3652	0.2674	**2**
	DL	0.1597	0.1822	0.2521	0.2563	0.1625	0.1822	**3**
Foraminifers	GLM	0.0503	-0.0279	0.8554	0.8789	0.0503	0.0491	**5**
	GAM	0.1116	0.0823	0.8274	0.8304	0.1116	0.0823	**4**
	RF	0.2424	0.2003	0.7586	0.7752	0.4252	0.2003	**1**
	GBM	0.3999	0.1926	0.6751	0.7789	0.3594	0.1926	**2**
	DL	0.1718	0.1367	0.7931	0.8054	0.1780	0.1367	**3**

as it is frequently reported in plankton studies as a measure of the fraction of variance explained (Zurell et al., 2020; Pinkerton et al., 2010, 2020), we chose to still include it.

All models tend to underestimate the total biomass on a global scale (-35% for pteropods and -5% for foraminifers of log-transformed biomass), with a stronger underestimation of the top 10th percentile biomass hotspots (on average -78% for pteropods and -53% for foraminifers). However, this underestimation is less pronounced in the more complex models (figures S19 and S20). On a basin-scale, highly productive regions are generally underestimated and low productivity areas overestimated with an average overestimation of the lowest 50% of log-transformed biomass by a factor of 8.7 for pteropods and a factor of 2.5 for foraminifers. Hence, biomass concentrations of both plankton groups are underestimated in the North Atlantic Ocean and the tropical Pacific and Atlantic, whereas predictions in the Indian Ocean and the region around Australia are on average too high (figures S19 and S20).

3.3 Environmental covariates

In general, the modeled responses of biomass to the fitted predictors converges across the ensemble members, except near the outer ranges of the predictor values, and for EKE (figure 4). Temperature shows an overall positive relation to pteropod biomass and a bimodal relation for foraminifer biomass with peaks around 5 ° to 7 °C and above 25°C. Chlorophyll-a is positively related to both pteropod and foraminifer biomass. At high chlorophyll-a concentrations ($\mathrm{Chl-a} > 1\,\mathrm{mg\,m^{-3}}$), biomass concentrations stagnate for pteropods and decrease slightly for foraminifers. MLD has a negative parabolic relation to pteropod biomass. Deepening MLD up to 30 m causes a decrease in biomass while a further deepening of the MLD leads to an increase in biomass concentrations. The effect of EKE on foraminifer biomass varies across the models, with a strong positive effect in the simpler GLM and GAM, a near neutral effect in the RF and GBM, and a negative influence in the DL (see figure 4).

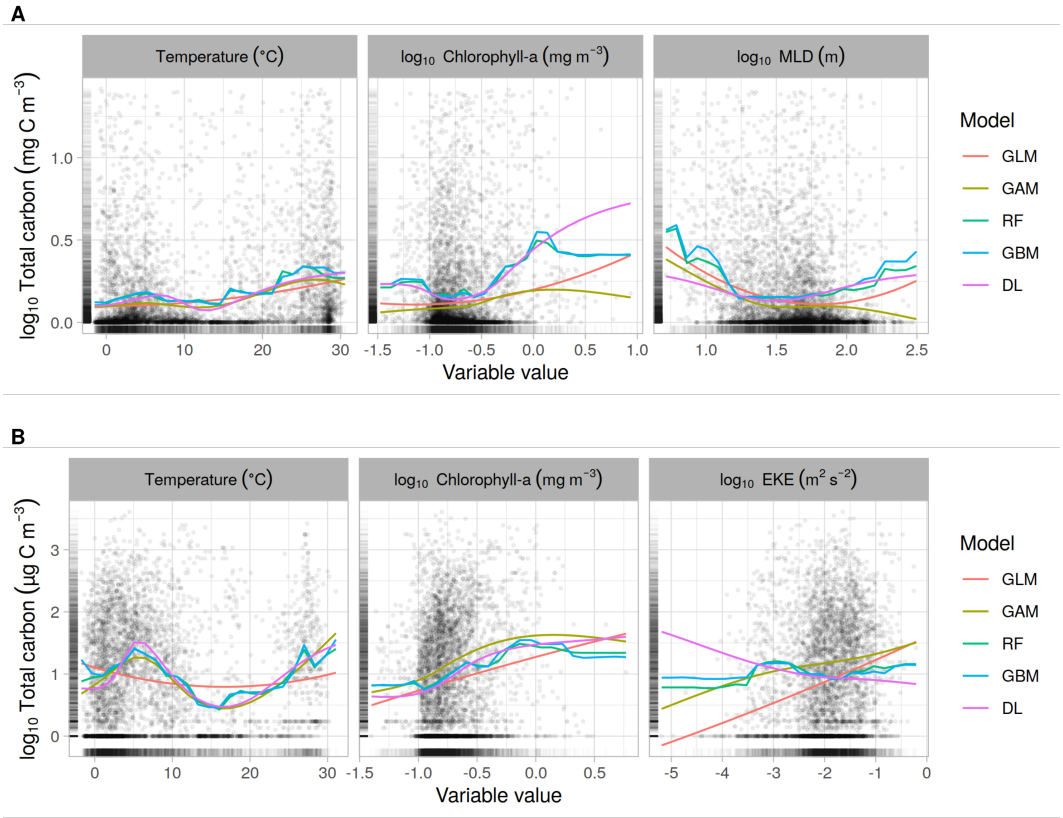

Figure 4. Partial dependence plots (PDP) for the environmental predictors in the pteropod (**A**) and foraminifer (**B**) models. The curves indicate the relations learned by the different SDMs and the rug on the x- and y-axis represents the distribution of the training data. MLD refers to the mixed layer depth, EKE to the eddy kinetic energy. The different model types are the Generalized Linear Model (GLM), Generalized Additive Model (GAM), Random Forest (RF), Boosted Regression Tree (GBM) and Neural Network (DL).

3.4 Global annual total inorganic carbon (TIC) export fluxes

Global mean annual biomass standing stocks are 52.2 Tg TC (ranging from 49.2 Tg TC to 57.3 Tg TC across SDM types) for pteropods and 0.9 Tg TC (0.6 Tg TC to 1.1 Tg TC) for foraminifers (table 3).

The corresponding global annual TIC fluxes were calculated based on growth rate parametrizations (section 2.3.2) and are on average 14.1 Tg TIC yr^{-1} (13.3 Tg TIC yr^{-1} to 15.5 Tg TIC yr^{-1}; table 3) for pteropods. Foraminifer TIC fluxes amount to on average 10.9 Tg TIC yr^{-1} (8.5 Tg TIC yr^{-1} to 14.3 Tg TIC yr^{-1}; table 3). The inter-SDMs range of the TIC fluxes increases by a factor of approximately 4—5 if the modelling uncertainty associated with the TIC-TC factor and the growth rate parametrization are included (table 3, see also section 3.5).

3.5 Uncertainty quantification

To assess the effects of SDM choice, growth rate parametrization and TIC-TC factor parametrization on the TIC flux predictions, we conducted a mANOVA and eval-

Table 3. Global mean annual surface pteropod and foraminifer total carbon (TC) biomass standing stocks and annual total inorganic carbon (TIC) flux estimates as calculated by the five species distribution model (SDMs).

	Pteropoda		Foraminifers	
Model	Standing stock (Tg TC)	Carbon flux (Tg TIC yr^{-1})	Standing stock (Tg TC)	Carbon flux (Tg TIC yr^{-1})
GLM	49.2	13.3 (8.5 - 19.1)	0.6	8.9 (4.0 - 16.4)
GAM	49.2	13.3 (8.5 - 19.1)	0.7	8.5 (3.0 - 19.0)
RF	57.3	15.5 (9.9 - 22.3)	1.0	14.2 (5.0 - 26.8)
GBM	56.9	15.4 (9.8 - 22.1)	1.1	13.2 (4.8 - 24.7)
DL	48.3	13.1 (8.4 - 18.9)	1.1	9.8 (3.7 - 20.3)
Average	**52.2**	**14.1**	**0.9**	**10.9**

uated spatial patterns of standard deviation between model predictions. The main sources of variability in global mean annual TIC fluxes differ between the plankton groups (figure S21). For pteropods, the growth rate and TIC-TC conversion factor choice are the major sources of uncertainty, as each explains 27% of the variability. SDM choice explains 10% of the variability in fluxes for pteropods. In contrast, the TIC flux variability for foraminifers is dominated by the parametrization of the foraminifer growth rate (71%), followed by the model choice (11%), and the TIC-TC factor ($< 10\%$).

From a spatial point of view, relative inter-SDMs variability is highest in regions of low productivity and where environmental conditions are outside the range of the training dataset (figure 3, panels **C** and **D**). This encompasses the Southern Hemispheric (SH) oceanic gyres and the low-productivity latitudinal band around 45°S for pteropods and around 30°S for foraminifers. Absolute biomass predictions differ the most in regions of high biomass, i.e., mainly the North Atlantic for both groups (figure 3, panels **A** and **B**).

4 Discussion

4.1 Biogeographic biomass patterns

The biogeographic distribution patterns found for pteropods and foraminifers largely agree with previous findings (Lalli & Gilmer, 1989; Bednaršek, Mozina, et al., 2012; Buitenhuis et al., 2019; Lombard et al., 2011; Schiebel, 2002). We found high biomass concentrations for both plankton groups in the warm tropical waters, at the high northern latitudes and in the upwelling systems.

The global warm-water belt around the equator has previously been identified as a region of high biomass for pteropods (Lalli & Gilmer, 1989; Bednaršek, Mozina, et al., 2012; Burridge et al., 2017) and foraminifers (Schiebel & Movellan, 2012). High biomass concentrations in the equatorial region for the two plankton groups are representative of total global mesozooplankton distributions (Moriarty et al., 2013; Strömberg et al., 2009), which also show peaks in the tropical ocean.

Earlier studies also found the high latitudes to be regions of high biomass for both plankton groups (Lalli & Gilmer, 1989; Bednaršek, Mozina, et al., 2012; Schiebel & Movellan, 2012; Hunt et al., 2008). Contrary to previous studies (Bednaršek, Mozina, et al., 2012; Lalli & Gilmer, 1989; Hunt et al., 2008), the Southern Ocean was not identified as a region of major pteropod productivity in our study. This is likely due to the influ-

ence of the SO-CPR dataset, which included a high fraction (95.8%) of absences. Removing all CPR data from our training dataset (i.e., SO-CPR and Aus-CPR) significantly increases biomass concentrations for pteropods by a factor of 4–8 in the Southern Ocean but not in other basins (figures S24 and S25). However, removing the CPR data also leads to significantly less well constrained PDP curves for low temperatures, which increases the uncertainty of these CPR-depleted SDMs projections. As previous studies were based on much fewer and spatially confined observations in the Southern Ocean (e.g., 141 data points south of 60° S in Bednaršek, Mozina, et al. (2012)), it is possible that they constitute local upper bound estimates of pteropod abundance and biomass in the Southern Ocean.

Similar to our findings, upwelling regions have previously been found to be associated with high abundances of pteropods (Dadon & Masello, 1999; Koppelmann et al., 2013; McGowan, 1967; Burridge et al., 2017) and foraminifers (Schiebel et al., 2004; Naidu & Malmgren, 1996; Ivanova et al., 1999). Upwelling systems are characterized by recurrent nutrient inputs that trigger high local primary productivity (Kämpf & Chapman, 2016), which produces optimal conditions for opportunistic foraminifer and pteropod species (Kucera, 2007; Schiebel & Hemleben, 2017). However, the upwelling systems are also associated with the upwelling of low pH waters (Joint et al., 2011; Hauri et al., 2013), and the shoaling of the calcite and aragonite saturation horizon (Leinweber & Gruber, 2013; Frenger et al., 2018). The effects of these changes in water chemistry in upwelling systems on pteropod and foraminifer abundances are discussed in section 4.2.

Overall, the modelled biogeographic patterns of pteropods and foraminifers are generally in line with earlier work (Bednaršek, Mozina, et al., 2012; Lalli & Gilmer, 1989; Schiebel & Movellan, 2012). Deviations, as the lower pteropod biomass in the Southern Ocean are probably caused by previously low sampling density and current biases in sampling methodology.

4.2 Environmental drivers

In agreement with other studies (Pinkerton et al., 2020; Beaugrand et al., 2013; Meilland et al., 2016; Jentzen et al., 2018), temperature was the strongest statistical covariate for the biomass distributions of pteropods and foraminifers in our study. This is not surprising since temperature influences all scales of biological processes, from intra-cellular reaction rates to species interactions (Chapperon & Seuront, 2011; Kirby & Beaugrand, 2009; Schmidt-Nielsen, 1997; Brown et al., 2004). Temperature is also related to the water column stratification, which in turn can affect plankton biomass by influencing nutrient availability (see section 2.2.1) and primary productivity (Chiswell et al., 2014). The present global dependencies of biomass on temperature can differ from the results of local studies (e.g., a negative dependency of pteropod biomass on temperature as found in Bednaršek et al. (2022)). As the geographic scale of the analysis is different, distinct effects are captured by the models, such as for example large-scale latitudinal effects in contrast to local upwelling influences.

The modelled bimodal structure of the biomass dependency of our SDMs on temperature for foraminifers, and—to a lesser extent–pteropods (peaks around 5-7°C and above 25° C, figure 4), likely reflects the existence of distinct assemblages of warm-water species and cold-water species within these groups (Bradshaw, 1959). Some foraminifer species are associated with one end of the temperature spectrum - for instance, *Neogloboquadrina pachyderma* is associated with temperatures below 10°C and *Globigerinoides ruber (white)* with temperatures above 18°C (Kucera, 2007; G. A. Schmidt & Mulitza, 2002), which broadly matches our identified peaks (Morard et al., 2015; Antell et al., 2021; Rillo et al., 2022). Furthermore, the temperature interval around 17°C constitutes a minimum in the foraminifer biomass dependency curve and it can be associated with the subtropical front (D. N. Schmidt et al., 2004). As very dynamic dispersal barriers, fronts

are regions of significant environmental variability where foraminifer body sizes were found to be significantly smaller (D. N. Schmidt et al., 2004). This could help explain why the subtropical front was associated with lower foraminifer biomass. However, most foraminifer species display wide thermal tolerances of around 10°C (Schiebel & Hemleben, 2017). Additionally, the sampling density was high in the cold regions of the Southern Ocean and at high temperatures in the tropics, but few data points (18.0% for pteropods and 23.1% for foraminifers) stem from the intermediate temperature range between 10°C and 20°C for both plankton groups. Hence, the bimodal structure might also be skewed due to an uneven sampling distribution (as seen in the uneven density of the x-axis rug plot in figure 4A).

In our SDMs, surface chlorophyll-a concentration emerged as the second-most important environmental covariate for the biomass of both plankton groups, which is also supported by the literature (Pinkerton et al., 2020; Schiebel et al., 2001; Meilland et al., 2016; Schiebel et al., 1995). Generally, a positive near-linear relationship between chlorophyll-a concentrations and pteropod and foraminifer biomasses is observed, particularly in the well-constrained range of the PDP curve (figure 4). As a measure of food availability, chlorophyll-a can be directly positively linked to zooplankton abundances and biomass (Schiebel et al., 2001; Pinkerton et al., 2020; Strömberg et al., 2009). However, both pteropods and foraminifers also feed on non-phytoplankton prey and organic particles to varying degrees (Lalli & Gilmer, 1989; Rhumbler, 1911; Caron & Bé, 1984; Spindler et al., 1984). Pteropods typically feed on particles that are one 100–1000th of their own size (Conley et al., 2018), while some foraminifers can digest prey larger than themselves (Schiebel & Hemleben, 2017). This can explain the smaller-scale deviations of the PDP curves from the near-linear trend and a certain decoupling at low chlorophyll-a concentrations (figure 4) as the zooplankton can feed on alternative organic particles.

The overall importance of the environmental variables driving biomass in models may vary with the spatio-temporal scale at which the analysis is conducted (Corney et al., 2006). Both MLD and EKE were found to be of minor importance as driving variables in our SDMs, which might be due to their predominantly mesoscale effect on mixing and food availability. MLD negatively influences pteropod biomass concentrations over most of the assessed range (figure 4). As flux-feeders, pteropods rely on a steady downward flux of particles, which can be hindered by a deep and turbulent water column mixing (Tsurumi et al., 2005). From a viewpoint of ecological successions over seasons, the shoaling of the deep winter mixed layer in spring is one of the main factors triggering spring phytoplankton blooms (Chiswell et al., 2014). Following these blooms, zooplankton productivity increases to feed on the remaining phytoplankton (Romagnan et al., 2015). This might explain the increase in pteropod biomass for shallow MLD values as an indirect consequence. EKE shows a slight positive impact on foraminifer biomass in the simpler models (figure 4). At the mesoscale, eddies can sustain increases in foraminifer biomass, as they can drive the mixing of the deep chlorophyll-a maximum into shallower surface layers, i.e., into the habitat of foraminifers (Turner, 2015; Kupferman et al., 1986; Beckmann et al., 1987; Fallet et al., 2011; Steinhardt et al., 2014; Schiebel et al., 1995). However, the effect of eddies varies as their direction of rotation determines the dominant vertical direction of water movement (Dufois et al., 2016). The direct large-scale effects of MLD and EKE on biomass patterns are not frequently assessed in the literature (exceptions for MLD are Pinkerton et al. (2020) and Schiebel et al. (2001)). On a local, short-term scale, however, they might have a strong influence on zooplankton biomass that cannot be captured by our global-scale monthly model.

Previous work identified carbonate chemistry as an important predictor for net calcification on a local scale (Bednaršek & Ohman, 2015; Manno et al., 2017; Lischka et al., 2011; Bednaršek et al., 2022; Mekkes, Renema, et al., 2021). CO_2 - rich waters characterized by low pH, low calcite, and low aragonite saturation states may negatively affect certain calcifying organisms by increasing their dissolution and lowering their cal-

cification rate (Bednaršek, Feely, et al., 2017; Bednaršek et al., 2022; Mekkes, Renema, et al., 2021; Mekkes, Sepúlveda-Rodríguez, et al., 2021). For pteropods, these changes in water chemistry can reduce their metabolic activity, increase shell dissolution, and decrease their growth and survival (Lischka et al., 2011; Lischka & Riebesell, 2012; Maas et al., 2015; Gardner et al., 2017; Manno et al., 2007; Bednaršek et al., 2016; Bednaršek, Klinger, et al., 2017; Bednaršek et al., 2022; Bednaršek, Feely, et al., 2017). Foraminifers are less sensitive to changes in saturation states as their shells are made of calcite (Orr et al., 2005; Weinkauf et al., 2016), but the specific sensitivities are not yet well quantified (Fabry et al., 2008), and calcite saturation has not yet decreased as much as aragonite saturation. As our models did not include any indicator of pteropod physiology or biominerology and were based on climatological environmental conditions, we could not account for these effects in the way that for example individual-based models do (Hofmann Elizondo & Vogt, 2022). So far, field studies have not found large-scale abundance decreases of either pteropods or foraminifers as a result of a changes in the carbonate chemistry (Ohman et al., 2009; Howes et al., 2015; Thibodeau et al., 2019), as the effects of other environmental variables such as temperature tend to prevail (Beare et al., 2013). However, the fitness reduction of individual organisms leads to delayed responses on the population level, such that large-scale changes may happen only in the near future under climate change (Bednaršek et al., 2022).

Overall, the relative importance and response curves shapes (figures 4, S18) of the various environmental predictors are in line with our current state of knowledge. Some response curves are affected by uneven sampling across environmental and geographic space and scale dependencies, but within the most commonly observed ranges of environmental conditions, the response curves of the five SDMs agree well with each other for both plankton groups.

4.3 Current global surface ocean biomass and TIC export fluxes

Estimates of global plankton standing stocks from observations have only become possible during the past decade (Buitenhuis, Vogt, et al., 2013) due to paucity in the available information about marine ecosystems. Hence, there are still large uncertainties, particularly for organisms such as zooplankton with patchy abundance patterns (Buitenhuis, Hashioka, & Quéré, 2013) and strongly uneven sampling distributions and methodologies (see also section 4.4 and figure S5 for an assessment of data patchiness). Estimates of standing stocks are highly uncertain, though less so than in marine systems than terrestrial ones (Bar-On et al., 2018; de Garidel-Thoron et al., 2022). In this context, we deem the partly large deviations of our estimates from previous studies as plausible.

On a global mean annual scale, our estimates of total plankton biomass standing stocks are a factor of 10 lower than previous MAREDAT observation-based estimates for pteropods (Bednaršek, Mozina, et al., 2012) and in the same range for foraminifers (Schiebel & Movellan, 2012) as shown in table 4. For both plankton groups, the previous standing stock estimates were 1) calculated using globally averaged, unweighted biomass concentrations, 2) based on a spatiotemporal subset of our current observational dataset, and 3) based only on non-zero abundance observations.

The discrepancy between our results and those of previous studies decreases when we calculate global standing stocks based on these different configurations (see table 4). Calculating standing stocks based on 1) MAREDAT methodology does not change the standing stock estimates strongly (46 TgTC to 57 TgTC for pteropoda and 0.5 TgTC to 1.1 TgTC for foraminifers). Additionally 2) subsetting our prediction fields at the original MAREDAT sampling points increases pteropod standing stock estimates by approximately 50% to 62 TgTC to 95 TgTC, while foraminifer estimates remain near constant at 0.6 TgTC to 1.9 TgTC. Finally, 3) excluding zero abundance observations before modelling increases standing stock estimates to 91 TgTC to 140 TgTC for pteropods and 2 TgTC

Table 4. Comparison between modeled total carbon (TC) standing stocks and total inorganic carbon (TIC) fluxes for pteropods and foraminifers with previous studies. All values were converted to represent TC and TIC, respectively. The results of the mechanistic studies from Gangstø et al. (2008) and Buitenhuis et al. (2019) denote the reported $CaCO_3$ production and not the export flux. The export flux calculations include dissolution of the sinking calcium carbonate shells. However, we do not take this into account in the current study. Thus, we compare the production terms before dissolution. The sensitivity analyses are shown in italics. For the comparisons to MAREDAT, the projected biomass maps were sampled at the MAREDAT observation points of the respective plankton group (Bednaršek, Mozina, et al., 2012; Schiebel & Movellan, 2012). To be consistent with the methodology used in Bednaršek, Mozina, et al. (2012) and Schiebel and Movellan (2012), the total standing stocks and fluxes were calculated from global non-weighted mean biomass concentrations and assuming one and nine complete overturn periods for pteropods and foraminifers, respectively.

	Pteropoda		Foraminifers	
Source	Standing stock (Tg TC)	Carbon flux (Tg TIC yr^{-1})	Standing stock (Tg TC)	Carbon flux (Tg TIC yr^{-1})
Estimates based on mechanistic modelling studies				
Buitenhuis et al. (2019)		152 - 4183[a]		100 - 141[a]
Gangstø et al. (2008)		300		
Estimates based on observational data				
Bednaršek, Tarling, et al. (2012)	444 - 505[b,c]	112 - 150[b,c]		
Schiebel and Movellan (2012)			1 - 5[b]	3 - 12[b]
Schiebel (2002)				157 - 389[b,d]
Our results	**49 - 57**	**8 - 22**	**1 - 2**	**3 - 35**
1: MAREDAT methodology	*46 - 57*	*12 - 15*	*0.5 - 1.1*	*5 - 10*
2: Sampled at MAREDAT points & methodology	*62 - 95*	*17 - 26*	*1 - 2*	*1 - 4*
3a: W/o zeros	*91 - 140*	*24 - 38*	*2 - 3*	*16 - 33*
3b: W/o zeros, MAREDAT points & methodology	*132 - 220*	*35 - 60*	*2 - 9*	*4 - 20*
W/o CPR data	*90 - 155*	*25 - 42*	*1 - 3*	*18 - 33*

[a]Based on calcite production, not flux, [b]Based on subset of observations used in this study,[c]Estimates based on non-zero observations only, [d]Flux at 100 m

to 3 TgTC for foraminifers. Combining all three modifications causes an increase of factor 3–4 for both plankton types. Following the same methodology, pteropod biomass estimates are still a factor of 2–4 lower than the MAREDAT estimates, while foraminifer biomass estimates are in the same range. A potential reason for this difference between the two plankton groups might be the variation in patchiness due to the larger body size of pteropoda. The original MAREDAT pteropod abundance observations are nearly four times as patchy as those of foraminifers (Buitenhuis, Vogt, et al., 2013), which could have led to a higher bias in the pteropod standing stock estimate.

In the context of the marine trophic foodweb, pteropods constitute approximately 6% to 8% of total macrozooplankton biomass, whereas foraminifers make up 0.1% to 0.6% of microzooplankton biomass as shown in figure 5 (Buitenhuis, Vogt, et al., 2013). Each plankton size class encompasses a broad range of taxonomic groups, so that the relatively small contributions of pteropods and foraminifers is logical. In contrast to the other PFTs estimates and the earlier MAREDAT estimates for pteropods and foraminifers, our results are based on global climatological biomass estimates instead of spatially discrete observation data. This causes a lower discrepancy between our mean and median estimates as well as a lower total standard deviation (figure 5), because high biomass extreme events are not as prevalent in our results as in the raw field observations (cf. also section 4.4 and figure S5).

Estimated pteropod TIC fluxes are a factor of 5–100 lower than in previous numerical modelling studies (table 4). The estimates by Buitenhuis et al. (2019) and Gangstø et al. (2008) are based on mechanistic models which used published laboratory evidence for model calibration and observational data from MAREDAT for model evaluation. How-

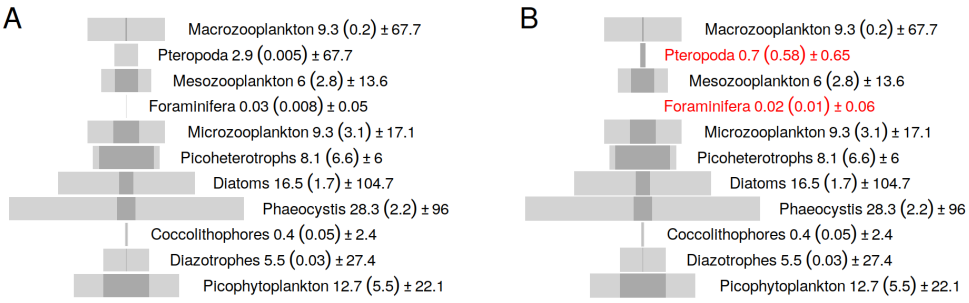

Figure 5. Trophic pyramid of autotrophic and heterotrophic plankton functional types (PFT). The bars show the mean (light grey filling) and median (dark grey filling, value in parentheses) biomass concentrations in $\mu g\,TC\,L^{-1}$ in the surface 200 m. The standard deviation is denoted for each PFT. **A** shows the original results from the MAREDAT project presented in Buitenhuis, Vogt, et al. (2013). **B** shows our updated estimates for pteropods and foraminifers as highlighted in red.

ever, the parametrization of the growth rate is based on copepod observations instead of pteropods in Buitenhuis, Vogt, et al. (2013) and hence could have introduced a bias. The difference in depth at which TIC-fluxes are reported (100 m in Buitenhuis et al. (2019) and 200 m in our study) likely introduce further uncertainties, however as neither of the results include dissolution effects, these are deemed minor. An additional reason for the discrepancy could be an incomplete representation of the true abundances in our observation data due to sampling biases (cf. section 4.4). Examples of such biases include net avoidance, diel vertical migration (DVM), and the use of sub-optimal mesh sizes for the target group (e.g. in the CPR), which can lead to underestimated abundances in our observational data (Zamelczyk et al., 2021; Pinkerton et al., 2020; Doubek et al., 2020). Excluding CPR data from our models approximately doubles the estimated TIC fluxes (table 4), however it also increases uncertainty in the environmental driver dependencies (cf. section 4.1).

Our foraminifer TIC flux estimates are of the same order of magnitude as the most recent observation-based estimates and mechanistic model-based studies, albeit on the lower end for the latter (Table 4). The earlier observational study by Schiebel (2002) is based on much smaller datasets with a spatial bias towards the highly productive North Atlantic Ocean and found substantially higher TIC fluxes. However, our results align well with the flux estimate calculated by more recent studies, such as Schiebel and Movellan (2012). In our work, we account only for large adults due to mesh size limitations, but including juvenile biomass might double foraminifer biomass and flux estimates(Schiebel and Movellan (2012), see also section 4.4). This uncertainty could also explain the deviations of our results from the mechanistic model-based estimate by Buitenhuis et al. (2019), which is a factor of 1.5–50 higher than our global annual TIC flux estimate. Similar as for pteropods, excluding CPR data prior to modelling approximately doubles the estimated global annual TIC fluxes (cf. table 4), which might be indicative of non-optimal representation of foraminifer abundances in this dataset.

Pteropoda contribute 0.5%–2.2% to total annual global carbonate fluxes and foraminifers contribute 0.2%–3.5%, assuming annual global fluxes amount to $1.0\,Pg\,TIC\,yr^{-1}$ to $1.6\,Pg\,TIC\,yr^{-1}$ (Iglesias-Rodriguez et al., 2002; Lee, 2001; Berelson et al., 2007). We can assume that the carbon fluxes calculated in our study represent a lower bound estimate due to biases and incompleteness of the observation dataset (see section 4.4). Coccolithophores are estimated to contribute 26%–52% to global carbonate fluxes (C. J. O'Brien, 2015),

which still leaves 40%–70% of global carbonate fluxes unaccounted for and points to an underestimation of the contribution from the calcifying zooplankton. Additional minor contributors to the marine $CaCO_3$ budget are fishes, atlantid heteropods, pseudothecosomes (particularly the fully shelled *Peracle* species), calcifying ostracods, dinoflagellates, ciliates and the larvae of both benthic molluscs and gymnosomates (Buitenhuis et al., 2019). However, their contribution to global carbonate fluxes is not well constrained, but may range between 3%–15% per group (Wilson et al., 2009; Schiebel, 2002; Buitenhuis et al., 2019), and hence warrants further investigation.

4.4 Limitations and uncertainties

Here, we use large global datasets and an exhaustive model ensemble approach to estimate pteropod and foraminifer biomass. We quantify and discuss the uncertainty arising from the model choice and key parametrizations and estimates for the growth rate and the TIC-TC factor. However, our biomass and carbon flux estimates are affected by the characteristics and errors underlying the observational data and the simplifying assumptions made for the model setup. These include the interaction of spatio-temporal biases in sampling effort with the inherent patchiness of plankton distribution, variations in sampling net mesh sizes, and limited taxonomic resolution for biomass conversions (de Garidel-Thoron et al., 2022).

Patchy sampling across space and time leads to spatiotemporal biases in the training dataset (figures 2, S3 and S4). Data coverage is low in the low productivity oligotrophic gyres and during the less productive months (figure S4). We find that a large fraction of the inter-model variability is due to environmental conditions outside of or at the outer ranges of the training data (section 3.5 and figures 3 and 4). Nonetheless, a large fraction of the global environmental space of our predictor variables is covered by the abundance datasets, which allows us to predict biomass values with higher certainty (figure S6). Furthermore, plankton distributions are generally characterized by a high level of seasonal and spatial patchiness (figure S5, Boltovskoy (1971); Beckmann et al. (1987); Siccha et al. (2012); Buitenhuis, Vogt, et al. (2013). This introduces high variance in the observed abundances (figure S5) and a mismatch between the gridded monthly climatologies used as environmental predictors and the mesoscale-affected biomass patterns (Righetti et al., 2019; Benedetti et al., 2021). However, previous studies found no significant benefit of using highly temporally resolved data over climatologies (Pinkerton et al., 2020), as the environmental conditions an organism experiences are based on their Langrangian movement over time (Hofmann Elizondo & Vogt, 2022). Finally, the use of coarse mesh sizes for sampling relatively small zooplankton can underestimate the true abundances as small and/or mobile individuals are missed (Tseng et al., 2011; Wells, 1973; Miloslavić et al., 2014; Mack et al., 2012; Skjoldal et al., 2013; Fabry, 1989; Zamelczyk et al., 2021). This is particularly relevant for the SO-CPR and Aus-CPR observations which make up 91% and 73% of our training data for pteropods and foraminifers, respectively (section 2.1.1) due to the large mesh size of 270 µm used (Richardson et al., 2006). These sampling data constraints hence cause our biomass and flux estimates to be lower end estimates.

Further uncertainties in the standing stock and flux estimates come from the simplified abundance to biomass conversions and the biomass to carbon flux derivation. We assumed species-level or group-level averages for the size-based biomass conversion functions (section 2.1.2). Yet, in practice these values vary based on ontogenetic stage, subspecies, ambient temperature (Bradshaw, 1959), and food availability (Meilland et al., 2016; Schiebel et al., 2001; Schiebel & Hemleben, 2005). These factors vary with latitude and we could not account for them explicitly in the present carbon conversions (cf. section 2.1.2) due to a lack of available parametrizations. Therefore, we likely underestimated the global latitudinal variability in our biomass predictions. To convert biomasses to TIC fluxes, growth rates and the TIC-TC conversion factor were based on spatially

constrained data and a limited number of species due to data availability (cf. section 2.1.2). The choices made for the growth rate function and the TIC-TC factor had a significant impact on flux estimates for pteropods, and for foraminifers to a lesser extent (section 3.5). Plankton observations identified at a finer taxonomic level and species-specific laboratory-based conversion factors and growth rates would likely increase the accuracy of our calculations. To estimate export fluxes at depth, particle sinking velocities and dissolution rates need to be considered (Takahashi & Bé, 1984; Schiebel et al., 2007). During periods of peak biomass production, high pulses of fast-sinking organisms occur and can drive higher export efficiency (Schiebel, 2002). However, the relative species abundances observed in our upper ocean foraminifera data (figure S26) are in good agreement with those found in sediment trap data in previous studies Kretschmer et al. (2018); Lombard et al. (2011). This shows that the foraminifer surface export fluxes and patterns found in our study are representative of export patterns found in the deeper ocean. For pteropods, to our knowledge, no comprehensive global sediment trap data analysis has yet been conducted. To assess comparability between fluxes at the surface and the deep ocean, such an analysis is hence much needed.

5 Conclusion

The aim of this study was to predict global monthly and annual patterns and drivers of shelled pteropod and planktic foraminifer TC biomass distributions, and their associated TIC fluxes, and to assess the importance of these groups for the global biogeochemical cycling of carbon and $CaCO_3$.

Globally, pteropods contribute 6%–8% and foraminifers 0.1%–0.6% to total global macrozooplankton and microzooplankton TC standing stocks, respectively. The sinking of their shells and tests constitutes approximately 1.5% each of the total global annual surface TIC fluxes. We found biomass hotspots for both plankton groups in the high Northern latitudes, around the equator, and in the upwelling systems. Temperature and chlorophyll-a concentrations were the two most important environmental covariates for modelling the biomass patterns.

Based on newly assembled abundance data for different organism groups, we can use our modelling pipeline to project global biomass patterns for various plankton functional groups (Le Quéré et al., 2005). Thus, we can validate newly developed mechanistic marine ecosystem models (Le Quéré et al., 2016; Clerc et al., 2022) of increased complexity and higher diversity in zooplankton functional types. Additionally, the models can be employed to assess future changes in plankton biomass by projecting the present models on future environmental fields under climate change scenarios (Benedetti et al., 2021; Tittensor et al., 2021). This is particularly relevant considering the high sensitivity of, for example, pteropods to ocean acidification and warming (Bednaršek et al., 2016; Manno et al., 2016). Thus, we can identify hotspots of future biomass changes (complementary to future changes in diversity as modeled in Benedetti et al. (2021)) and potentially link these to risk assessments based on other ocean health indices (Halpern et al., 2012).

Furthermore, the pipeline can be used to model other types of quantitative data, such as sediment trap data (Kretschmer et al., 2018) or measurements based on novel approaches like underwater imaging techniques or omics (Pesant et al., 2015). As a large fraction of the carbonate export fluxes still remains unaccounted for based on our results, we could calculate flux contributions of different organism groups such as fish and shelled heteropods (Wilson et al., 2009; Buitenhuis et al., 2019; Wall-Palmer et al., 2016). Comparing estimates based on upper ocean data with those based on sediment traps could help to improve our understanding of export patterns driven by different organism groups as well as the impacts of carbonate dissolution and sinking rates on such patterns.

Open Research Section

The observational datasets used to train the models as well as the model outputs will be made publicly available on AtlantECO's GeoNode portal (https://atlanteco-geonode.eu/) upon acceptance of the manuscript. An adapted version of the modelling pipeline, applicable to any species abundance or biomass dataset in the AtlantECO format is available on the GitHub account of N.K. (https://github.com/nielja).

Acknowledgments

We thank all contributors involved in the zooplankton field sampling and identification and we acknowledge the efforts made by the community to share such data through publicly available archives. This project has received funding from the European Union's Horizon 2020 research and innovation programme under grant agreement no. 862923. This output reflects only the author's view, and the European Union cannot be held responsible for any use that may be made of the information contained therein. We thank David Johns for preparing and sharing the calcifying pteropod counts of the CPR survey. We are grateful to Anthony J. Richardson and Claire Davies for facilitating the access to the Aus-CPR survey. The Aus-CPR data was sourced from Australia's Integrated Marine Observing System (IMOS) – IMOS is enabled by the National Collaborative Research Infrastructure Strategy (NCRIS). We are also very grateful to John Kitchener for facilitating the access to the SO-CPR survey. Nina Bednaršek acknowledges support from the Slovene Research Agency (ARRS "Biomarkers of subcellular stress in the Northern Adriatic under global environmental change", #J12468).

References

Anderson, O. R., Spindler, M., Bé, A. W. H., & Hemleben, C. (1979). Trophic activity of planktonic foraminifera. *Journal of the Marine Biological Association of the United Kingdom*, *59*(3), 791–799. Retrieved from `https://www.cambridge.org/core/article/trophic-activity-of-planktonic-foraminifera/F9AC18BAA017EC7EAE64CB0D6E3A805C` doi: DOI:10.1017/S002531540004577X

Anglada-Ortiz, G., Zamelczyk, K., Meilland, J., Ziveri, P., Chierici, M., Fransson, A., & Rasmussen, T. L. (2021). Planktic Foraminiferal and Pteropod Contributions to Carbon Dynamics in the Arctic Ocean (North Svalbard Margin). *Frontiers in Marine Science*, *8*(June). doi: 10.3389/fmars.2021.661158

Antell, G. S., Fenton, I. S., Valdes, P. J., & Saupe, E. E. (2021). Thermal niches of planktonic foraminifera are static throughout glacial-interglacial climate change. *Proceedings of the National Academy of Sciences of the United States of America*, *118*(18), 1–9. doi: 10.1073/pnas.2017105118

Bar-On, Y. M., Phillips, R., & Milo, R. (2018). The biomass distribution on Earth. *Proceedings of the National Academy of Sciences of the United States of America*, *115*(25), 6506–6511. doi: 10.1073/pnas.1711842115

Barton, A. D., Irwin, A. J., Finkel, Z. V., & Stock, C. A. (2016). Anthropogenic climate change drives shift and shuffle in North Atlantic phytoplankton communities. *Proceedings of the National Academy of Sciences of the United States of America*, *113*(11), 2964–2969. doi: 10.1073/pnas.1519080113

Bé, A. W. H., & Gilmer, R. W. (1977). A zoogeographic and taxonomic review of euthecosomatous Pteropoda. *Oceanic micropaleontology*, *1*(6), 733–808.

Beare, D., McQuatters-Gollop, A., van der Hammen, T., Machiels, M., Teoh, S. J., & Hall-Spencer, J. M. (2013, 5). Long-Term Trends in Calcifying Plankton and pH in the North Sea. *PLOS ONE*, *8*(5), e61175. Retrieved from `https://doi.org/10.1371/journal.pone.0061175`

Beaugrand, G., Edwards, M., & Legendre, L. (2010). Marine biodiversity, ecosys-

tem functioning, and carbon cycles. *Proceedings of the National Academy of Sciences of the United States of America*, *107*(22), 10120–10124. doi: 10.1073/pnas.0913855107

Beaugrand, G., Mcquatters-Gollop, A., Edwards, M., & Goberville, E. (2013). Long-term responses of North Atlantic calcifying plankton to climate change. *Nature Climate Change*, *3*(3), 263–267. doi: 10.1038/nclimate1753

Beckmann, W., Auras, A., & Hemleben, C. (1987). Cyclonic cold-core eddy in the eastern North Atlantic. III. Zooplankton. *Marine Ecology Progress Series*, 165–173.

Bednaršek, N., Carter, B. R., Mccabe, R. M., Feely, R. A., & Howard, E. (2022). Pelagic calcifiers face increased mortality and habitat loss with warming and ocean acidification. *Authorea*. doi: DOI:10.22541/au.164865092.29568156/v1

Bednaršek, N., Feely, R. A., Beck, M. W., Glippa, O., Kanerva, M., & Engström-Öst, J. (2018). El Niño-related thermal stress coupled with upwelling-related ocean acidification negatively impacts cellular to population-level responses in pteropods along the California current system with implications for increased bioenergetic costs. *Frontiers in Marine Science*, *5*(DEC), 1–17. doi: 10.3389/fmars.2018.00486

Bednaršek, N., Feely, R. A., Tolimieri, N., Hermann, A. J., Siedlecki, S. A., Waldbusser, G. G., ... Pörtner, H. O. (2017). Exposure history determines pteropod vulnerability to ocean acidification along the US West Coast article. *Scientific Reports*, *7*(1), 1–12. doi: 10.1038/s41598-017-03934-z

Bednaršek, N., Harvey, C. J., Kaplan, I. C., Feely, R. A., & Možina, J. (2016). Pteropods on the edge: Cumulative effects of ocean acidification, warming, and deoxygenation. *Progress in Oceanography*, *145*, 1–24. doi: 10.1016/j.pocean.2016.04.002

Bednaršek, N., Klinger, T., Harvey, C. J., Weisberg, S., McCabe, R. M., Feely, R. A., ... Tolimieri, N. (2017). New ocean, new needs: Application of pteropod shell dissolution as a biological indicator for marine resource management. *Ecological Indicators*, *76*, 240–244. doi: 10.1016/j.ecolind.2017.01.025

Bednaršek, N., Mozina, J., Vogt, M., O'Brien, C., & Tarling, G. A. (2012). The global distribution of pteropods and their contribution to carbonate and carbon biomass in the modern ocean. *Earth System Science Data*, *4*(1), 167–186. doi: 10.5194/essd-4-167-2012

Bednaršek, N., & Ohman, M. D. (2015). Changes in pteropod distributions and shell dissolution across a frontal system in the California Current System. *Marine Ecology Progress Series*, *523*, 93–103. doi: 10.3354/meps11199

Bednaršek, N., Tarling, G. A., Fielding, S., & Bakker, D. C. (2012). Population dynamics and biogeochemical significance of Limacina helicina antarctica in the Scotia Sea (Southern Ocean). *Deep-Sea Research Part II: Topical Studies in Oceanography*, *59-60*, 105–116. doi: 10.1016/j.dsr2.2011.08.003

Bell, D. M., & Schlaepfer, D. R. (2016). On the dangers of model complexity without ecological justification in species distribution modeling. *Ecological Modelling*, *330*, 50–59. Retrieved from `http://dx.doi.org/10.1016/j.ecolmodel.2016.03.012` doi: 10.1016/j.ecolmodel.2016.03.012

Benedetti, F., Vogt, M., Elizondo, U. H., Righetti, D., Zimmermann, N. E., & Gruber, N. (2021). Major restructuring of marine plankton assemblages under global warming. *Nature Communications*, *12*(1), 1–15. Retrieved from `http://dx.doi.org/10.1038/s41467-021-25385-x` doi: 10.1038/s41467-021-25385-x

Berelson, W. M., Balch, W. M., Najjar, R., Feely, R. A., Sabine, C., & Lee, K. (2007). Relating estimates of CaCO3 production, export, and dissolution in the water column to measurements of CaCO3 rain into sediment traps and dissolution on the sea floor: A revised global carbonate budget. *Global Biogeochemical Cycles*, *21*(1).

Boehmke, B., & Greenwell, B. (2019a). Deep Learning. In *Hands-on machine learning with r* (1st ed., chap. 12). New York: Chapman and Hall/CRC. doi: https://doi.org/10.1201/9780367816377

Boehmke, B., & Greenwell, B. (2019b). Gradient Boosting. In *Hands-on machine learning with r* (1st ed., chap. 11). New York: Chapman and Hall/CRC. doi: https://doi.org/10.1201/9780367816377

Boehmke, B., & Greenwell, B. (2019c). Interpretable Machine Learning. In *Hands-on machine learning with r* (chap. 16). New York: Chapman and Hall/CRC. doi: https://doi.org/10.1201/9780367816377

Boehmke, B., & Greenwell, B. (2019d). Modeling Process. In *Hands-on machine learning with r2* (1st ed., chap. 2). New York: Chapman and Hall/CRC.

Boehmke, B., & Greenwell, B. (2019e). Random Forests. In *Hands-on machine learning with r* (1st ed., chap. 11). New York: Chapman and Hall/CRC. doi: https://doi.org/10.1201/9780367816377

Boltovskoy, E. (1971). Patchiness in the distribution of planktonic foraminifera. In *Proceedings of the 2. planktonic conference* (pp. 107–115). Rome, Italy: Ed. Tecnoscienza.

Boyce, D. G., Lewis, M. R., & Worm, B. (2010). Global phytoplankton decline over the past century. *Nature*, *466*(7306), 591–596. doi: 10.1038/nature09268

Boyer, T. P., García, H. E., Locarnini, R. A., Zweng, M. M., Mishonov, A. V., Reagan, J. R., ... Smolyar, I. V. (2018). *World Ocean Atlas 2018.* Retrieved from `https://www.ncei.noaa.gov/archive/accession/NCEI-WOA18`

Bradshaw, J. S. (1959). Ecology of living planktonic foraminifera in the north and equatorial Pacific. *Ocean. Cushman Found. Foram. Res. Contr.*, *10*(2), 25–64.

Brandão, M. C., Benedetti, F., Martini, S., Soviadan, Y. D., Irisson, J. O., Romagnan, J. B., ... Lombard, F. (2021). Macroscale patterns of oceanic zooplankton composition and size structure. *Scientific Reports*, *11*(1), 1–19. doi: 10.1038/s41598-021-94615-5

Brown, J. H., Gillooly, J. F., Allen, A. P., Savage, V. M., & West, G. B. (2004). Toward a metabolic theory of ecology. *Ecology*, *85*(7), 1771–1789.

Brun, P., Kiørboe, T., Licandro, P., & Payne, M. R. (2016). The predictive skill of species distribution models for plankton in a changing climate. *Global change biology*, *22*(9), 3170–3181. doi: 10.1111/gcb.13274

Brun, P., Thuiller, W., Chauvier, Y., Pellissier, L., Wüest, R. O., Wang, Z., & Zimmermann, N. E. (2020). Model complexity affects species distribution projections under climate change. *Journal of Biogeography*, *47*(1), 130–142. doi: 10.1111/jbi.13734

Brun, P., Vogt, M., Payne, M. R., Gruber, N., O'Brien, C. J., Buitenhuis, E. T., ... Luo, Y. W. (2015). Ecological niches of open ocean phytoplankton taxa. *Limnology and Oceanography*, *60*(3), 1020–1038. doi: 10.1002/lno.10074

Buitenhuis, E. T., Hashioka, T., & Quéré, C. L. (2013). Combined constraints on global ocean primary production using observations and models. *Global Biogeochemical Cycles*, *27*(3), 847–858. doi: 10.1002/gbc.20074

Buitenhuis, E. T., Le Quéré, C., Bednaršek, N., & Schiebel, R. (2019). Large Contribution of Pteropods to Shallow CaCO3 Export. *Global Biogeochemical Cycles*, *33*(3), 458–468. doi: 10.1029/2018GB006110

Buitenhuis, E. T., Vogt, M., Moriarty, R., Bednaršek, N., Doney, S. C., Leblanc, K., ... Swan, C. (2013). MAREDAT: Towards a world atlas of MARine Ecosystem DATa. *Earth System Science Data*, *5*(2), 227–239. doi: 10.5194/essd-5-227-2013

Burba, G., & Anderson, D. (2005). *A Brief Practical Guide to Eddy Covariance Flux Measurements* (Tech. Rep.). Lincoln: LI-COR Biosciences. doi: 10.1076/ceyr.18.1.62.5393

Burridge, A. K., Goetze, E., Wall-Palmer, D., Le Double, S. L., Huisman, J., & Peijnenburg, K. T. (2017). Diversity and abundance of pteropods and het-

eropods along a latitudinal gradient across the Atlantic Ocean. *Progress in Oceanography*, *158*, 213–223. Retrieved from `http://dx.doi.org/10.1016/j.pocean.2016.10.001` doi: 10.1016/j.pocean.2016.10.001

Caron, D. A., & Bé, A. W. H. (1984). Predicted and observed feeding rates of the spinose planktonic foraminifer Globigerinoides sacculifer. *Bulletin of Marine Science*, *35*(1), 1–10.

Carton, J. A., Chepurin, G. A., & Chen, L. (2018). SODA3: A new ocean climate reanalysis. *Journal of Climate*, *31*(17), 6967–6983. doi: 10.1175/jcli-d-18-0149.1

Chapperon, C., & Seuront, L. (2011). Behavioral thermoregulation in a tropical gastropod: links to climate change scenarios. *Global Change Biology*, *17*(4), 1740–1749.

Chiswell, S. M., Calil, P. H., & Boyd, P. W. (2014). Spring blooms and annual cycles of phytoplankton: A unified perspective. *Journal of Plankton Research*, *37*(3), 500–508. doi: 10.1093/plankt/fbv021

Clerc, C., Bopp, L., Benedetti, F., Vogt, M., & Aumont, O. (2022). Including filter-feeding gelatinous macrozooplankton in a global marine biogeochemical model: model-data comparison and impact on the ocean carbon cycle. *Authorea Preprints*.

Conley, K. R., Lombard, F., & Sutherland, K. R. (2018). Mammoth grazers on the ocean's minuteness: A review of selective feeding using mucous meshes. *Proceedings of the Royal Society B: Biological Sciences*, *285*(1878). doi: 10.1098/rspb.2018.0056

Copernicus. (2021). *Climate Data Store of the Copernicus Marine Environment.* Retrieved from `https://cds.climate.copernicus.eu/cdsapp#!/dataset/10.24381/cds.4c328c78?tab=doc` doi: 10.24381/cds.4c328c78

Corney, P. M., Duc, M. G., Smart, S. M., Kirby, K. J., Bunce, R. G., & Marrs, R. H. (2006). Relationships between the species composition of forest field-layer vegetation and environmental drivers, assessed using a national scale survey. *Journal of Ecology*, *94*(2), 383–401. doi: 10.1111/j.1365-2745.2006.01094.x

Dadon, J. R., & Masello, J. F. (1999). Mechanisms generating and maintaining the admixture of zooplanktonic molluscs (Euthecosomata: Opistobranchiata: Gastropoda) in the Subtropical Front of the South Atlantic. *Marine Biology*, *135*(1), 171–179. doi: 10.1007/s002270050614

Davis, C. S., & Wiebe, P. H. (1985). Macrozooplankton biomass in a warm-core Gulf Stream ring: time series changes in size structure, taxonomic composition, and vertical distribution. *Journal of Geophysical Research*, *90*(C5), 8871–8884. doi: 10.1029/JC090iC05p08871

De Broyer, C., et al. (Eds.). (2014). *Biogeographic Atlas of the Southern Ocean.* Cambridge, United Kingdom: SCAR.

de Garidel-Thoron, T., Chaabane, S., Giraud, X., Meilland, J., Jonkers, L., Kucera, M., ... Schiebel, R. (2022). The Foraminiferal Response to Climate Stressors Project: Tracking the Community Response of Planktonic Foraminifera to Historical Climate Change. *Frontiers in Marine Science*, *9*(May), 1–6. doi: 10.3389/fmars.2022.827962

Dietrich, G., Kalle, K., Krauss, W., & Siedler, G. (1975). *Allgemeine Meereskunde* (3rd ed.). Berlin/Stuttgart: Gebrüder Bornträger.

Dormann, C. F., Elith, J., Bacher, S., Buchmann, C., Carl, G., Carré, G., ... Lautenbach, S. (2013). Collinearity: A review of methods to deal with it and a simulation study evaluating their performance. *Ecography*, *36*(1), 27–46. doi: 10.1111/j.1600-0587.2012.07348.x

Doubek, J. P., Goldfarb, S. K., & Stockwell, J. D. (2020). Should we be sampling zooplankton at night? *Limnology and Oceanography Letters*, *5*(4), 313–321. doi: 10.1002/lol2.10151

Dufois, F., Hardman-Mountford, N. J., Greenwood, J., Richardson, A. J., Feng, M., & Matear, R. J. (2016). Anticyclonic eddies are more productive than cyclonic eddies in subtropical gyres because of winter mixing. *Science Advances*, *2*(5), 1–7. doi: 10.1126/sciadv.1600282

Elith, J., Kearney, M., & Phillips, S. (2010). The art of modelling range-shifting species. *Methods in Ecology and Evolution*, *1*(4), 330–342. doi: 10.1111/j.2041-210x.2010.00036.x

Elith, J., & Leathwick, J. R. (2009). Species distribution models: Ecological explanation and prediction across space and time. *Annual Review of Ecology, Evolution, and Systematics*, *40*, 677–697. doi: 10.1146/annurev.ecolsys.110308.120159

Fabry, V. J. (1989). Aragonite production by pteropod molluscs in the subarctic Pacific. *Deep Sea Research Part A, Oceanographic Research Papers*, *36*(11), 1735–1751. doi: 10.1016/0198-0149(89)90069-1

Fabry, V. J., Seibel, B. A., Feely, R. A., & Orr, J. C. (2008). Impacts of ocean acidification on marine fauna and ecosystem processes. *ICES Journal of Marine Science*, *65*(3), 414–432.

Fallet, U., Ullgren, J. E., Castañeda, I. S., van Aken, H. M., Schouten, S., Ridderinkhof, H., & Brummer, G.-J. A. (2011). Contrasting variability in foraminiferal and organic paleotemperature proxies in sedimenting particles of the Mozambique Channel (SW Indian Ocean). *Geochimica et Cosmochimica Acta*, *75*(20), 5834–5848. Retrieved from `https://www.sciencedirect.com/science/article/pii/S0016703711004650` doi: https://doi.org/10.1016/j.gca.2011.08.009

Fisher, R. A., & Yates, F. (1953). *Statistical tables for biological, agricultural and medical research.* Hafner Publishing Company.

Frenger, I., Bianchi, D., Stührenberg, C., Oschlies, A., Dunne, J., Deutsch, C., ... Schütte, F. (2018). Biogeochemical Role of Subsurface Coherent Eddies in the Ocean: Tracer Cannonballs, Hypoxic Storms, and Microbial Stewpots? *Global Biogeochemical Cycles*, *32*(2), 226–249. doi: 10.1002/2017GB005743

Frerichs, W. E., Heiman, M. E., Borgman, L. E., & Be, A. W. H. (1972). Latitudal variations in planktonic foraminiferal test porosity; Part 1, Optical studies. *The Journal of Foraminiferal Research*, *2*(1), 6–13.

Gangstø, R., Gehlen, M., Schneider, B., Bopp, L., Aumont, O., & Joos, F. (2008). Modeling the marine aragonite cycle: Changes under rising carbon dioxide and its role in shallow water CaCO3 dissolution. *Biogeosciences*, *5*(4), 1057–1072. doi: 10.5194/bg-5-1057-2008

Garcia, H. E., Weathers, K. W., Paver, C. R., Smolyar, I., Boyer, T. P., Locarnini, M. M., ... Seidov, D. (2019a). *World ocean atlas 2018. Vol. 4: Dissolved inorganic nutrients (phosphate, nitrate and nitrate + nitrite, silicate)* (Tech. Rep.). NOAA. Retrieved from `https://data.nodc.noaa.gov/woa/WOA18/DOC/woa18_vol4.pdf`

Garcia, H. E., Weathers, K. W., Paver, C. R., Smolyar, I., Boyer, T. P., Locarnini, M. M., ... Seidov, D. (2019b). *World Ocean Atlas 2018, Volume 3: Dissolved Oxygen, Apparent Oxygen Utilization, and Dissolved Oxygen Saturation.* (Tech. Rep.). NOAA. Retrieved from `https://www.ncei.noaa.gov/access/world-ocean-atlas-2018/bin/woa18oxnu.pl?parameter=o`

Gardner, J., Manno, C., Bakker, D. C. E., Peck, V. L., & Tarling, G. A. (2017). Southern Ocean pteropods at risk from ocean warming and acidification. *Marine Biology*, *165*(1), 8. Retrieved from `https://doi.org/10.1007/s00227-017-3261-3` doi: 10.1007/s00227-017-3261-3

Gilmer, R. W., & Harbison, G. R. (1986). Morphology and field behavior of pteropod molluscs: feeding methods in the families Cavoliniidae, Limacinidae and Peraclididae (Gastropoda: Thecosomata). *Marine Biology*, *91*(1), 47–57.

Govoni, J. J., Hare, J. A., Davenport, E. D., Chen, M. H., & Marancik, K. E.

(2010). Mesoscale, cyclonic eddies as larval fish habitat along the southeast United States shelf: A Lagrangian description of the zooplankton community. *ICES Journal of Marine Science*, *67*(3), 403–411. doi: 10.1093/icesjms/fsp269

Gregor, L., & Gruber, N. (2021). OceanSODA-ETHZ: a global gridded data set of the surface ocean carbonate system for seasonal to decadal studies of ocean acidification. *Earth System Science Data*, *13*(2), 777–808.

Guisan, A., & Zimmermann, N. E. (2000). Predictive habitat distribution models in ecology. *Ecological Modelling*, *135*(2-3), 147–186. doi: 10.1016/S0304-3800(00)00354-9

H2O.ai. (2021). *R Interface for H2O.* Retrieved from `https://github.com/h2oai/h2o-3`

Halpern, B. S., Longo, C., Hardy, D., McLeod, K. L., Samhouri, J. F., Katona, S. K., ... Zeller, D. (2012). An index to assess the health and benefits of the global ocean. *Nature*, *488*(7413), 615–620. doi: 10.1038/nature11397

Hastie, T. J., & Tibshirani, R. J. (1990). Generalized additive models. In *Generalized additive models* (1st ed., pp. 136–173). New York: Routledge. doi: https://doi.org/10.1201/9780203753781

Hauri, C., Gruber, N., McDonnell, A. M., & Vogt, M. (2013). The intensity, duration, and severity of low aragonite saturation state events on the California continental shelf. *Geophysical Research Letters*, *40*(13), 3424–3428. doi: 10.1002/grl.50618

Helaouët, P., & Beaugrand, G. (2009). Physiology, ecological niches and species distribution. *Ecosystems*, *12*(8), 1235–1245. doi: 10.1007/s10021-009-9261-5

Hemleben, C., Spindler, M., & Anderson, O. R. (1989). Host and symbiont relationships. In *Modern planktonic foraminifera* (pp. 86–111). Springer.

Hofmann Elizondo, U., Righetti, D., Benedetti, F., & Vogt, M. (2021). Biome partitioning of the global ocean based on phytoplankton biogeography. *Progress in Oceanography*, *194*(February), 102530. Retrieved from `https://doi.org/10.1016/j.pocean.2021.102530` doi: 10.1016/j.pocean.2021.102530

Hofmann Elizondo, U., & Vogt, M. (2022). Individual-based modeling of shelled pteropods. *Ecological Modelling*, *468*, 109944. doi: 10.1016/j.ecolmodel.2022.109944

Horton, T., Gofas, S., Kroh, A., Poore, G. C., Read, G., Rosenberg, G., ... Vranken, S. (2017). Improving nomenclatural consistency: a decade of experience in the World Register of Marine Species. *European Journal of Taxonomy*, *389*, 1–24. Retrieved from `https://www.marinespecies.org/aphia.php?p=sourcedetails&id=287923` doi: 10.5852/ejt.2017.389

Hosie, G. (2021). *Southern Ocean Continuous Plankton Recorder Zooplankton Records, Ver. 9.* Australian Antarctic Data Centre. doi: doi:10.26179/ksds-s610

Hosmer Jr, D. W., Lemeshow, S., & Sturdivant, R. X. (2013). Assessing the Fit of the Model. In *Applied logistic regression* (Vol. 398, pp. 153–225). John Wiley & Sons.

Howes, E. L., Stemmann, L., Assailly, C., Irisson, J. O., Dima, M., Bijma, J., & Gattuso, J. P. (2015). Pteropod time series from the North Western Mediterranean (1967-2003): Impacts of pH and climate variability. *Marine Ecology Progress Series*, *531*, 193–206. doi: 10.3354/meps11322

Hunt, B. P., Pakhomov, E. A., Hosie, G. W., Siegel, V., Ward, P., & Bernard, K. (2008). Pteropods in Southern Ocean ecosystems. *Progress in Oceanography*, *78*(3), 193–221. doi: 10.1016/j.pocean.2008.06.001

Iglesias-Rodriguez, M. D., Armstrong, R., Feely, R., Hood, R., Kleypas, J., Milliman, J. D., ... Sarmiento, J. (2002). Progress made in study of ocean's calcium carbonate budget. *Eos*, *83*(34), 2000–2002. doi: 10.1029/2002EO000267

IMOS. (2022). *IMOS - AusCPR: Zooplankton Abundance.* NASA/Global Change

Master Directory (GCMD) Earth Science Keywords. Version 6.0.0.0.0. Retrieved from https://catalogue-imos.aodn.org.au/geonetwork/srv/eng/catalog.search#/metadata/c1344e70-480e-0993-e044-00144f7bc0f4

Ivanova, E. M., Conan, S. M.-H., Peeters, F. J. C., & Troelstra, S. R. (1999). Living Neogloboquadrina pachyderma sin and its distribution in the sediments from Oman and Somalia upwelling areas. *Marine Micropaleontology*, *36*(2-3), 91–107.

Jentzen, A., Schönfeld, J., & Schiebel, R. (2018). Assessment of the effect of increasing temperature on the ecology and assemblage structure of modern planktic foraminifers in the Caribbean and surrounding seas. *Journal of Foraminiferal Research*, *48*(3), 251–272. doi: 10.2113/gsjfr.48.3.251

Jin., X., Gruber, N., Dune, J. P., Sarmiento, J. L., & Armstrong, R. A. (2006). Diagnosing the contributions of phytoplankton functional groups to the production and export of particulate organic carbon, CaCO3, and opal from global nutrient and alkalinity distributions. *Global Biogeochemical Cycles*, *20*(2), 1–17. doi: 10.1029/2005GB002532

Johns, D. M. B. A. o. t. U. M. (2021). *Continuous Plankton Recorder data for all coccolithophores, foraminifera and thecosomata - all areas.* The Archive for Marine Species and Habitats Data (DASSH). doi: https://doi.org/10.17031/1763

Joint, I., Doney, S. C., & Karl, D. M. (2011). Will ocean acidification affect marine microbes. *ISME Journal*, *5*(1), 1–7. doi: 10.1038/ismej.2010.79

Jonkers, L., Hillebrand, H., & Kucera, M. (2019). Global change drives modern plankton communities away from the pre-industrial state. *Nature*, *570*(7761), 372–375. Retrieved from http://dx.doi.org/10.1038/s41586-019-1230-3 doi: 10.1038/s41586-019-1230-3

Kämpf, J., & Chapman, P. (2016). *Upwelling systems of the world.* Springer.

Kirby, R. R., & Beaugrand, G. (2009). Trophic amplification of climate warming. *Proceedings of the Royal Society B: Biological Sciences*, *276*(1676), 4095–4103.

Koppelmann, R., Kullmann, B., Lahajnar, N., Martin, B., & Mohrholz, V. (2013). Onshore - offshore distribution of Thecosomata (Gastropoda) in the Benguela Current upwelling region off Namibia: species diversity and trophic position. *Journal of the Marine Biological Association of the United Kingdom*, *93*(6), 1625–1640. Retrieved from https://www.cambridge.org/core/article/onshoreoffshore-distribution-of-thecosomata-gastropoda-in-the-benguela-current-upwelling-region-off-namibia-species-diversity-and-trophic-position/9231CA48082E65EFFCC11D50AFDE45F4 doi: DOI:10.1017/S0025315413000052

Kretschmer, K., Jonkers, L., Kucera, M., & Schulz, M. (2018). Modeling seasonal and vertical habitats of planktonic foraminifera on a global scale. *Biogeosciences*, *15*(14), 4405–4429. doi: 10.5194/bg-15-4405-2018

Kruskal, W. H., & Wallis, W. A. (1952). Use of Ranks in One-Criterion Variance Analysis. *Journal of the American Statistical Association*, *47*(260), 583–621. doi: 10.1080/01621459.1952.10483441

Kucera, M. (2007). Chapter Six Planktonic Foraminifera as Tracers of Past Oceanic Environments. *Developments in Marine Geology*, *1*(07), 213–262. doi: 10.1016/S1572-5480(07)01011-1

Kupferman, S. L., Becker, G. A., Simmons, W. F., Schauer, U., Marietta, M. G., & Nies, H. (1986). An intense cold core eddy in the North-East Atlantic. *Nature*, *319*(6053), 474–477.

Lalli, C. M., & Gilmer, R. W. (1989). *Pelagic snails: the biology of holoplanktonic gastropod mollusks.* Stanford University Press.

Larson, R. J. (1986). Water content, organic content, and carbon and nitrogen composition of medusae from the northeast Pacific. *Journal of Experimental Marine Biology and Ecology*, *99*(2), 107–120. doi: 10.1016/0022-0981(86)90231-5

Lee, K. (2001). Global net community production estimated from the annual cycle of surface water total dissolved inorganic carbon. *Limnology and Oceanography*, *46*(6), 1287–1297.

Leinweber, A., & Gruber, N. (2013). Variability and trends of ocean acidification in the Southern California Current System: A time series from Santa Monica Bay. *Journal of Geophysical Research: Oceans*, *118*(7), 3622–3633. doi: 10.1002/jgrc.20259

Le Quéré, C., Buitenhuis, E. T., Moriarty, R., Alvain, S., Aumont, O., Bopp, L., ... Vallina, S. M. (2016). Role of zooplankton dynamics for Southern Ocean phytoplankton biomass and global biogeochemical cycles. *Biogeosciences*, *13*(14), 4111–4133. doi: 10.5194/bg-13-4111-2016

Le Quéré, C., Harrison, S. P., Colin Prentice, I., Buitenhuis, E. T., Aumont, O., Bopp, L., ... Giraud, X. (2005). Ecosystem dynamics based on plankton functional types for global ocean biogeochemistry models. *Global Change Biology*, *11*(11), 2016–2040.

Lischka, S., Büdenbender, J., Boxhammer, T., & Riebesell, U. (2011). Impact of ocean acidification and elevated temperatures on early juveniles of the polar shelled pteropod Limacina helicina: Mortality, shell degradation, and shell growth. *Biogeosciences*, *8*(4), 919–932. doi: 10.5194/bg-8-919-2011

Lischka, S., & Riebesell, U. (2012). Synergistic effects of ocean acidification and warming on overwintering pteropods in the Arctic. *Global Change Biology*, *18*(12), 3517–3528. doi: 10.1111/gcb.12020

Locarnini, M. M., Mishonov, A. V., Baranova, O. K., Boyer, T. P., Zweng, M. M., Garcia, H. E., ... Smolyar, I. (2018). *World ocean atlas 2018, Vol. 1: Temperature* (Tech. Rep.). NOAA. Retrieved from `https://www.ncei.noaa.gov/access/world-ocean-atlas-2018/bin/woa18.pl?parameter=t`

Lombard, F., Labeyrie, L., Michel, E., Bopp, L., Cortijo, E., Retailleau, S., ... Jorissen, F. (2011). Modelling planktic foraminifer growth and distribution using an ecophysiological multi-species approach. *Biogeosciences*, *8*(4), 853–873. doi: 10.5194/bg-8-853-2011

Lombard, F., Labeyrie, L., Michel, E., Spero, H. J., & Lea, D. W. (2009). Modelling the temperature dependent growth rates of planktic foraminifera. *Marine Micropaleontology*, *70*(1-2), 1–7. Retrieved from `http://dx.doi.org/10.1016/j.marmicro.2008.09.004` doi: 10.1016/j.marmicro.2008.09.004

Longhurst, A. R. (2007). Physical Control of Ecological Processes. In A. R. Longhurst (Ed.), *Ecological geography of the sea* (2nd ed., pp. 51–70). Burlington: Academic Press. doi: 10.1016/b978-012455521-1/50005-x

Maas, A. E., Lawson, G. L., & Tarrant, A. M. (2015). Transcriptome-wide analysis of the response of the thecosome pteropod Clio pyramidata to short-term CO2 exposure. *Comparative Biochemistry and Physiology Part D: Genomics and Proteomics*, *16*, 1–9. Retrieved from `https://www.sciencedirect.com/science/article/pii/S1744117X15000398` doi: https://doi.org/10.1016/j.cbd.2015.06.002

Mack, H. R., Conroy, J. D., Blocksom, K. A., Stein, R. A., & Ludsin, S. A. (2012). A comparative analysis of zooplankton field collection and sample enumeration methods. *Limnology and Oceanography: Methods*, *10*(JANUARY), 41–53. doi: 10.4319/lom.2012.10.41

MacKas, D. L., & Galbraith, M. D. (2012). Pteropod time-series from the NE Pacific. *ICES Journal of Marine Science*, *69*(3), 448–459. doi: 10.1093/icesjms/fsr163

Mackas, D. L., Tsurumi, M., Galbraith, M. D., & Yelland, D. R. (2005). Zooplankton distribution and dynamics in a North Pacific Eddy of coastal origin: II. Mechanisms of eddy colonization by and retention of offshore species. *Deep-Sea Research Part II: Topical Studies in Oceanography*, *52*(7-8), 1011–1035. doi: 10.1016/j.dsr2.2005.02.008

Manno, C., Bednaršek, N., Tarling, G. A., Peck, V. L., Comeau, S., Adhikari, D., ... Ziveri, P. (2017). Shelled pteropods in peril: Assessing vulnerability in a high CO2 ocean. *Earth-Science Reviews*, *169*(April), 132–145. doi: 10.1016/j.earscirev.2017.04.005

Manno, C., Peck, V. L., & Tarling, G. A. (2016). Pteropod eggs released at high pCO2 lack resilience to ocean acidification. *Scientific Reports*, *6*(November 2015), 1–10. doi: 10.1038/srep25752

Manno, C., Sandrini, S., Tositti, L., & Accornero, A. (2007). First stages of degradation of Limacina helicina shells observed above the aragonite chemical lysocline in Terra Nova Bay (Antarctica). *Journal of Marine Systems*, *68*(1-2), 91–102.

McGowan, J. A. (1967). Distributional atlas of pelagic molluscs in the California Current region. *CalCOFI Atlas*, *6*.

Meilland, J., Fabri-Ruiz, S., Koubbi, P., Monaco, C. L., Cotte, C., Hosie, G. W., ... Howa, H. (2016). Planktonic foraminiferal biogeography in the Indian sector of the Southern Ocean: Contribution from CPR data. *Deep-Sea Research Part I: Oceanographic Research Papers*, *110*, 75–89. Retrieved from `http://dx.doi.org/10.1016/j.dsr.2015.12.014` doi: 10.1016/j.dsr.2015.12.014

Mekkes, L., Renema, W., Bednaršek, N., Alin, S. R., Feely, R. A., Huisman, J., ... Peijnenburg, K. T. C. A. (2021). Pteropods make thinner shells in the upwelling region of the California Current Ecosystem. *Scientific Reports*, *11*(1), 1–11. Retrieved from `https://doi.org/10.1038/s41598-021-81131-9` doi: 10.1038/s41598-021-81131-9

Mekkes, L., Sepúlveda-Rodríguez, G., Bielkinaitė, G., Wall-Palmer, D., Brummer, G. J. A., Dämmer, L. K., ... Peijnenburg, K. T. (2021). Effects of Ocean Acidification on Calcification of the Sub-Antarctic Pteropod Limacina retroversa. *Frontiers in Marine Science*, *8*(March), 1–12. doi: 10.3389/fmars.2021.581432

Merow, C., Smith, M. J., Edwards, T. C., Guisan, A., Mcmahon, S. M., Normand, S., ... Elith, J. (2014). What do we gain from simplicity versus complexity in species distribution models? *Ecography*, *37*(12), 1267–1281. doi: 10.1111/ecog.00845

Michaels, A. F., Caron, D. A., Swanberg, N. R., & Howse, F. A. (1995). Primary productivity by symbiont-bearing planktonic sarcodines (Acantharia, Radiolaria, Foraminifera) in surface waters near Bermuda. *Journal of Plankton Research*, *17*(1), 103–129. doi: 10.1093/plankt/17.1.103

Miloslavić, M., Lučić, D., Gangai, B., & Onofri, I. (2014). Mesh size effects on mesozooplankton community structure in a semi-enclosed coastal area and surrounding sea (South Adriatic Sea). *Marine Ecology*, *35*(4), 445–455. doi: 10.1111/maec.12101

Morard, R., Darling, K. F., Mahé, F., Audic, S., Ujiié, Y., Weiner, A. K. M., ... Quillévéré, F. (2015). PFR2: a curated database of planktonic foraminifera 18S ribosomal DNA as a resource for studies of plankton ecology, biogeography and evolution. *Molecular Ecology Resources*, *15*(6), 1472–1485.

Moriarty, R., Buitenhuis, E. T., & Le Quéré, C. (2013). Distribution of known macrozooplankton abundance and biomass in the global ocean. *Earth System Science Data*, *5*(2), 241–257. doi: 10.5194/essd-5-241-2013

Mucci, A. (1983). The solubility of calcite and aragonite in seawater at various salinities, temperatures, and one atmosphere total pressure. *Am. J. Sci*, *283*(7), 780–799.

Myers, T. D. (1968). *Horizontal and vertical distribution of thecosomatous pteropods off Cape Hatteras*. Duke University.

Naidu, P. D., & Malmgren, B. A. (1996). A high-resolution record of late Quaternary upwelling along the Oman Margin, Arabian Sea based on planktonic foraminifera. *Paleoceanography*, *11*(1), 129–140.

NASA OB.DAAC. (2018a). *Sea-viewing Wide Field-of-view Sensor (SeaWiFS) Chlorophyll Data.* Retrieved from https://oceandata.sci.gsfc.nasa.gov/directaccess/SeaWiFS/Mapped/Monthly_Climatology/9km/chlor_a/ doi: 10.5067/ORBVIEW-2/SEAWIFS/L3M/CHL/2018

NASA OB.DAAC. (2018b). *Sea-viewing Wide Field-of-view Sensor (SeaWiFS) Downwelling Diffuse Attenuation Coefficient Data.* Retrieved from https://oceandata.sci.gsfc.nasa.gov/directaccess/SeaWiFS/Mapped/Monthly_Climatology/9km/Kd_490/ doi: 10.5067/ORBVIEW-2/SEAWIFS/L3M/KD/2018

NASA OB.DAAC. (2018c). *Sea-viewing Wide Field-of-view Sensor (SeaWiFS) Euphotic Depth Data.* Retrieved from https://oceandata.sci.gsfc.nasa.gov/directaccess/SeaWiFS/Mapped/Monthly_Climatology/9km/Zeu_lee/ doi: 10.5067/ORBVIEW-2/SEAWIFS/L3M/ZLEE/2018

NASA OB.DAAC. (2018d). *Sea-viewing Wide Field-of-view Sensor (SeaWiFS) Garver-Siegel-Maritorena (GSM) Model Data.* Retrieved from https://oceandata.sci.gsfc.nasa.gov/directaccess/SeaWiFS/Mapped/Monthly_Climatology/9km/bbp_443_gsm/ doi: 10.5067/ORBVIEW-2/SEAWIFS/L3M/GSM/2018

NASA OB.DAAC. (2018e). *Sea-viewing Wide Field-of-view Sensor (SeaWiFS) Photosynthetically Available Radiation Data.* doi: 10.5067/ORBVIEW-2/SEAWIFS/L3M/PAR/2018

Nash, J. E., & Sutcliffe, J. V. (1970). River flow forecasting through conceptual models part I - A discussion of principles. *Journal of hydrology*, *10*(3), 282–290.

Nelder, J. A., & Wedderburn, R. W. M. (1972). Generalized linear models. *Journal of the Royal Statistical Society: Series A (General)*, *135*(3), 370–384.

OB.DAAC, N. (2018). *Sea-viewing Wide Field-of-view Sensor (SeaWiFS).*

O'Brien, C. J. (2015). *Global-scale distributions of marine haptophyte phytoplankton* (Unpublished doctoral dissertation). ETH Zurich.

O'Brien, C. J., Vogt, M., & Gruber, N. (2016). Global coccolithophore diversity: Drivers and future change. *Progress in Oceanography*, *140*, 27–42. Retrieved from http://dx.doi.org/10.1016/j.pocean.2015.10.003 doi: 10.1016/j.pocean.2015.10.003

O'Brien, T. D. (2010). *COPEPOD, a global plankton database : a review of the 2010 database contents, processing methods, and access interface.* Retrieved from https://repository.library.noaa.gov/view/noaa/5040

Ohman, M. D., Lavaniegos, B. E., & Townsend, A. W. (2009). Multi-decadal variations in calcareous holozooplankton in the California Current System: thecosome pteropods, heteropods, and foraminifera. *Geophysical Research Letters*, *36*(18), 2–6. doi: 10.1029/2009GL039901

Orr, J. C., Fabry, V. J., Aumont, O., Bopp, L., Doney, S. C., Feely, R. A., ... Yool, A. (2005). Anthropogenic ocean acidification over the twenty-first century and its impact on calcifying organisms. *Nature*, *437*(7059), 681–686. doi: 10.1038/nature04095

Peijnenburg, K. T. C. A. (2021). *Personal communication.*

Peijnenburg, K. T. C. A., Janssen, A. W., Wall-Palmer, D., Goetze, E., Maas, A. E., Todd, J. A., & Marlétaz, F. (2020). The origin and diversification of pteropods precede past perturbations in the Earth's carbon cycle. *Proceedings of the National Academy of Sciences of the United States of America*, *117*(41), 25609–25617. doi: 10.1073/pnas.1920918117

Pesant, S., Not, F., Picheral, M., Kandels-Lewis, S., Le Bescot, N., Gorsky, G., ... Coordinators, T. O. C. (2015). Open science resources for the discovery and analysis of Tara Oceans data. *Scientific Data*, *2*(1), 150023. Retrieved from https://doi.org/10.1038/sdata.2015.23 doi: 10.1038/sdata.2015.23

Pinkerton, M. H., Décima, M., Kitchener, J. A., Takahashi, K. T., Robinson, K. V.,

Stewart, R., & Hosie, G. W. (2020). Zooplankton in the Southern Ocean from the continuous plankton recorder: Distributions and long-term change. *Deep-Sea Research Part I: Oceanographic Research Papers*, *162*(May 2019). doi: 10.1016/j.dsr.2020.103303

Pinkerton, M. H., Smith, A. N., Raymond, B., Hosie, G. W., Sharp, B., Leathwick, J. R., & Bradford-Grieve, J. M. (2010). Spatial and seasonal distribution of adult Oithona similis in the Southern Ocean: Predictions using boosted regression trees. *Deep-Sea Research Part I: Oceanographic Research Papers*, *57*(4), 469–485. Retrieved from `http://dx.doi.org/10.1016/j.dsr.2009.12.010` doi: 10.1016/j.dsr.2009.12.010

Qiao, H., Feng, X., Escobar, L. E., Peterson, A. T., Soberón, J., Zhu, G., & Papeş, M. (2019). An evaluation of transferability of ecological niche models. *Ecography*, *42*(3), 521–534. doi: 10.1111/ecog.03986

Rembauville, M., Meilland, J., Ziveri, P., Schiebel, R., Blain, S., & Salter, I. (2016). Planktic foraminifer and coccolith contribution to carbonate export fluxes over the central Kerguelen Plateau. *Deep-Sea Research Part I: Oceanographic Research Papers*, *111*, 91–101. Retrieved from `http://dx.doi.org/10.1016/j.dsr.2016.02.017` doi: 10.1016/j.dsr.2016.02.017

Rhumbler, L. (1911). Die Foraminiferen (Thalamophoren) der Plankton Expedition, Pt. 1, Die Allgemeinen Organizationsverhaltnisse der Foraminifera. *Lipsius & Tischer, Kiel und Leipzig*, *331*.

Richardson, A. J., Walne, A. W., John, A. W., Jonas, T. D., Lindley, J. A., Sims, D. W., ... Witt, M. (2006). Using continuous plankton recorder data. *Progress in Oceanography*, *68*(1), 27–74. doi: 10.1016/j.pocean.2005.09.011

Righetti, D., Vogt, M., Gruber, N., Psomas, A., & Zimmermann, N. E. (2019). Global pattern of phytoplankton diversity driven by temperature and environmental variability. *Science Advances*, *5*(5), 1–11. doi: 10.1126/sciadv.aau6253

Rillo, M. C., Woolley, S., & Hillebrand, H. (2022). Drivers of global pre-industrial patterns of species turnover in planktonic foraminifera. *Ecography*, *2022*(1), 1–11. doi: 10.1111/ecog.05892

Romagnan, J.-B., Legendre, L., Guidi, L., Jamet, J.-L., Jamet, D., Mousseau, L., ... Sardet, C. (2015). Comprehensive model of annual plankton succession based on the whole-plankton time series approach. *PLoS One*, *10*(3), e0119219.

Rost, B., & Riebesell, U. (2004). Coccolithophores and the biological pump: responses to environmental changes. In H. R. Thierstein & J. R. Young (Eds.), *Coccolithophores* (pp. 99–125). Springer. doi: 10.1007/978-3-662-06278-4{_}5

Rothschild, B. J., & Osborn, T. R. (1988). Small-scale turbulence and plankton contact rates. *Journal of plankton Research*, *10*(3), 465–474.

Sallée, J. B., Pellichero, V., Akhoudas, C., Pauthenet, E., Vignes, L., Schmidtko, S., ... Kuusela, M. (2021). Summertime increases in upper-ocean stratification and mixed-layer depth. *Nature*, *591*(7851), 592–598. doi: 10.1038/s41586-021-03303-x

Sarmiento, J., & Gruber, N. (2006). Calcium Carbonate Cycle. In *Ocean biogeochemical dynamics* (p. 359 - 391). Princeton University Press.

Sarmiento, J. L., & Gruber, N. (2006). Carbon Cycle. In *Ocean biogeochemical dynamics* (pp. 318–358). Princeton University Press.

Schiebel, R. (2002). Planktic foraminiferal sedimentation and the marine calcite budget. *Global Biogeochemical Cycles*, *16*(4), 3–1. doi: 10.1029/2001gb001459

Schiebel, R. (2021). *Personal Communication.*

Schiebel, R., Barker, S., Lendt, R., Thomas, H., & Bollmann, J. (2007). Planktic foraminiferal dissolution in the twilight zone. *Deep Sea Research Part II: Topical Studies in Oceanography*, *54*(5-7), 676–686.

Schiebel, R., & Hemleben, C. (2000). Interannual variability of planktic foraminiferal populations and test flux in the eastern North Atlantic Ocean (JGOFS). *Deep-Sea Research Part II: Topical Studies in Oceanography*, *47*(9-11), 1809–1852.

doi: 10.1016/S0967-0645(00)00008-4

Schiebel, R., & Hemleben, C. (2005). Modern planktic foraminifera. *Paläontologische Zeitschrift*, *79*(1), 135–148. doi: 10.1007/bf03021758

Schiebel, R., & Hemleben, C. (2017). *Planktic foraminifers in the modern ocean* (2nd ed.). Berlin, Heidelberg: Springer. doi: 10.1007/978-3-662-50297-6

Schiebel, R., Hiller, B., & Hemleben, C. (1995). Impacts of storms on Recent planktic foraminiferal test production and CaCO3 flux in the North Atlantic at 47 °N, 20 °W (JGOFS). *Marine Micropaleontology*, *26*(1-4), 115–129. doi: 10.1016/0377-8398(95)00035-6

Schiebel, R., & Movellan, A. (2012). First-order estimate of the planktic foraminifer biomass in the modern ocean. *Earth System Science Data*, *4*(1), 75–89. doi: 10.5194/essd-4-75-2012

Schiebel, R., Waniek, J., Bork, M., & Hemleben, C. (2001). Planktic foraminiferal production stimulated by chlorophyll redistribution and entrainment of nutrients. *Deep-Sea Research Part I: Oceanographic Research Papers*, *48*(3), 721–740. doi: 10.1016/S0967-0637(00)00065-0

Schiebel, R., Waniek, J., Zeltner, A., & Alves, M. (2002). Impact of the Azores Front on the distribution of planktic foraminifers, shelled gastropods, and coccolithophorids. *Deep-Sea Research Part II: Topical Studies in Oceanography*, *49*(19), 4035–4050. doi: 10.1016/S0967-0645(02)00141-8

Schiebel, R., Zeltner, A., Treppke, U. F., Waniek, J. J., Bollmann, J., Rixen, T., & Hemleben, C. (2004). Distribution of diatoms, coccolithophores and planktic foraminifers along a trophic gradient during SW monsoon in the Arabian Sea. *Marine Micropaleontology*, *51*(3-4), 345–371. doi: 10.1016/j.marmicro.2004.02.001

Schmidt, D. N., Renaud, S., Bollmann, J., Schiebel, R., & Thierstein, H. R. (2004). Size distribution of Holocene planktic foraminifer assemblages: Biogeography, ecology and adaptation. *Marine Micropaleontology*, *50*(3-4), 319–338. doi: 10.1016/S0377-8398(03)00098-7

Schmidt, G. A., & Mulitza, S. (2002). Global calibration of ecological models for planktic foraminifera from coretop carbonate oxygen-18. *Marine Micropaleontology*, *44*(3-4), 125–140. doi: 10.1016/S0377-8398(01)00041-X

Schmidt-Nielsen, K. (1997). *Animal physiology: adaptation and environment*. Cambridge university press.

Seuront, L., Schmitt, F., & Lagadeuc, Y. (2001). Turbulence intermittency, small-scale phytoplankton patchiness and encounter rates in plankton: Where do we go from here? *Deep-Sea Research Part I: Oceanographic Research Papers*, *48*(5), 1199–1215. doi: 10.1016/S0967-0637(00)00089-3

Shapiro, S. S., & Wilk, M. B. (1965, 12). An analysis of variance test for normality (complete samples). *Biometrika*, *52*(3-4), 591–611. Retrieved from `https://doi.org/10.1093/biomet/52.3-4.591` doi: 10.1093/biomet/52.3-4.591

Siccha, M., Schiebel, R., Schmidt, S., & Howa, H. (2012). Short-term and small-scale variability in planktic foraminifera test flux in the Bay of Biscay. *Deep Sea Research Part I: Oceanographic Research Papers*, *64*, 146–156.

Skjoldal, H. R., Wiebe, P. H., Postel, L., Knutsen, T., Kaartvedt, S., & Sameoto, D. D. (2013). Intercomparison of zooplankton (net) sampling systems: Results from the ICES/GLOBEC sea-going workshop. *Progress in Oceanography*, *108*, 1–42. Retrieved from `http://dx.doi.org/10.1016/j.pocean.2012.10.006` doi: 10.1016/j.pocean.2012.10.006

Soviadan, Y. D., Benedetti, F., Brandão, M. C., Ayata, S. D., Irisson, J. O., Jamet, J. L., ... Stemmann, L. (2022). Patterns of mesozooplankton community composition and vertical fluxes in the global ocean. *Progress in Oceanography*, *200*(September 2021). doi: 10.1016/j.pocean.2021.102717

Spiess, A.-N., & Neumeyer, N. (2010, 6). An evaluation of R2 as an inadequate measure for nonlinear models in pharmacological and biochemical research: a

Monte Carlo approach. *BMC pharmacology*, *10*, 6. Retrieved from https://pubmed.ncbi.nlm.nih.gov/20529254https://www.ncbi.nlm.nih.gov/pmc/articles/PMC2892436/ doi: 10.1186/1471-2210-10-6

Spindler, M., Hemleben, C., Salomons, J. B., & Smit, L. P. (1984). Feeding behavior of some planktonic foraminifers in laboratory cultures. *The Journal of Foraminiferal Research*, *14*(4), 237–249.

Steinhardt, J., Cléroux, C., Ullgren, J., de Nooijer, L., Durgadoo, J. V., Brummer, G.-J., & Reichart, G.-J. (2014). Anti-cyclonic eddy imprint on calcite geochemistry of several planktonic foraminiferal species in the Mozambique Channel. *Marine Micropaleontology*, *113*, 20–33.

Stepien, J. C. (1980). The occurrence of chaetognaths, pteropods and euphausiids in relation to deep flow reversals in the Straits of Florida. *Deep Sea Research Part A. Oceanographic Research Papers*, *27*(12), 987–1011.

Strömberg, K. H., Smyth, T. J., Allen, J. I., Pitois, S., & O'Brien, T. D. (2009). Estimation of global zooplankton biomass from satellite ocean colour. *Journal of Marine Systems*, *78*(1), 18–27. Retrieved from http://dx.doi.org/10.1016/j.jmarsys.2009.02.004 doi: 10.1016/j.jmarsys.2009.02.004

Student. (1908). The Probable Error of A Mean. *Biometrika*, *6*(1), 1–25.

Takahashi, K., & Bé, A. W. (1984). Planktonic foraminifera: factors controlling sinking speeds. *Deep Sea Research Part A, Oceanographic Research Papers*, *31*(12), 1477–1500. doi: 10.1016/0198-0149(84)90083-9

Thibodeau, P. S., Steinberg, D. K., Stammerjohn, S. E., & Hauri, C. (2019). Environmental controls on pteropod biogeography along the Western Antarctic Peninsula. *Limnology and Oceanography*, *64*, S240-S256. doi: 10.1002/lno.11041

Thuiller, W., Guéguen, M., Renaud, J., Karger, D. N., & Zimmermann, N. E. (2019). Uncertainty in ensembles of global biodiversity scenarios. *Nature Communications*, *10*(1), 1–9. Retrieved from http://dx.doi.org/10.1038/s41467-019-09519-w doi: 10.1038/s41467-019-09519-w

Tittensor, D. P., Novaglio, C., Harrison, C. S., Heneghan, R. F., Barrier, N., Bianchi, D., ... Blanchard, J. L. (2021). Next-generation ensemble projections reveal higher climate risks for marine ecosystems. *Nature Climate Change*, *11*(11), 973–981. doi: 10.1038/s41558-021-01173-9

Tseng, L. C., Dahms, H. U., Hung, J. J., Chen, Q. C., & Hwang, J. S. (2011). Can different mesh sizes affect the results of copepod community studies? *Journal of Experimental Marine Biology and Ecology*, *398*(1-2), 47–55. Retrieved from http://dx.doi.org/10.1016/j.jembe.2010.12.007 doi: 10.1016/j.jembe.2010.12.007

Tsurumi, M., Mackas, D. L., Whitney, F. A., DiBacco, C., Galbraith, M. D., & Wong, C. S. (2005). Pteropods, eddies, carbon flux, and climate variability in the Alaska Gyre. *Deep Sea Research Part II: Topical Studies in Oceanography*, *52*(7-8), 1037–1053.

Turner, J. T. (2015). Zooplankton fecal pellets, marine snow, phytodetritus and the ocean's biological pump. *Progress in Oceanography*, *130*, 205–248. Retrieved from http://dx.doi.org/10.1016/j.pocean.2014.08.005 doi: 10.1016/j.pocean.2014.08.005

Vereshchaka, A. L., Lunina, A. A., & Mikaelyan, A. S. (2022). Surface chlorophyll concentration as a mesoplankton biomass assessment tool in the Southern Ocean region. *Global Ecology and Biogeography*, *31*(3), 405–424. doi: 10.1111/geb.13435

Waldock, C., Stuart-Smith, R. D., Albouy, C., Cheung, W. W. L., Edgar, G. J., Mouillot, D., ... Pellissier, L. (2022, 1). A quantitative review of abundance-based species distribution models. *Ecography*, *2022*(1). Retrieved from https://doi.org/10.1111/ecog.05694 doi: https://doi.org/10.1111/ecog.05694

Wall-Palmer, D., Smart, C. W., Kirby, R., Hart, M. B., Peijnenburg, K. T., & Janssen, A. W. (2016). A review of the ecology, palaeontology and distribution of atlantid heteropods (Caenogastropoda: Pterotracheoidea: Atlantidae). *Journal of Molluscan Studies*, *82*(2), 221–234. doi: 10.1093/mollus/eyv063

Wang, K., Hunt, B. P., Liang, C., Pauly, D., & Pakhomov, E. A. (2017). Reassessment of the life cycle of the pteropod Limacina helicina from a high resolution interannual time series in the temperate North Pacific. *ICES Journal of Marine Science*, *74*(7), 1906–1920. doi: 10.1093/icesjms/fsx014

Weinfurt, K. P. (1995). Multivariate analysis of variance. In G. L. Grimm & P. R. Yarnold (Eds.), *Reading and understanding multivariate statistics* (p. 245 - 276). American Psychological Association.

Weinkauf, M. F., Kunze, J. G., Waniek, J. J., & Kučera, M. (2016). Seasonal variation in shell calcification of planktonic foraminifera in the ne atlantic reveals species-specific response to temperature, productivity, and optimum growth conditions. *PLoS ONE*, *11*(2), 1–33. doi: 10.1371/journal.pone.0148363

Wells, F. E. (1973). Effects of mesh size on estimation of population densities of tropical euthecosomatous pteropods. *Marine Biology*, *20*(4), 347–350. doi: 10.1007/BF00354276

Wilson, R. W., Millero, F. J., Taylor, J. R., Walsh, P. J., Christensen, V., Jennings, S., & Grosell, M. (2009). Contribution of fish to the marine inorganic carbon cycle. *Science*, *323*(5912), 359–362.

Wormuth, J. H. (1981). Vertical distributions and diel migrations of Euthecosomata in the northwest Sargasso Sea. *Deep Sea Research Part A. Oceanographic Research Papers*, *28*(12), 1493–1515.

Zamelczyk, K., Fransson, A., Chierici, M., Jones, E., Meilland, J., Anglada-Ortiz, G., & Lødemel, H. H. (2021). Distribution and Abundances of Planktic Foraminifera and Shelled Pteropods During the Polar Night in the Sea-Ice Covered Northern Barents Sea. *Frontiers in Marine Science*, *8*(October), 1–19. doi: 10.3389/fmars.2021.644094

Zurell, D., Franklin, J., König, C., Bouchet, P. J., Dormann, C. F., Elith, J., ... Merow, C. (2020). A standard protocol for reporting species distribution models. *Ecography*, *43*(9), 1261–1277. doi: 10.1111/ecog.04960

Zweng, M. M., Seidov, D., Boyer, T., Locarnini, M., Garcia, H., Mishonov, A., ... Smolyar, I. (2019). *World ocean atlas 2018, Vol. 2: Salinity* (Tech. Rep.). NOAA. Retrieved from `https://www.ncei.noaa.gov/access/world-ocean-atlas-2018/bin/woa18.pl?parameter=s`

Figure 1.

Plankton observation data – *2.1*

Abundance counts
- COPEPOD, MAREDAT, NA-NP CPR, SO-CPR, AUS-CPR, AMT, unpublished datasets

Preprocessing and biomass calculation – *2.1.1 – 2.1.3*

- Taxonomic harmonization
- Remove incomplete data
- Biomass calculation
- Exclude coastal data, NA-NP CPR and gymnosomata
- Surface data aggregation
- Outlier removal
- Match to environmental conditions

Environmental predictor data – *2.2.1*

Monthly gridded products
- World Ocean Atlas 2018
- SeaWiFs

Environmental predictor choice – *2.2.1*

- Exclude highly correlated predictors
- Choose predictors that explain the highest fraction of TC biomass variance

SDMs – *2.2.2*

- Generalized Linear Model (GLM)
- Generalized Additive Model (GAM)
- Random Forest (RF)
- Boosted Regression Tree (GBM)
- Neural Network (DL)

Growth rate parametrization – *2.3.2*

- Pteropoda: average overturn periods (Bednaršek, Mozina, et al., 2012)
- Foraminifera: temperature-dependent growth rates (Lombard et al., 2009)

TC biomass distribution predictions – *2.3.1*

- Monthly gridded global predictions

TIC surface flux estimates – *2.3.2*

- Global annual TIC flux magnitude

Assessment & uncertainty analysis – *2.3.3 – 2.3.4*

- Environmental driver analysis
  - Permuation analysis
  - Partial dependence plots
- Model performance
  - RMSE, r2, residual patterns
- Uncertainty
  - Spatial inter-model uncertainty
  - Effect of model parameter choice on predictions

Figure 2.

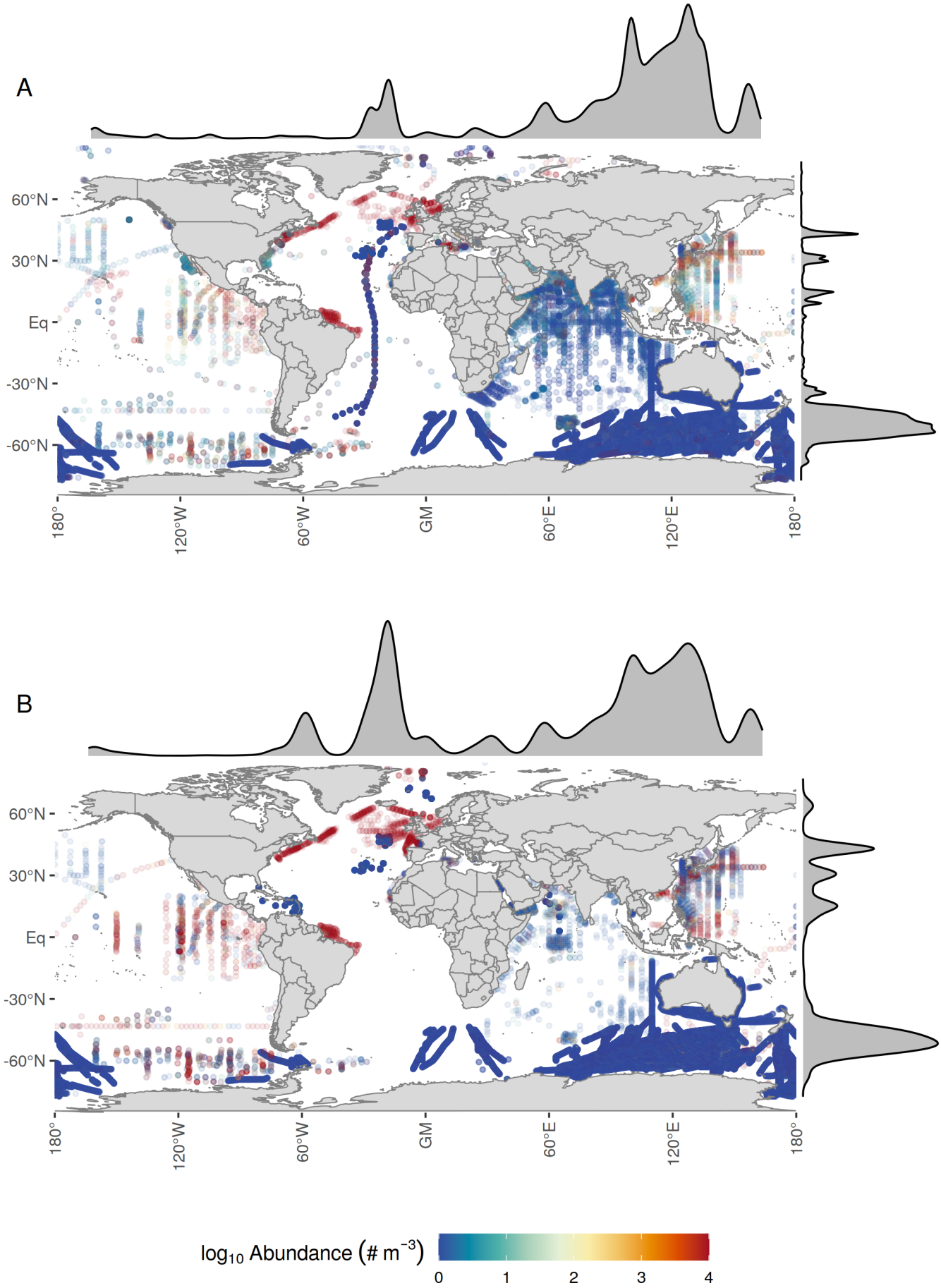
A
B
60°N
30°N
Eq
-30°N
-60°N
180°
120°W
60°W
GM
60°E
120°E
180°
log10 Abundance (# m-3)
0
1
2
3
4

Figure 3.

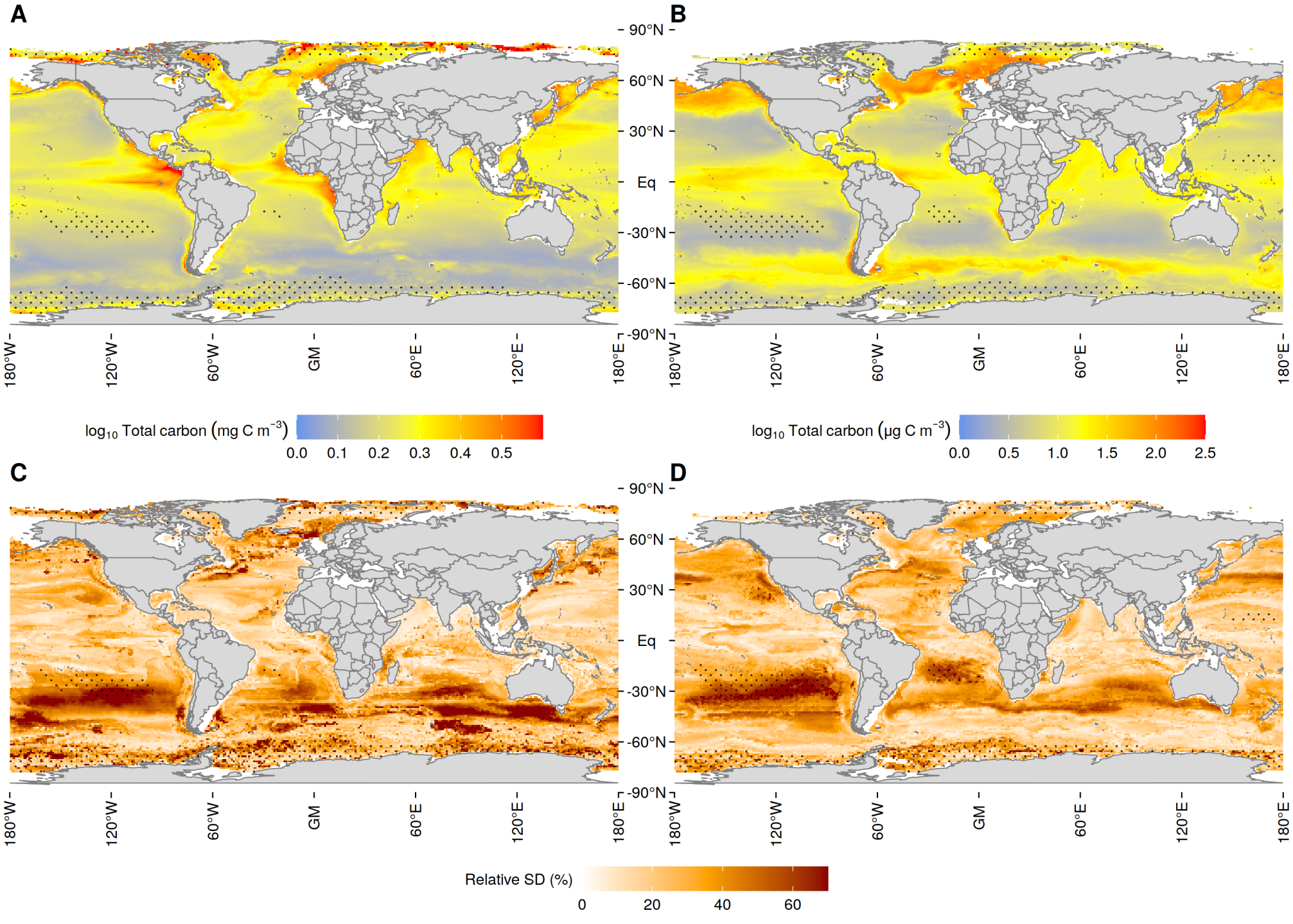
A
B
C
D
90°N
60°N
30°N
Eq
-30°N
-60°N
-90°N
180°W
120°W
60°W
GM
60°E
120°E
180°E
log10 Total carbon (mg C m-3)
0.0 0.1 0.2 0.3 0.4 0.5
log10 Total carbon (µg C m-3)
0.0 0.5 1.0 1.5 2.0 2.5
Relative SD (%)
0 20 40 60

Figure 4.

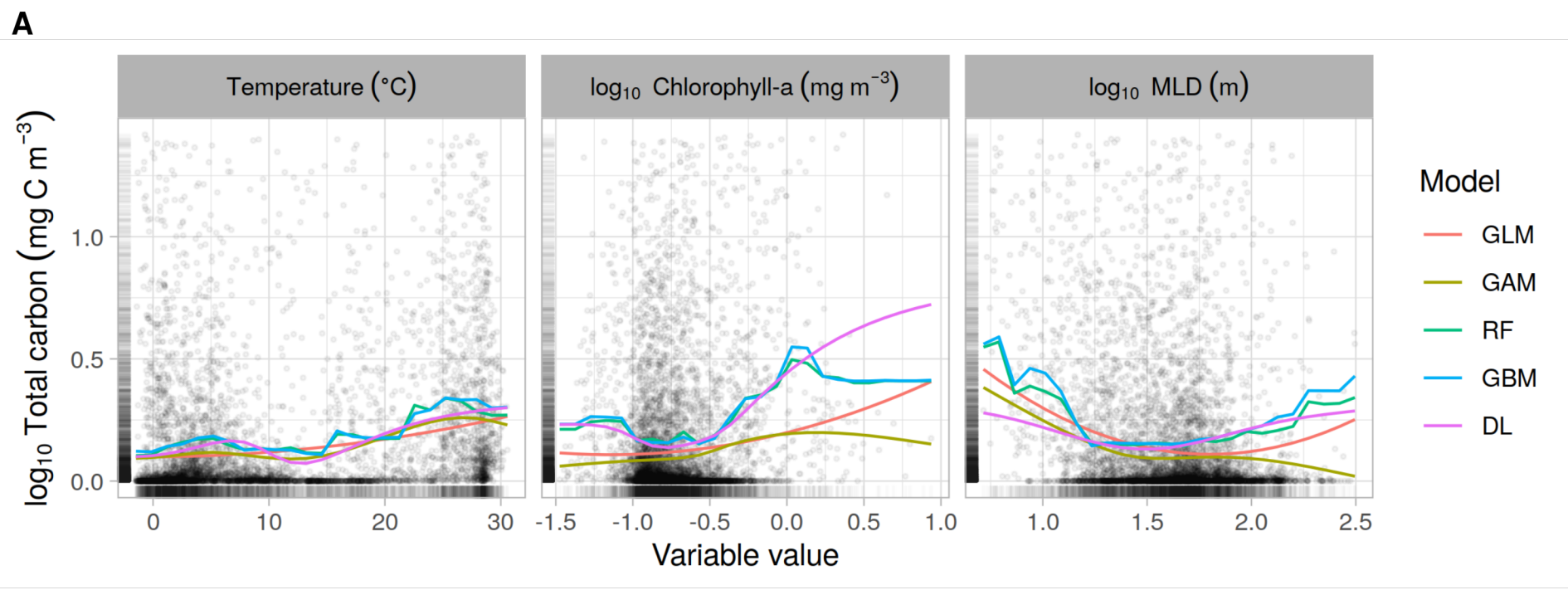
A
Temperature (°C)
log10 Chlorophyll-a (mg m-3)
log10 MLD (m)
log10 Total carbon (mg C m-3)
Variable value
Model
GLM
GAM
RF
GBM
DL

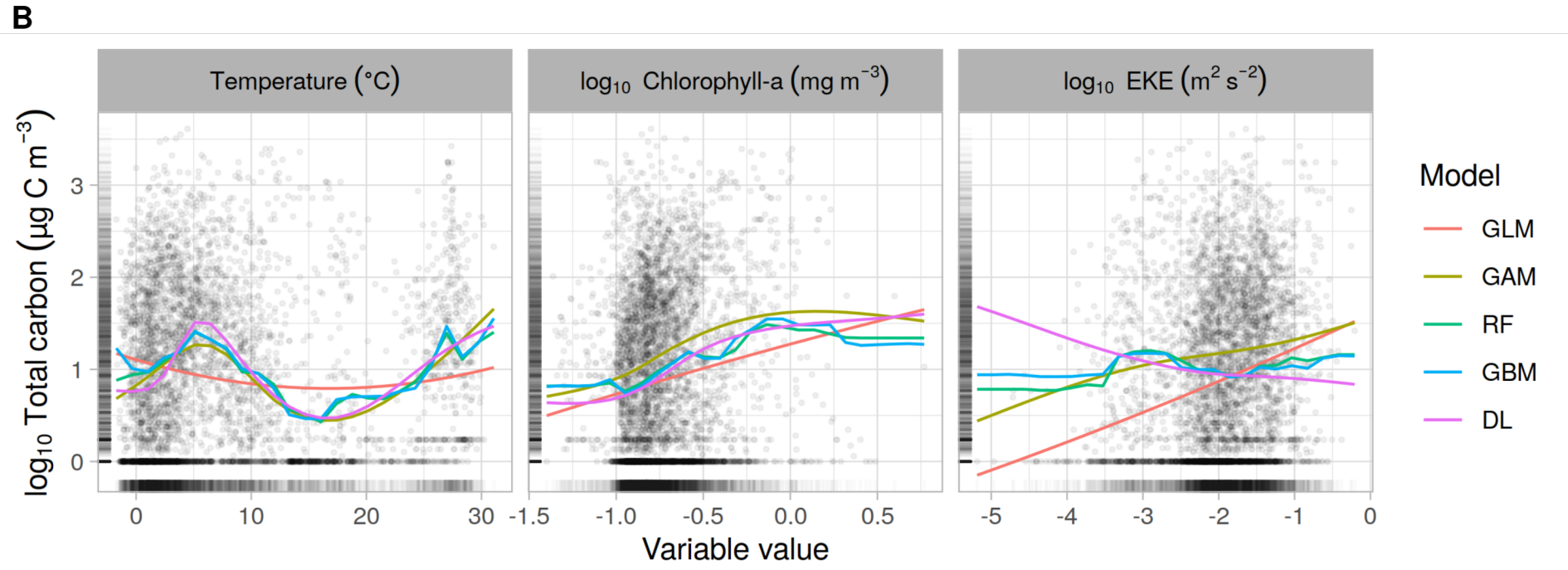
B
Temperature (°C)
log10 Chlorophyll-a (mg m-3)
log10 EKE (m2 s-2)
log10 Total carbon (µg C m-3)
Variable value
Model
GLM
GAM
RF
GBM
DL

Figure 5.

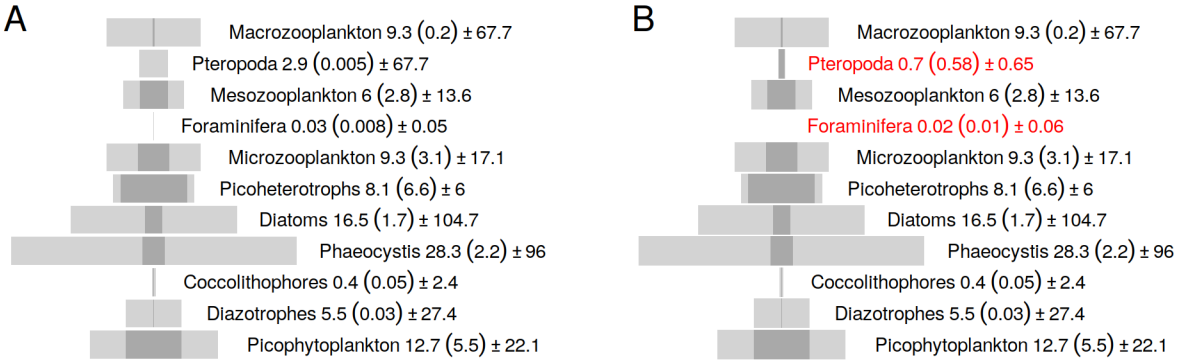
A
Macrozooplankton 9.3 (0.2) ± 67.7
Pteropoda 2.9 (0.005) ± 67.7
Mesozooplankton 6 (2.8) ± 13.6
Foraminifera 0.03 (0.008) ± 0.05
Microzooplankton 9.3 (3.1) ± 17.1
Picoheterotrophs 8.1 (6.6) ± 6
Diatoms 16.5 (1.7) ± 104.7
Phaeocystis 28.3 (2.2) ± 96
Coccolithophores 0.4 (0.05) ± 2.4
Diazotrophes 5.5 (0.03) ± 27.4
Picophytoplankton 12.7 (5.5) ± 22.1
B
Macrozooplankton 9.3 (0.2) ± 67.7
Pteropoda 0.7 (0.58) ± 0.65
Mesozooplankton 6 (2.8) ± 13.6
Foraminifera 0.02 (0.01) ± 0.06
Microzooplankton 9.3 (3.1) ± 17.1
Picoheterotrophs 8.1 (6.6) ± 6
Diatoms 16.5 (1.7) ± 104.7
Phaeocystis 28.3 (2.2) ± 96
Coccolithophores 0.4 (0.05) ± 2.4
Diazotrophes 5.5 (0.03) ± 27.4
Picophytoplankton 12.7 (5.5) ± 22.1

Supporting Information for "The impact of zooplankton calcifiers on the marine carbon cycle"

[1]Nielja S. Knecht, [1]Fabio Benedetti, [1]Urs Hofmann Elizondo, [2,3]Nina Bednaršek, [4,5,6]Sonia Chaabane, [7]Catharina de Weerd, [7,8]Katja T. C. A. Peijnenburg, [6]Ralf Schiebel, [1]Meike Vogt

[1]Environmental Physics, Institute of Biogeochemistry and Pollutant Dynamics, ETH Zurich, Zurich, Switzerland

[2]National Institute of Biology, Marine Biological Station, Piran, Slovenia

[3]Cooperative Institute for Marine Resources Studies, Oregon State University, Oregon, USA

[4]Aix-Marseille Université, CNRS, IRD, INRAE, CEREGE, Aix-en-Provence, France

[5]French Foundation for Research on Biodiversity (FRB-CESAB), Paris, France

[6]Department of Climate Geochemistry, Max-Planck-Institute for Chemistry, Mainz, Germany

[7]Plankton Diversity and Evolution, Naturalis Biodiversity Center, Leiden, The Netherlands

[8]Institute for Biodiversity and Ecosystem Dynamics, University of Amsterdam, Amsterdam, The Netherlands

Contents of this file

Corresponding author: N. S. Knecht, Environmental Physics, Institute of Biogeochemistry and Pollutant Dynamics, ETH Zurich, Zurich, Switzerland (nknecht@ethz.ch)

Introduction

The supporting information includes additional figures and tables relating to the original observation data, the abundance-to-biomass conversions and the modelling process. The outputs of various sensitivity analyses are also shown as described and referenced in the main text.

Figures

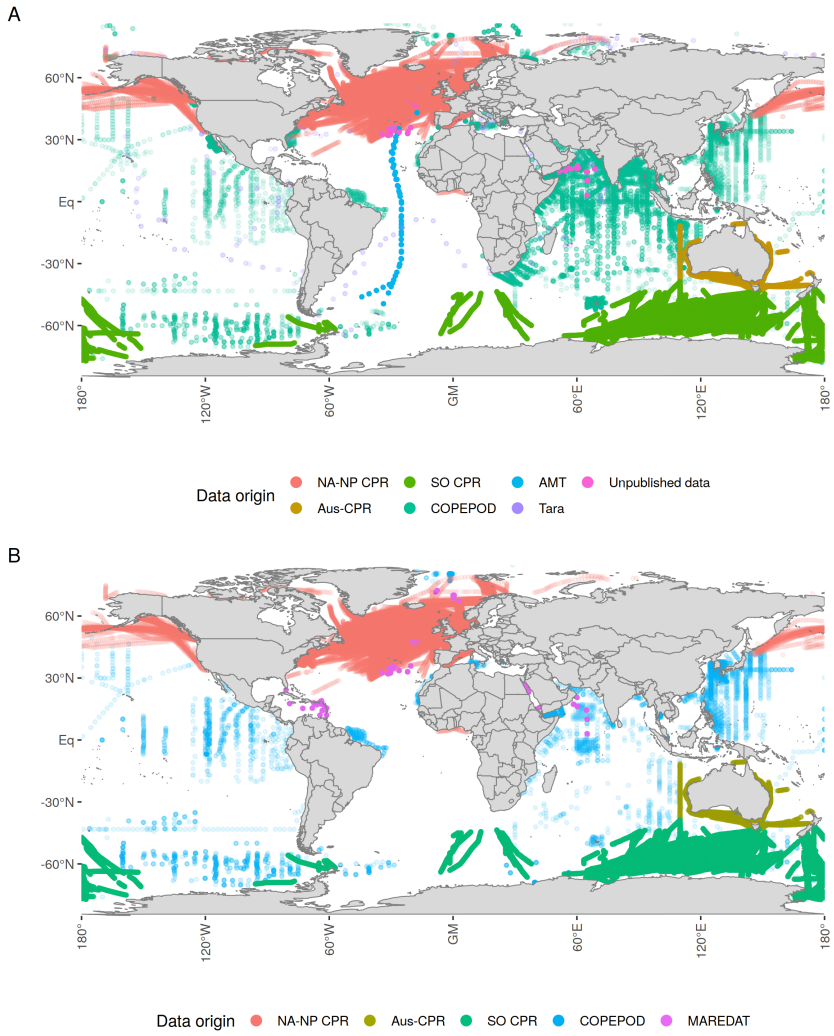

Figure S1. Pteropoda (**A**) and planktic foraminifers (**B**) data sources. CPR refers to the Continuous Plankton Recorder (NA-NP: North Atlantic and North Pacific, Aus: Australia, SO: Southern Ocean), COPEPOD to the Coastal and Oceanic Plankton Ecology, Production and Observation Database, AMT to the Atlantic Meridional Transect and MAREDAT to the MARine Ecosystem DATabase. See section 2.1.1 for more details.

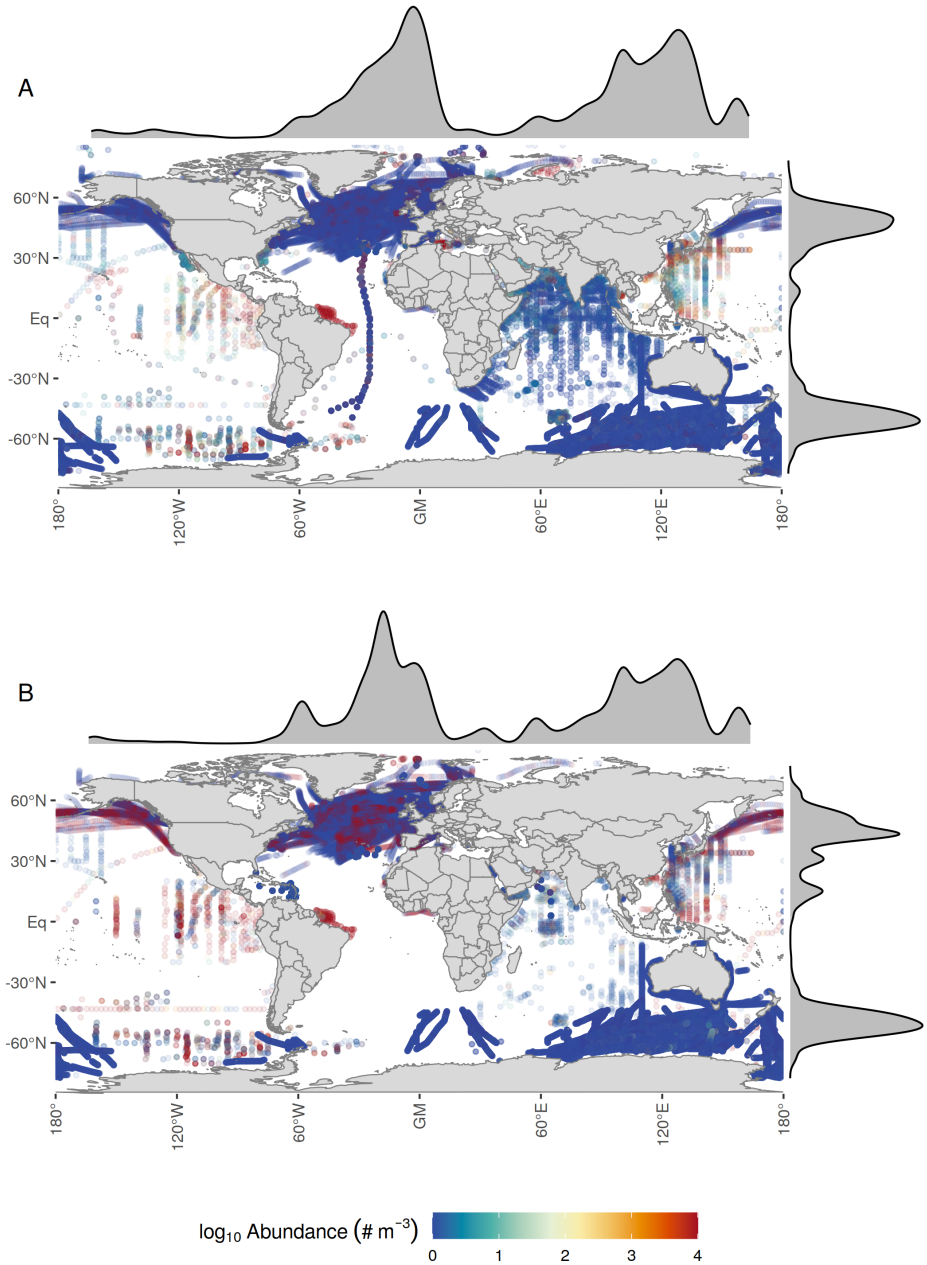

Figure S2. Pteropoda (**A**) and planktic foraminifers (**B**) abundance observation data from the full quality controlled AtlantECO dataset. The marginal plots show the density of observations and highlight the dominant role of the North Atlantic and North Pacific Continuous Plankton Recorder (NA-NP CPR) survey, the Southern Ocean CPR (SO-CPR) survey as well as a spatially confined, highly resolved dataset in the North Atlantic.

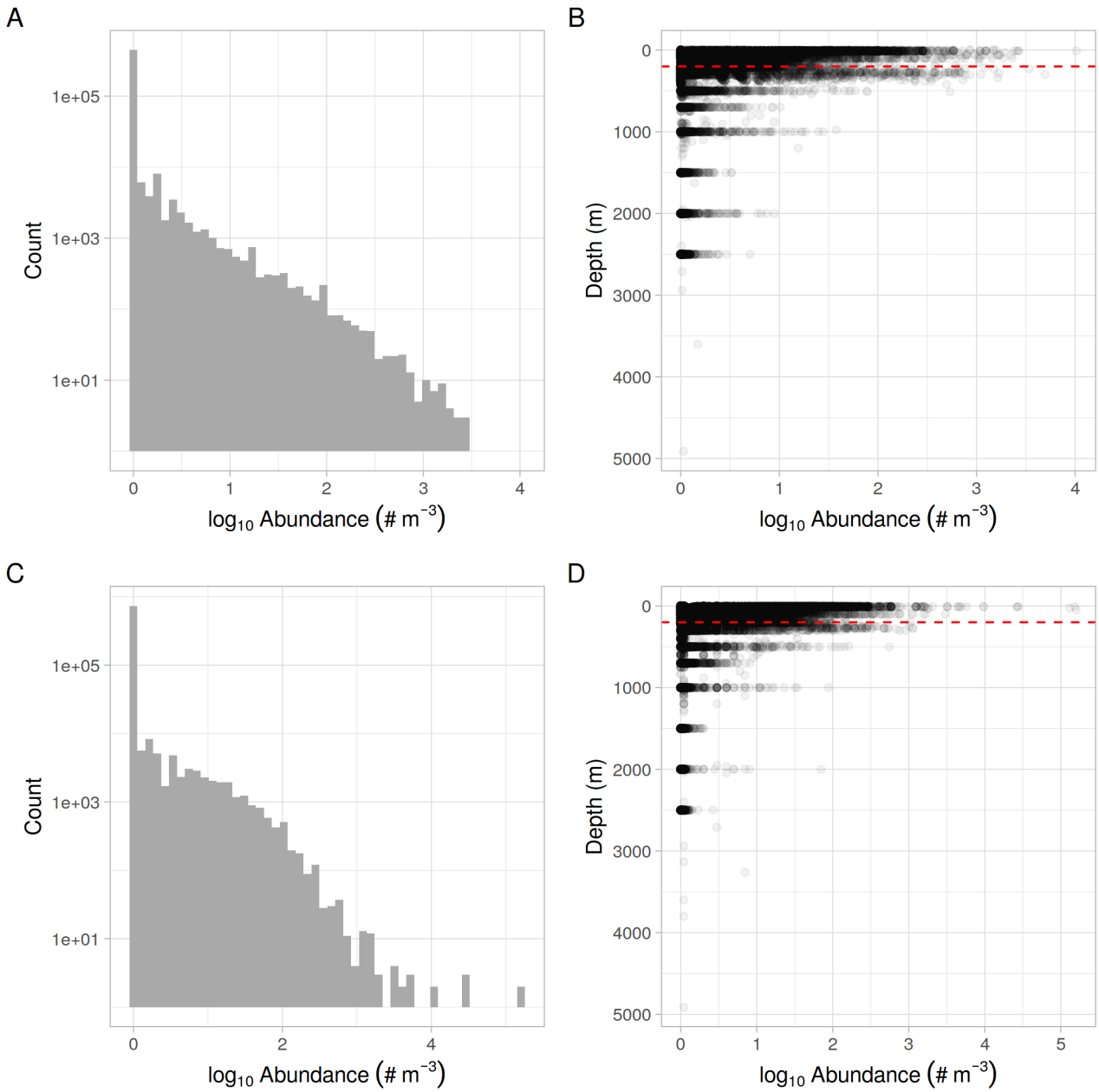

Figure S3. **A, C**: histogram of abundance observations for pteropods (**A**) and planktic foraminifers (**C**). The prevalence of zero abundances is evident. **B, D**: depth distribution of the sampling data for pteropods (**B**) and foraminifers (**D**). The dashed red line indicates the cut-off of 200 m. All data above this depth were used for the modelling.

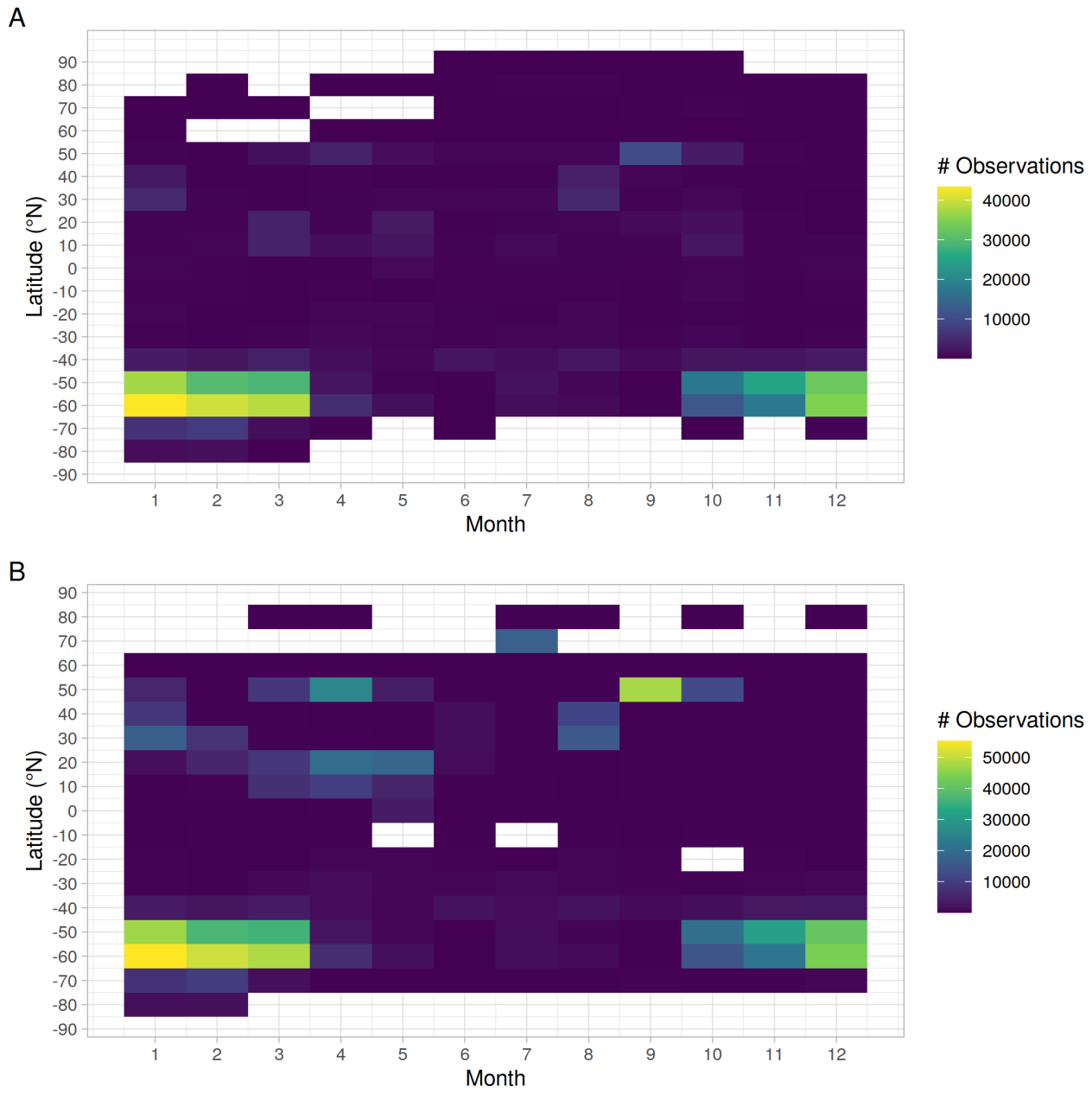

Figure S4. Hovmoeller diagrams showing the density of pteropod (**A**) and planktic foraminifer (**B**) sampling points as a function of month and latitude. The dominance of the Southern Ocean Continuous Plankton Recorder (SO-CPR) during the summer of the Southern Hemisphere as well as increased sampling effort in the Northern Hemispheric summer can be seen for both groups.

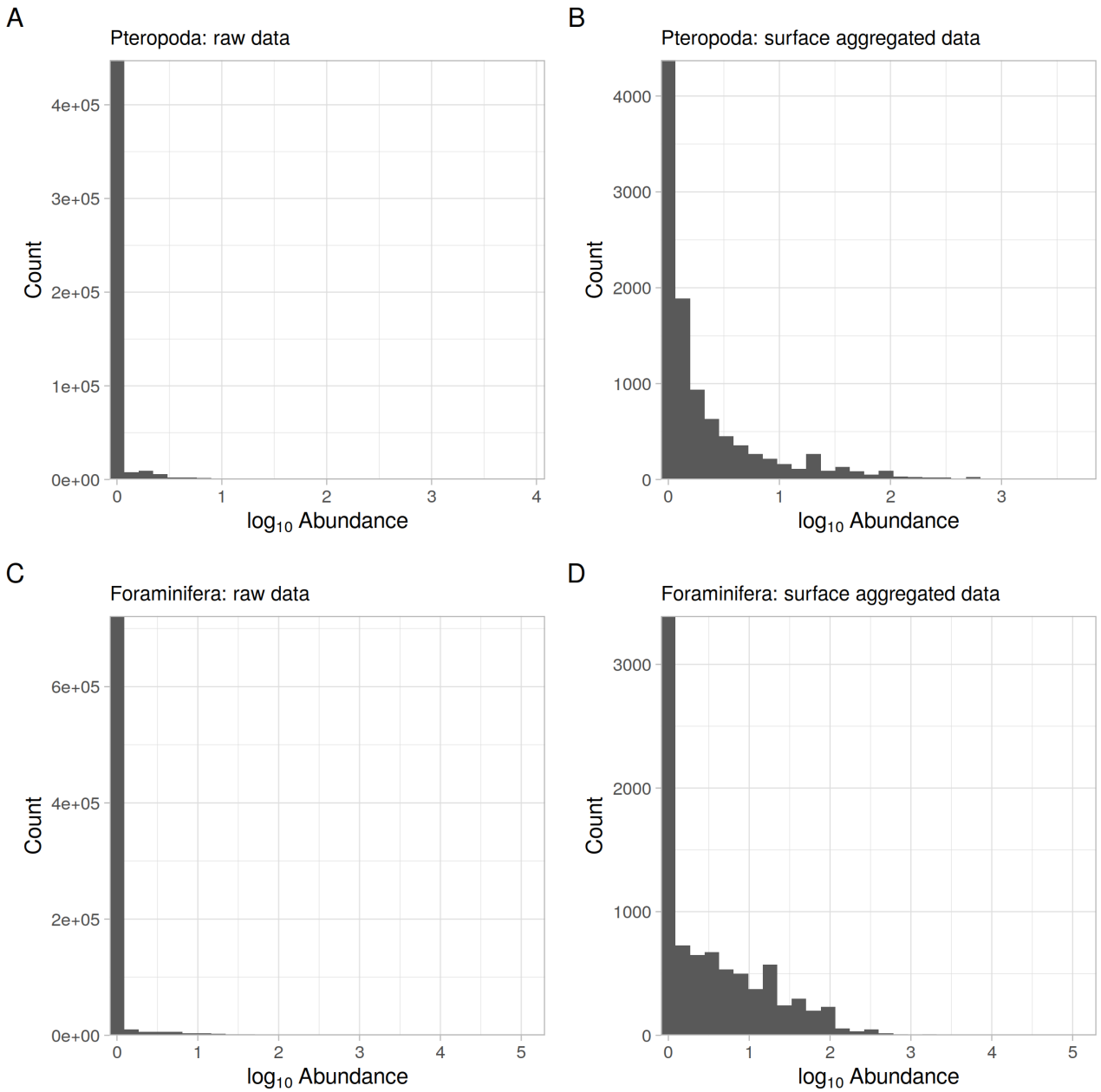

Figure S5. Effect of surface data aggregation on abundance data distribution, note the different axes limits. **A** and **C** show the distribution of raw observation data for pteropods and planktic foraminifers, respectively. Plots **B** and **D** show the histograms after the surface ocean aggregation. There is a notable reduction in points with zero abundance and the histograms are less skewed.

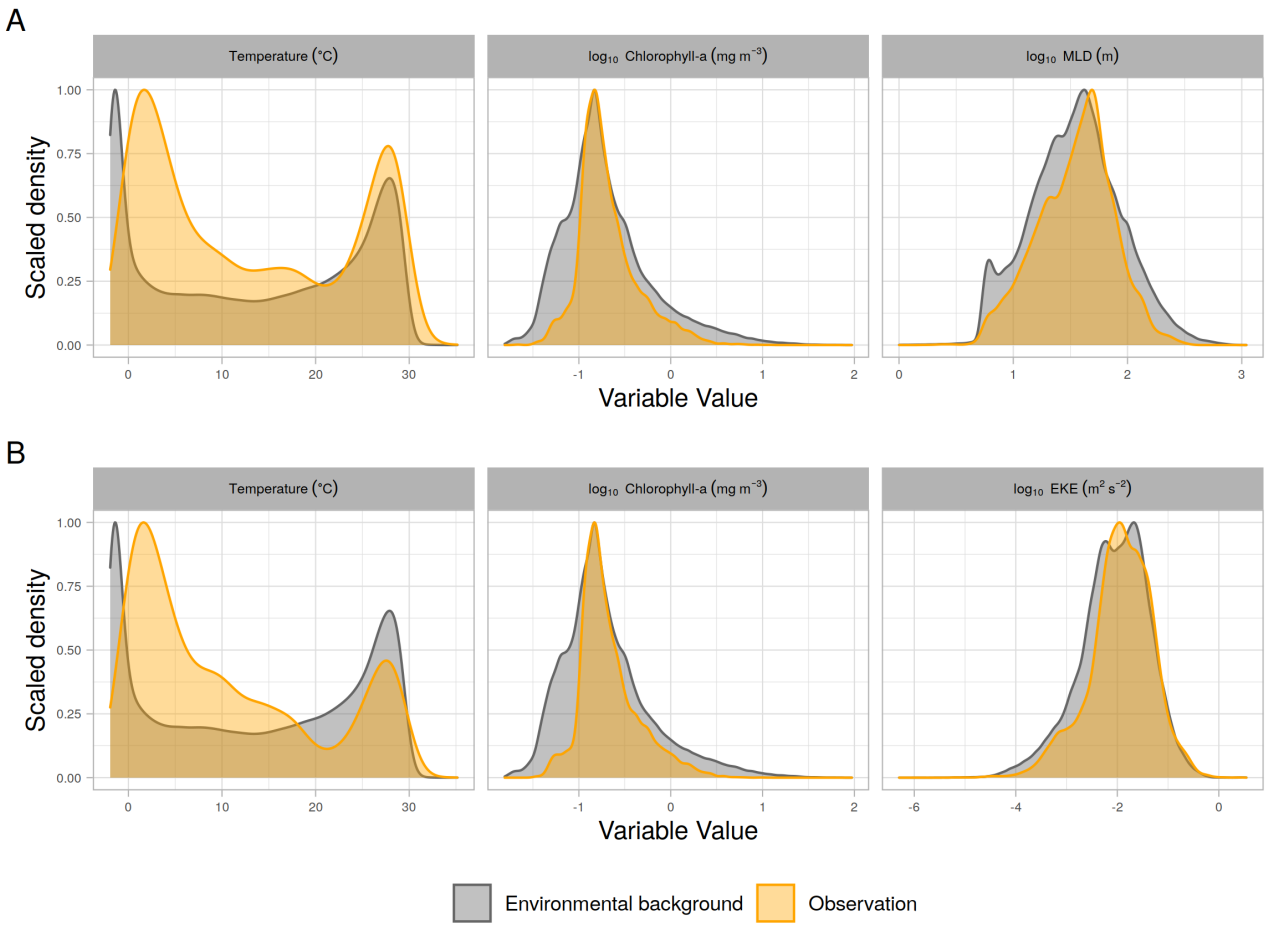

Figure S6. Coverage of the total global environmental background space by the observation data for **A** pteropods and **B** planktic foraminifers. Grey shading indicates the environmental background data and orange shading the environmental conditions at the spatio-temporal location of the sampling points after the surface ocean aggregation. The density curves are scaled to reach a maximum value of 1.

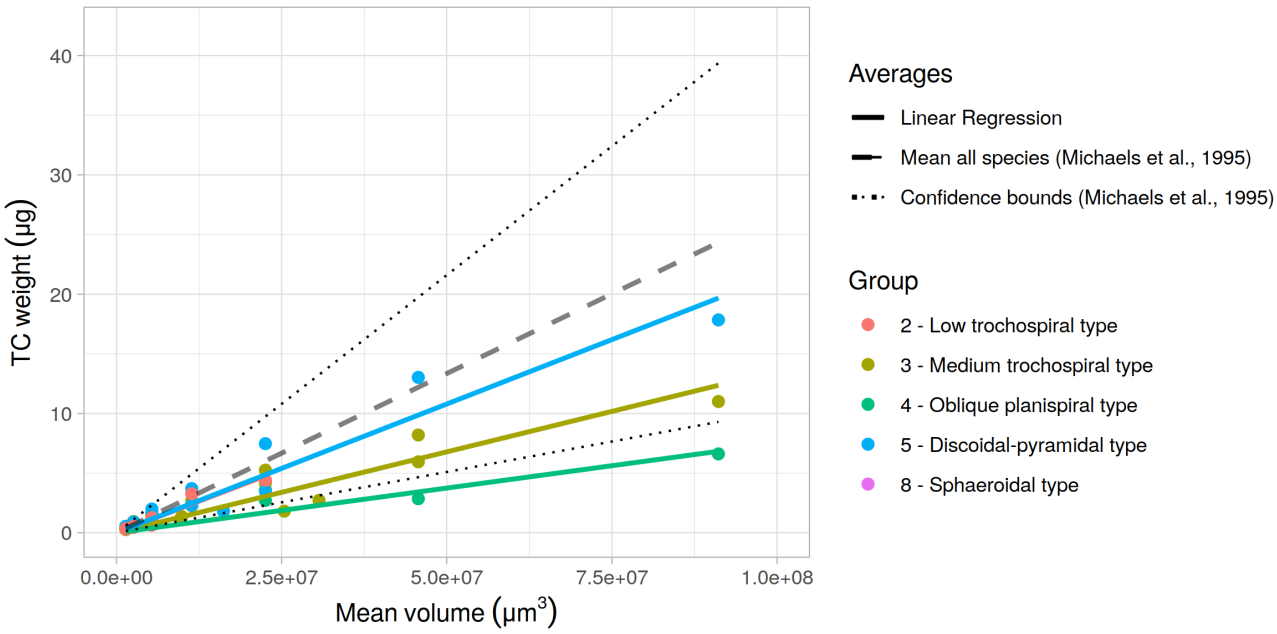

Figure S7. Linear fits of foraminifer total carbon (TC) weight as a function of mean volume based on sampling data from Schiebel and Hemleben (2000) and Takahashi and Bé (1984). The colors indicate the different shape groups. The dashed line denotes the mean value as calculated per Michaels et al. (1995) and the dotted lines the corresponding confidence interval.

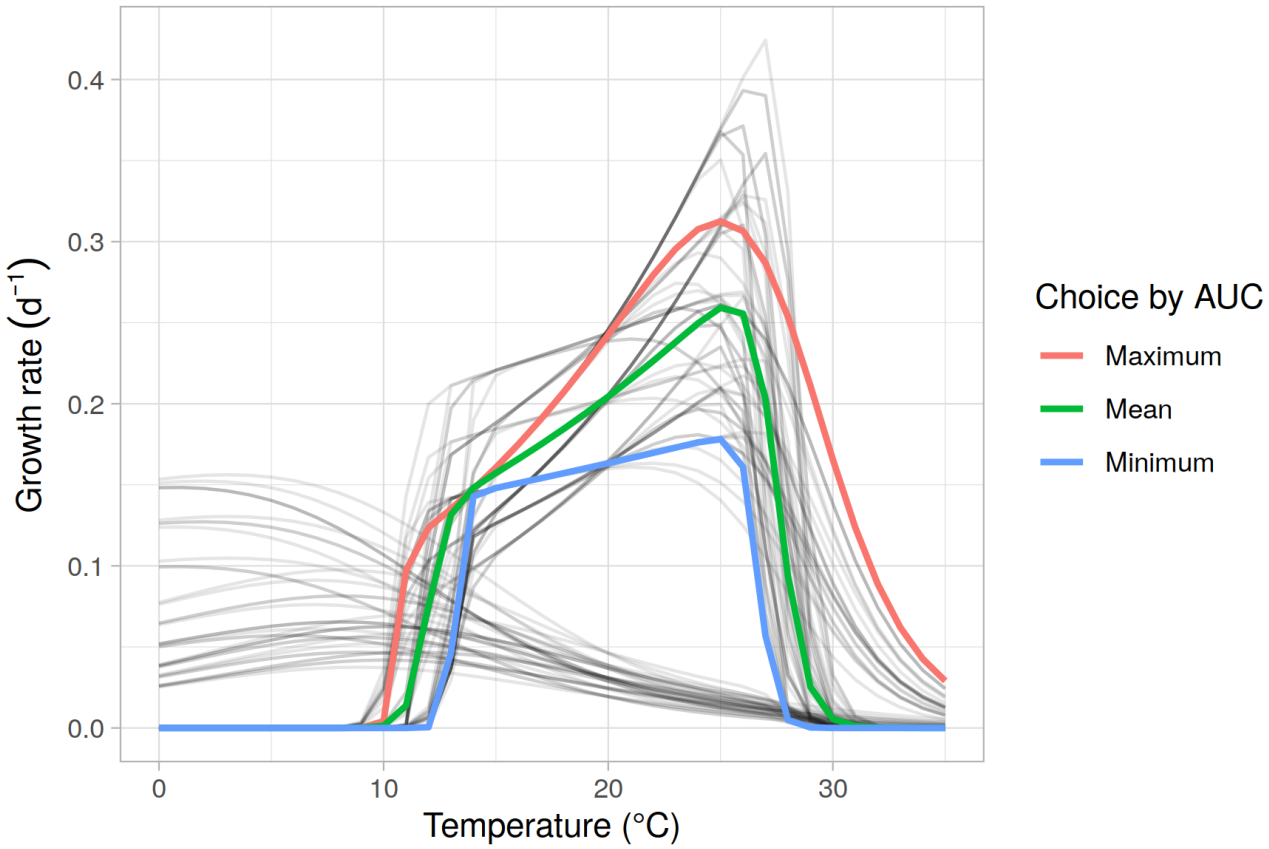

Figure S8. Foraminifer daily growth rates as derived from Lombard et al. (2009). Black lines indicate all possible curves from the range of parameter values given. Colored lines indicate the final choices for the modelling. Minimum and maximum curves were chosen based on the minimal (maximal) area under the curve (AUC) between 0°C and 30°C while retaining ecologically sensible shapes. This means the curves with a growth rate maximum between 0°C and 10°C were not chosen despite their lower AUC as they are deemed non-representative of the entire foraminifera phylum.

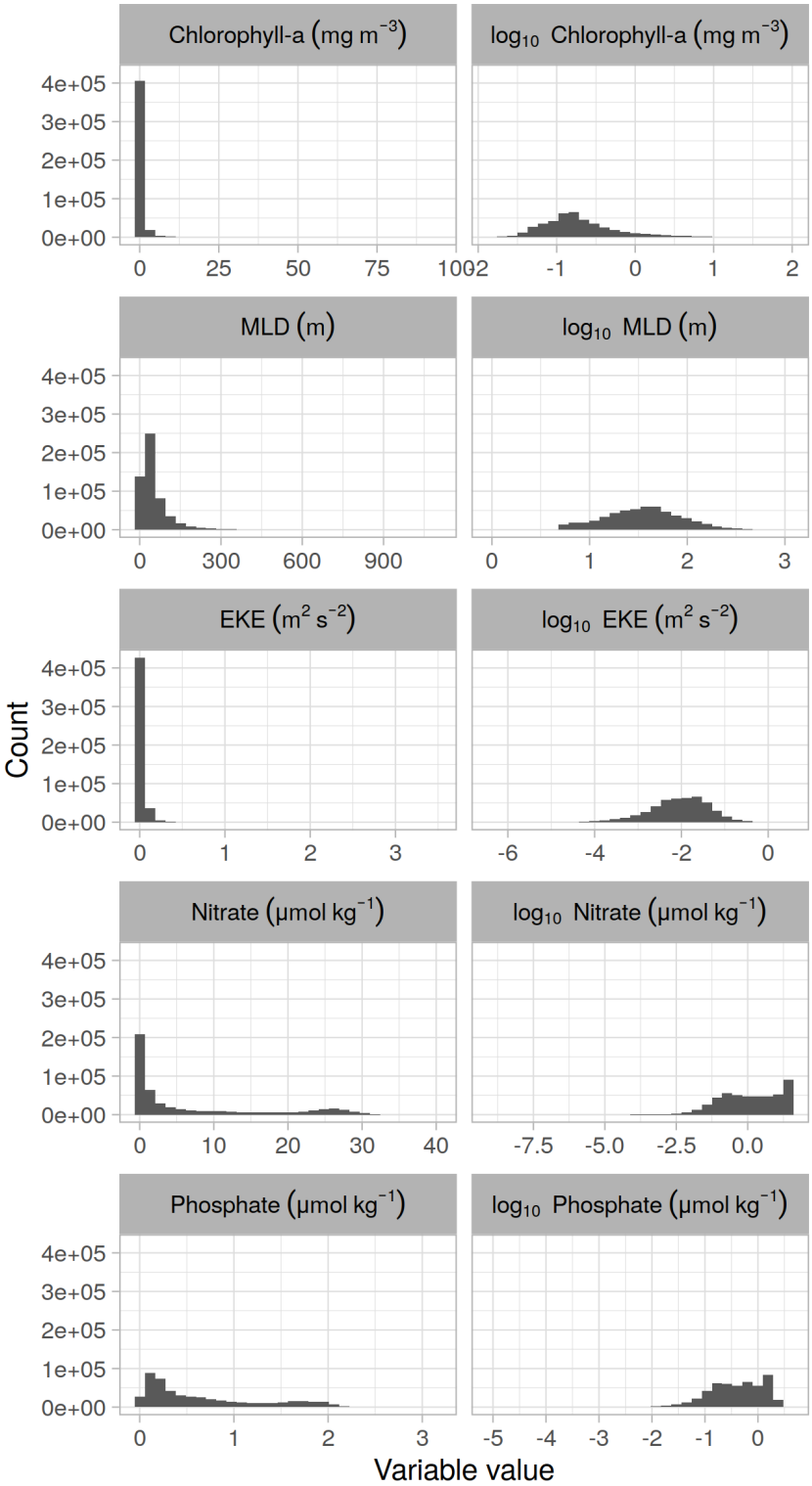

Figure S9. Histograms depicting the global distribution of values for the environmental predictors that were later log-transformed. The left column shows the histograms for the original values and the right column those for the log-transformed ones. One can see that the transformation causes all variables to be more normally distributed than originally.

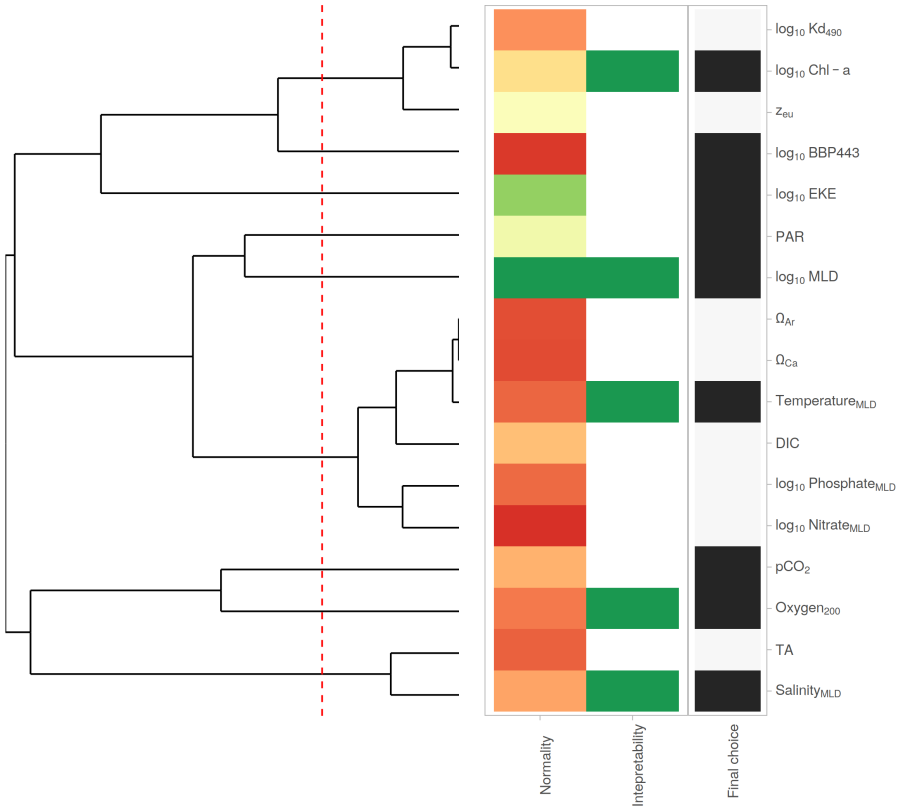

Figure S10. Plot depicting the steps taken to select the final set of environmental predictors for the pteropod species distribution models (SDMs). The dendrogram on the left shows the correlation structure of the environmental predictors as assessed at the grid points where observation data are present. The red dashed line indicates a correlation level of $|r| = 0.7$, i.e. all clusters right of this line are correlated to a higher degree. From each cluster, only one environmental predictor can be chosen and the red-green tile plot in the middle shows an evaluation of the two selection criteria, with green indicating a positive choice and red a negative one. 1) More normally distributed predictors are preferred. The normality column in the tile plot is a measure of the normality of the distribution of each environmental predictor. The values shown are the log-transformed and subsequently normalized p-values of the Shapiro-Wilk test. 2) Predictors with clearer known relevance for zooplankton abundances and hence simpler interpretability are preferred. These choices were made manually, with green shading indicating the most easily interpretable predictor. Finally, the last, black-and-white column highlights the final chosen predictors which were in the next step assessed for their predictive power.

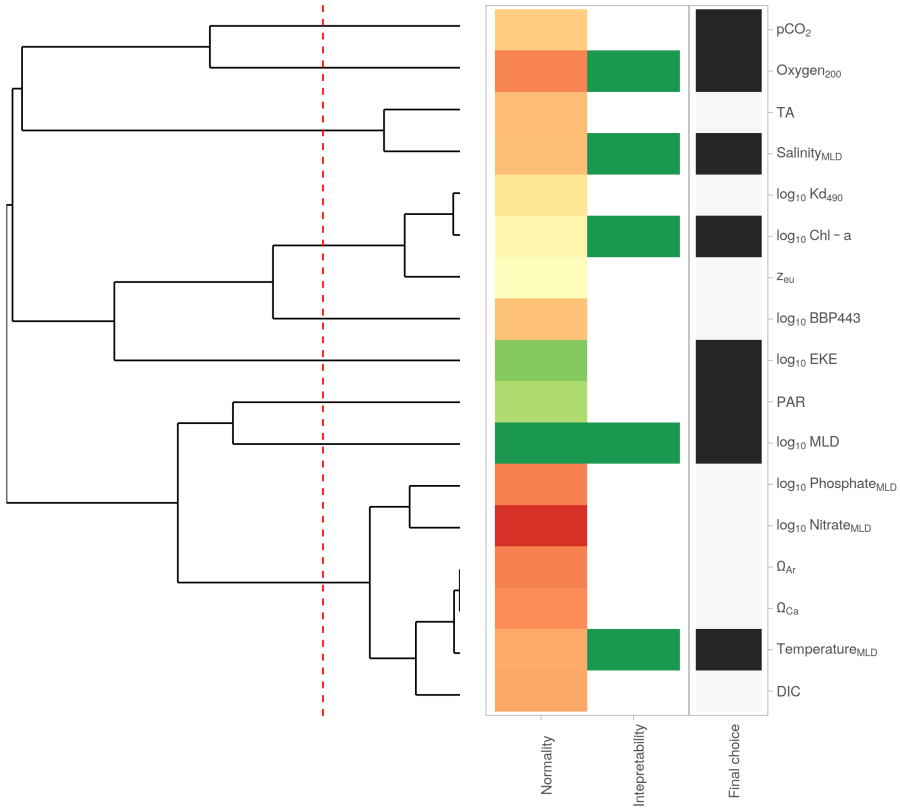

Figure S11. Plot depicting the steps taken to select the final set of environmental predictors for the foraminifer species distribution models (SDMs). See figure S10 for an extensive explanation of the plot structure.

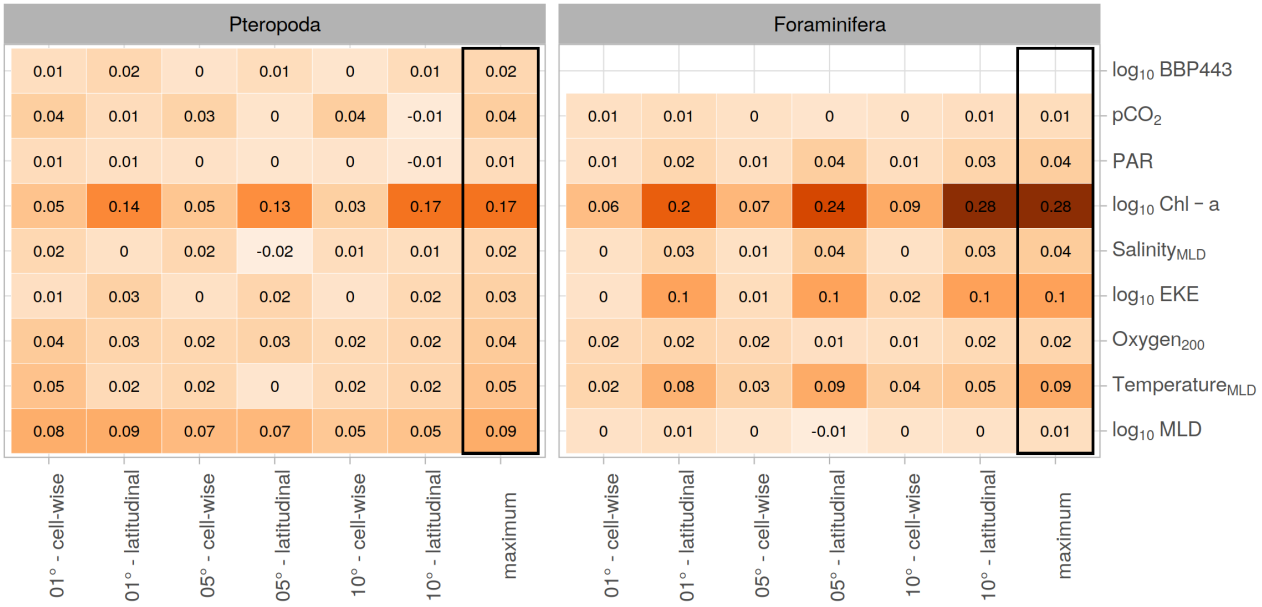

Figure S12. Variance explained by the different environmental predictors as assessed by three univariate models (GLM, GLM with quadratic terms and GAM) across the grid-wise and latitudinal aggregation levels for pteropods and foraminifers. The last column of both plots shows the maximum deviance explained across any of the assessed spatial aggregation levels. These are the values used for deciding which predictors to include in the species distribution models. The subscript MLD refers to variables that were averaged over the mixed layer depth. The value of oxygen was taken at 200 m depth.

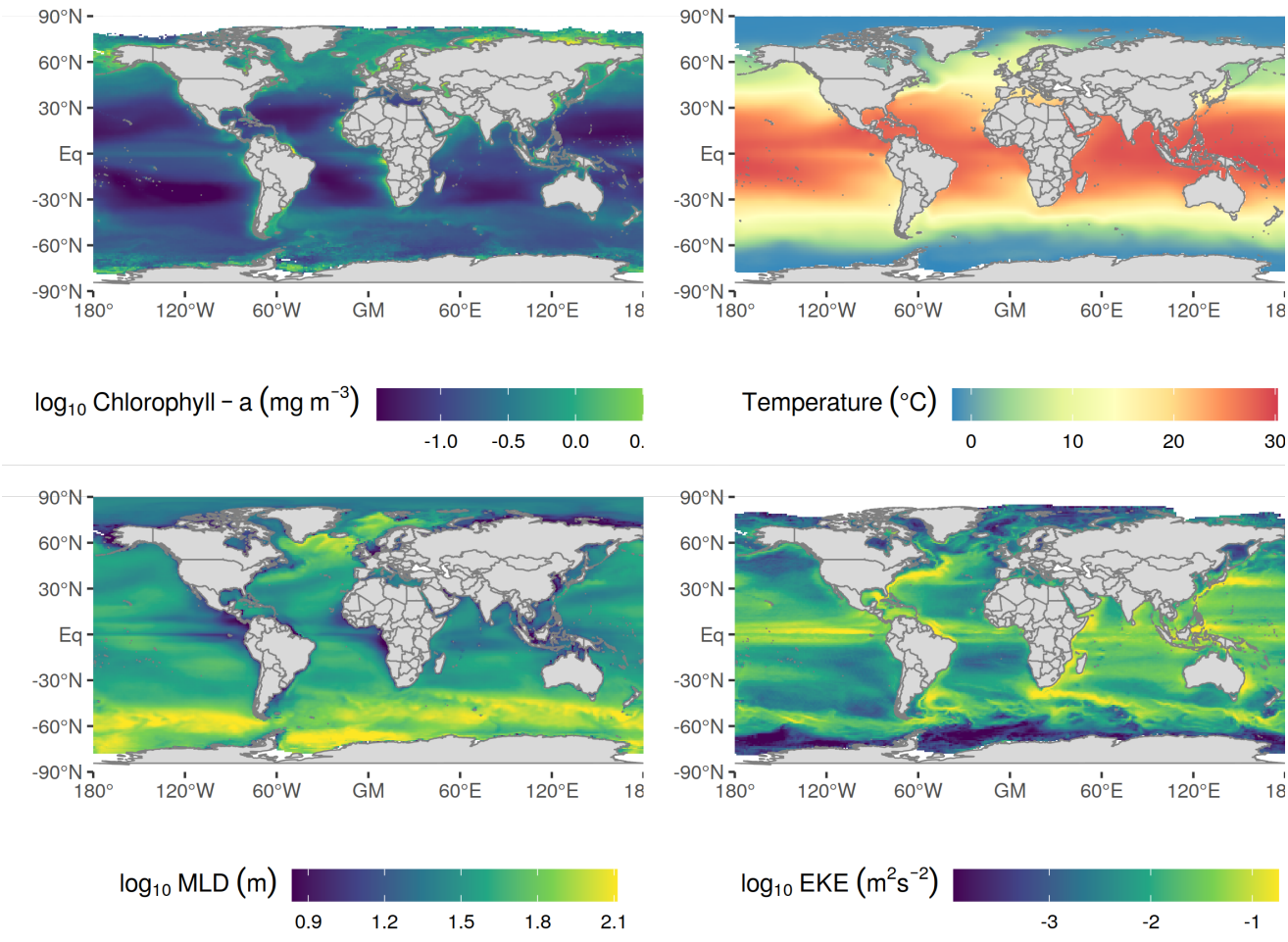

Figure S13. Annually averaged distribution of the four environmental predictors used in the modelling process.

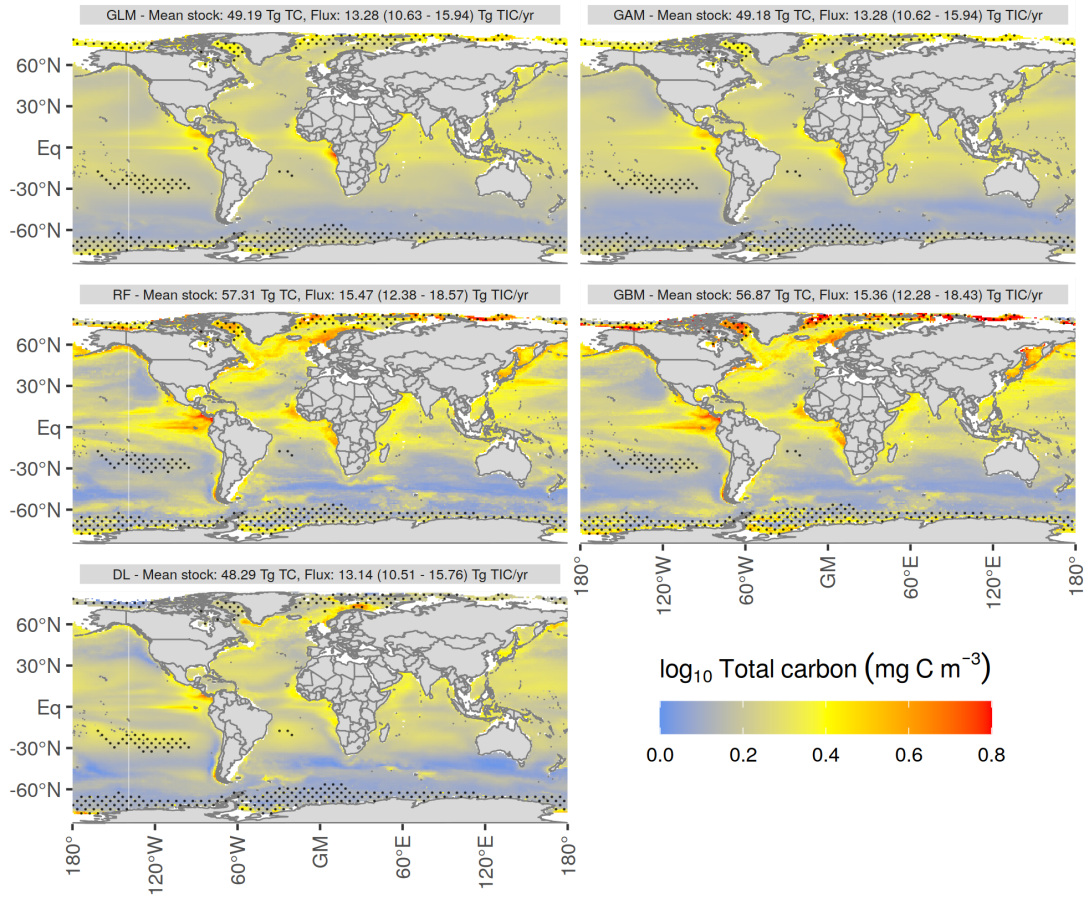

Figure S14. Mean annual pteropod total carbon (TC) biomass predictions as calculated by the five different models. Values are shown as $\log_{10}(TC + 1)$. Stippled areas indicate grid points where the environmental conditions were outside the training dataset for more than six months of the year as calculated with the Multivariate Environmental Similarity Surfaces (MESS) analysis. The headers denote the mean TC biomass stock and the annual global total inorganic carbon (TIC) flux with the range of uncertainty resulting from different choices of the TIC-TC conversion factor and the growth rate formulation.

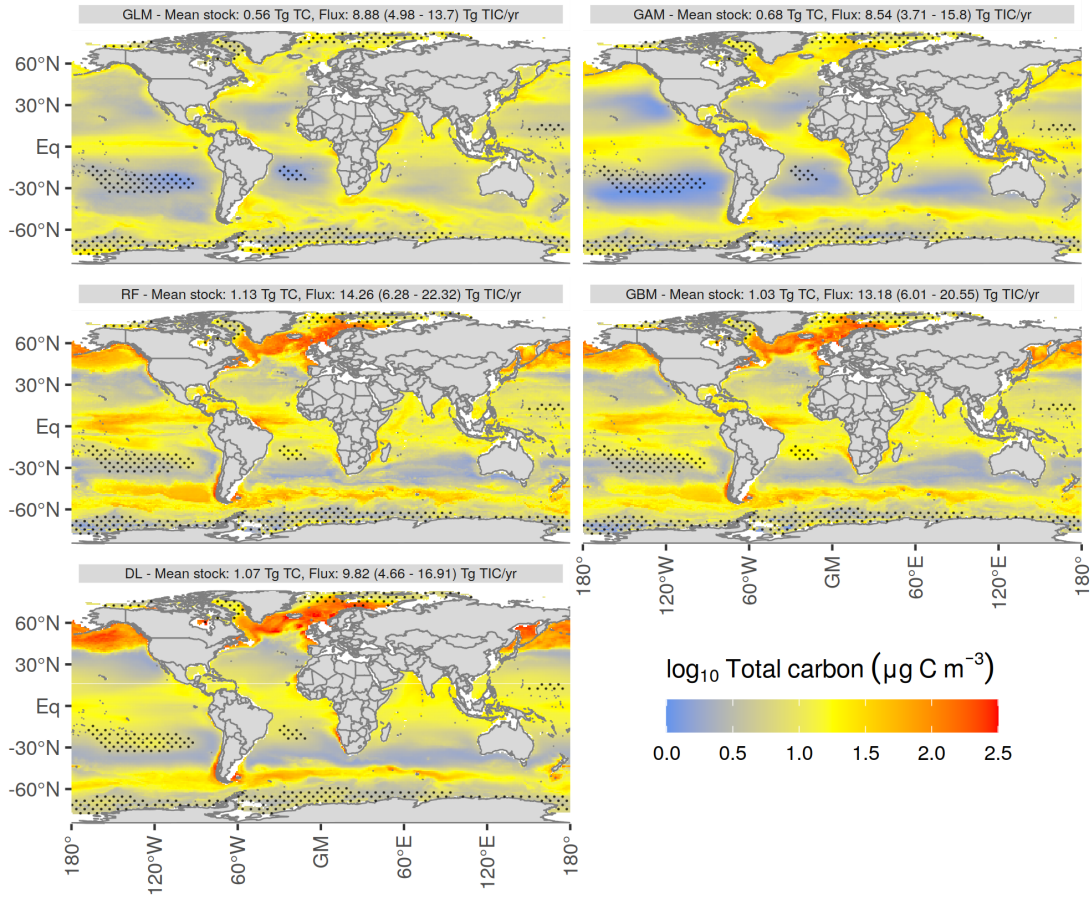

Figure S15. Mean annual foraminifer total carbon (TC) biomass predictions as calculated by the five different models. Values are shown as $\log_{10}(TC + 1)$. Stippled areas indicate grid points where the environmental conditions were outside the training dataset for more than six months of the year as calculated with the Multivariate Environmental Similarity Surfaces (MESS) analysis. The headers denote the mean TC biomass stock and the annual global total inorganic carbon (TIC) flux with the range of uncertainty resulting from different choices of the TIC-TC conversion factor and the growth rate formulation.

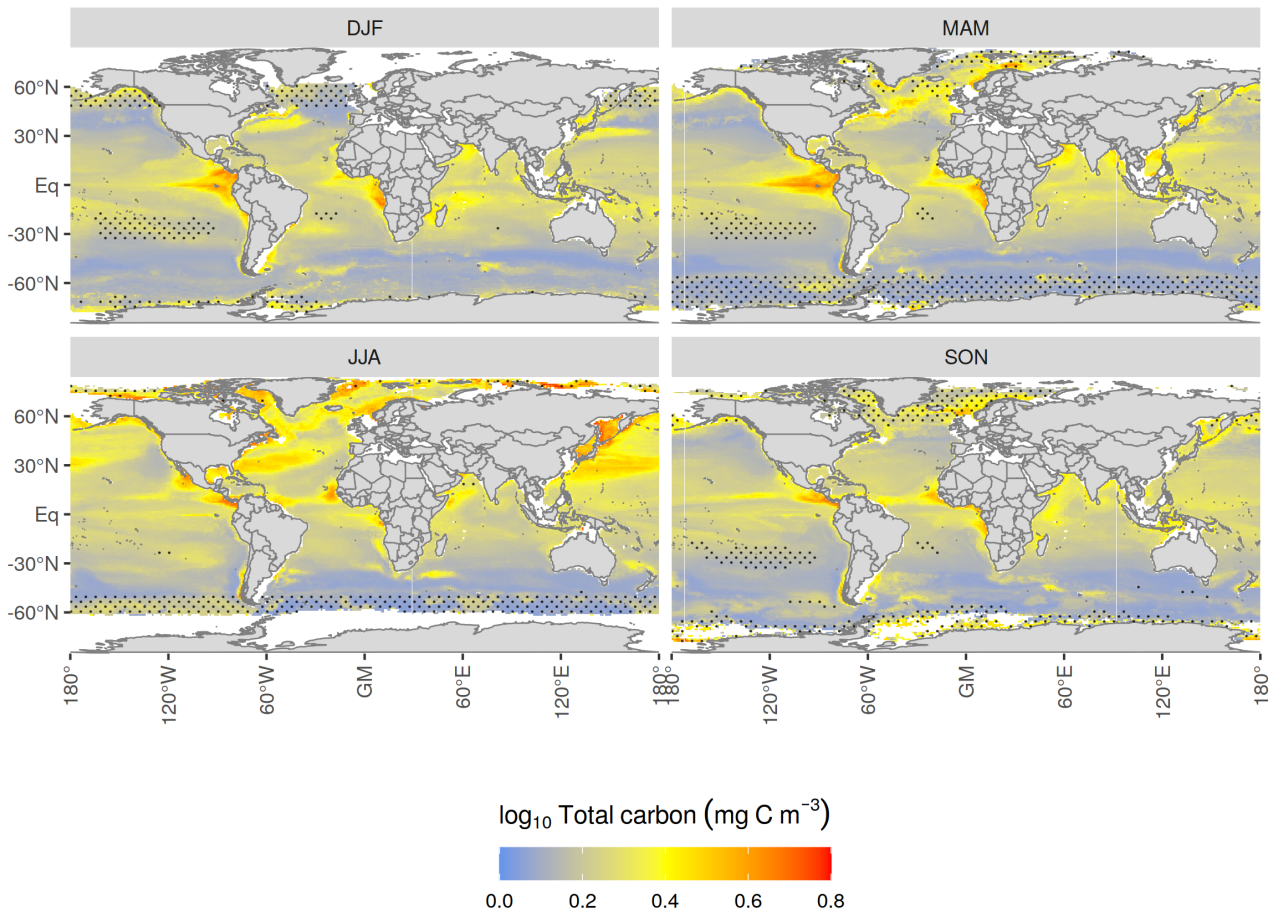

Figure S16. Seasonal mean pteropod total carbon (TC) biomass predictions as mean over the five models (DJF = December - February, MAM = March - May, JJA = June - August, SON = September - November). Values are shown as $\log_{10}(TC + 1)$. Stippled areas indicate grid points where the environmental conditions were outside the training dataset for more than one month of the respective season as calculated with the Multivariate Environmental Similarity Surfaces (MESS) analysis.

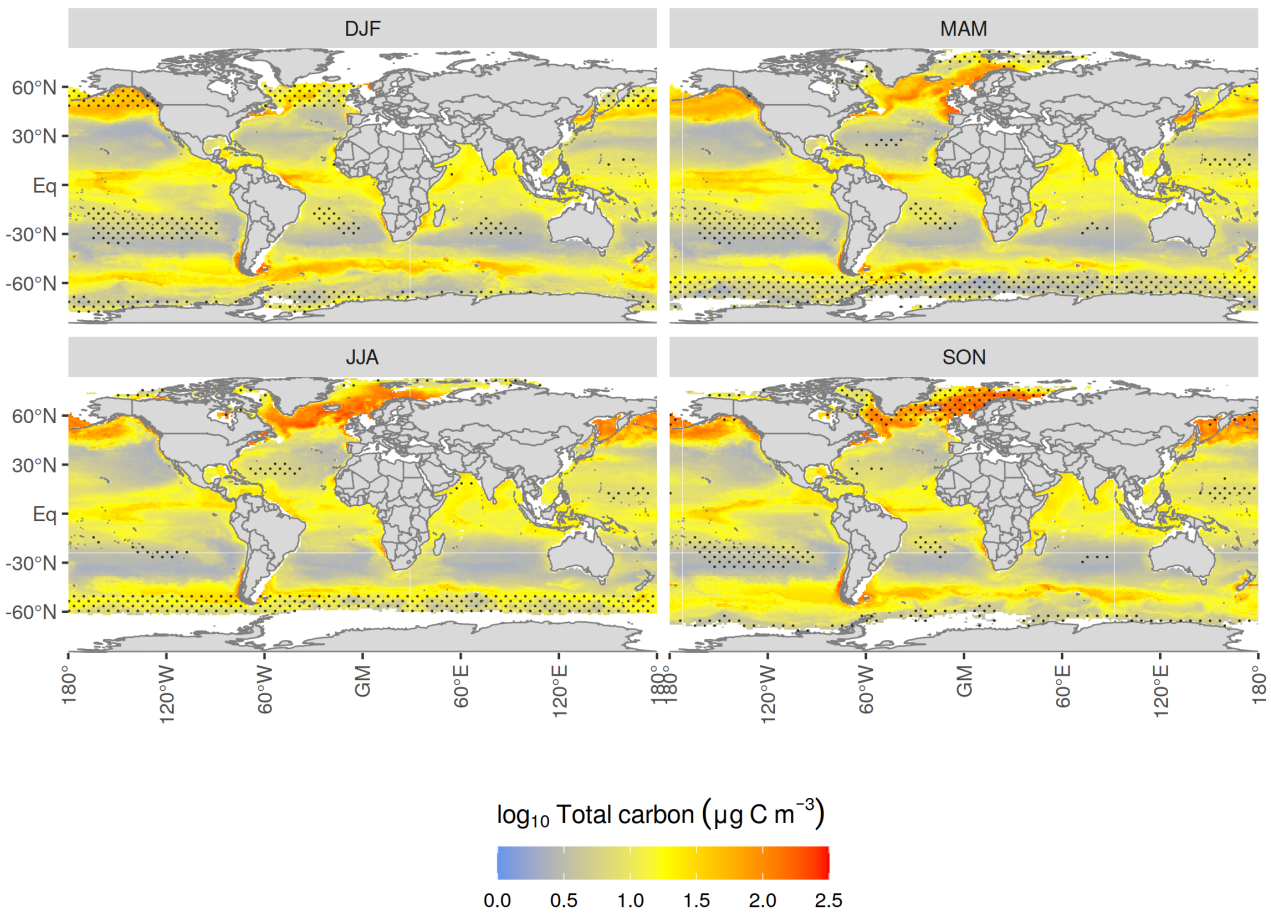

Figure S17. Seasonal mean foraminifer total carbon (TC) biomass predictions as mean over the five models (DJF = December - February, MAM = March - May, JJA = June - August, SON = September - November). Values are shown as $\log_{10}(TC + 1)$. Stippled areas indicate grid points where the environmental conditions were outside the training dataset for more than 1 months of the respective season as calculated with the Multivariate Environmental Similarity Surfaces (MESS) analysis.

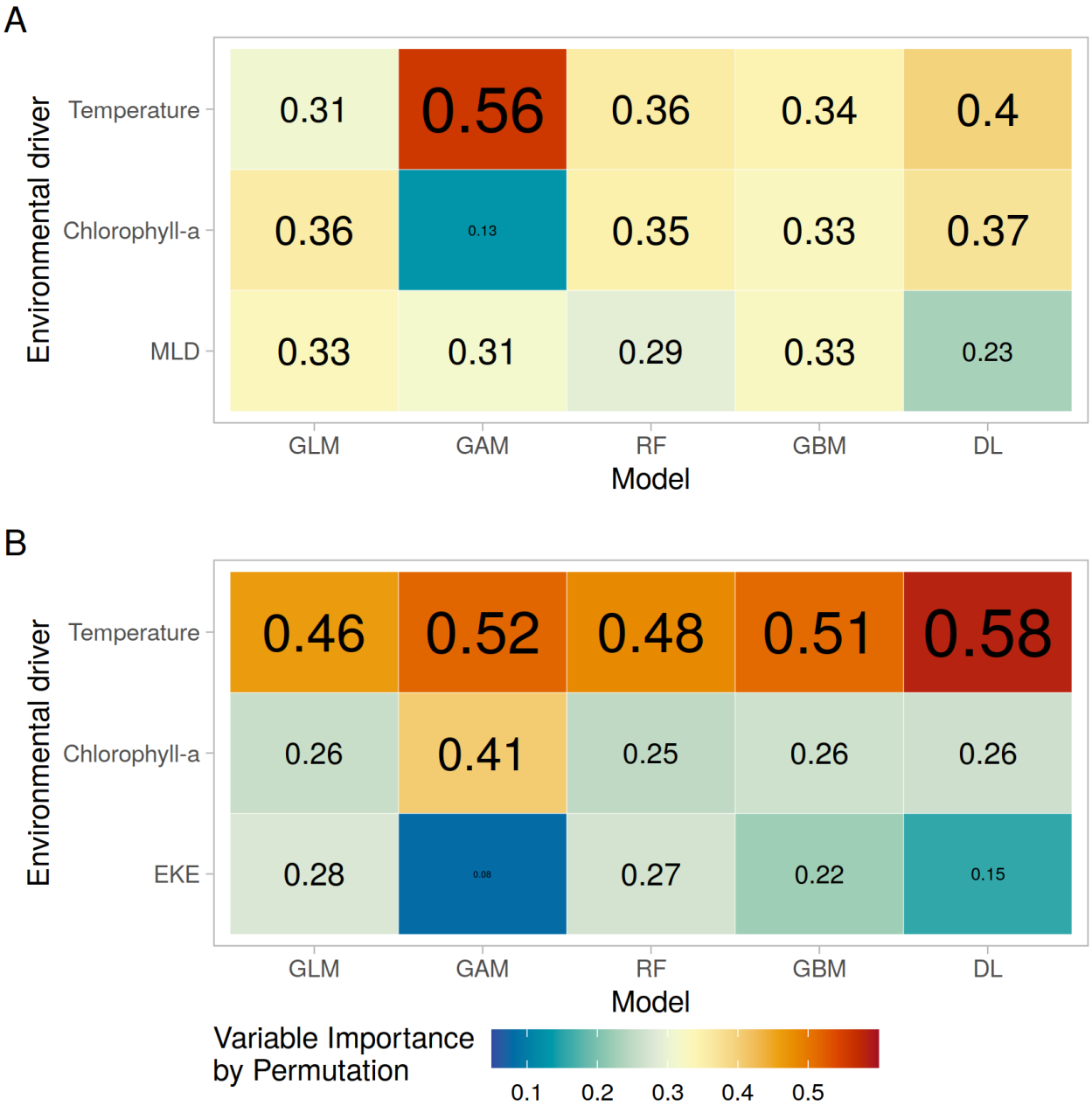

Figure S18. Normalized pteropod (**A**) and foraminifer (**B**) predictor variable importance as calculated with a permutation analysis across the five species distribution models (SDMs). A high value indicates that a change in this variable has a large effect on the predicted biomass values. All importance values are normalized to sum to one for each model.

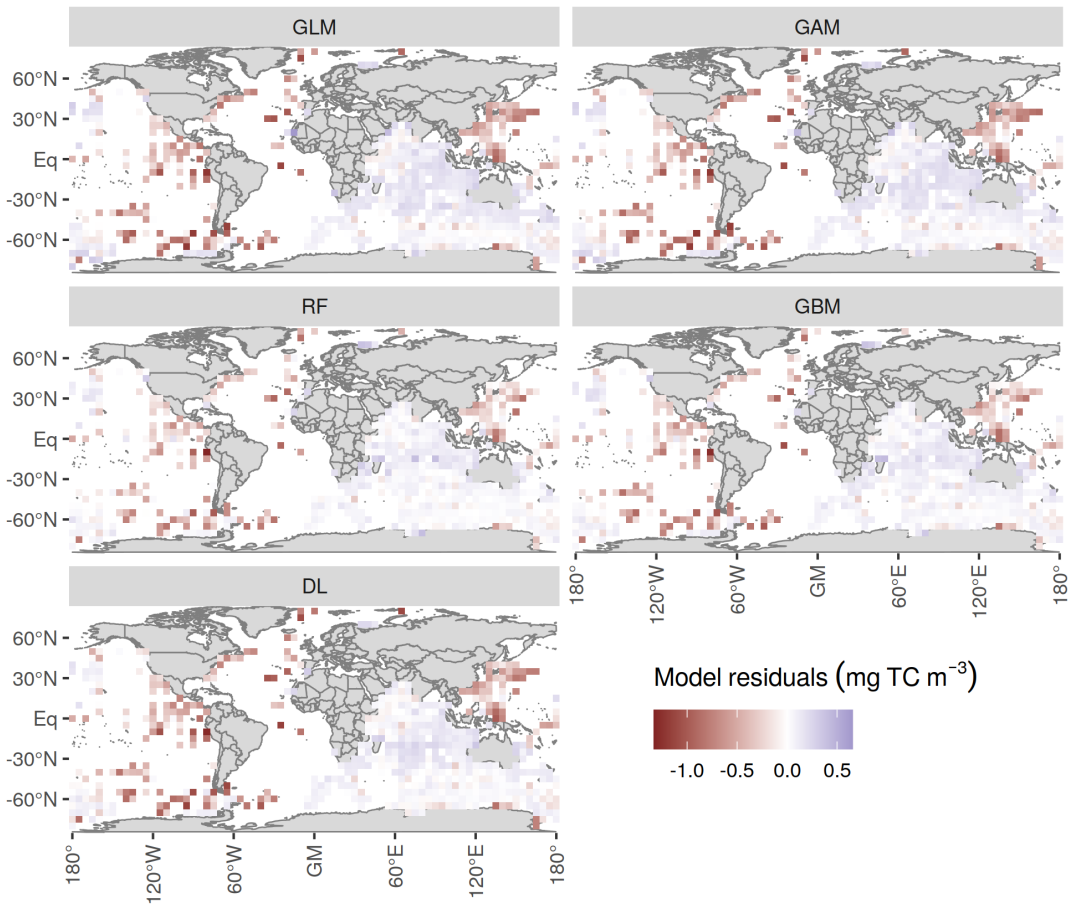

Figure S19. Pteropod total carbon (TC) biomass prediction residuals, averaged over all months and 5°grid bins. Negative residuals, i.e. an underestimation of the true values can be seen in the tropical ocean as well as the North Atlantic and the South-eastern Pacific. In contrast, an overestimation of the true values occurs mostly in the Indian Ocean and to a small extent in the Southern Ocean between 0°E and 150°E. These patterns correspond to the biomass predictions in that regions of high productivity are generally still underestimated, as the bloom dynamics here cause very high biomass concentrations. Areas of lower productivity are generally slightly overestimated.

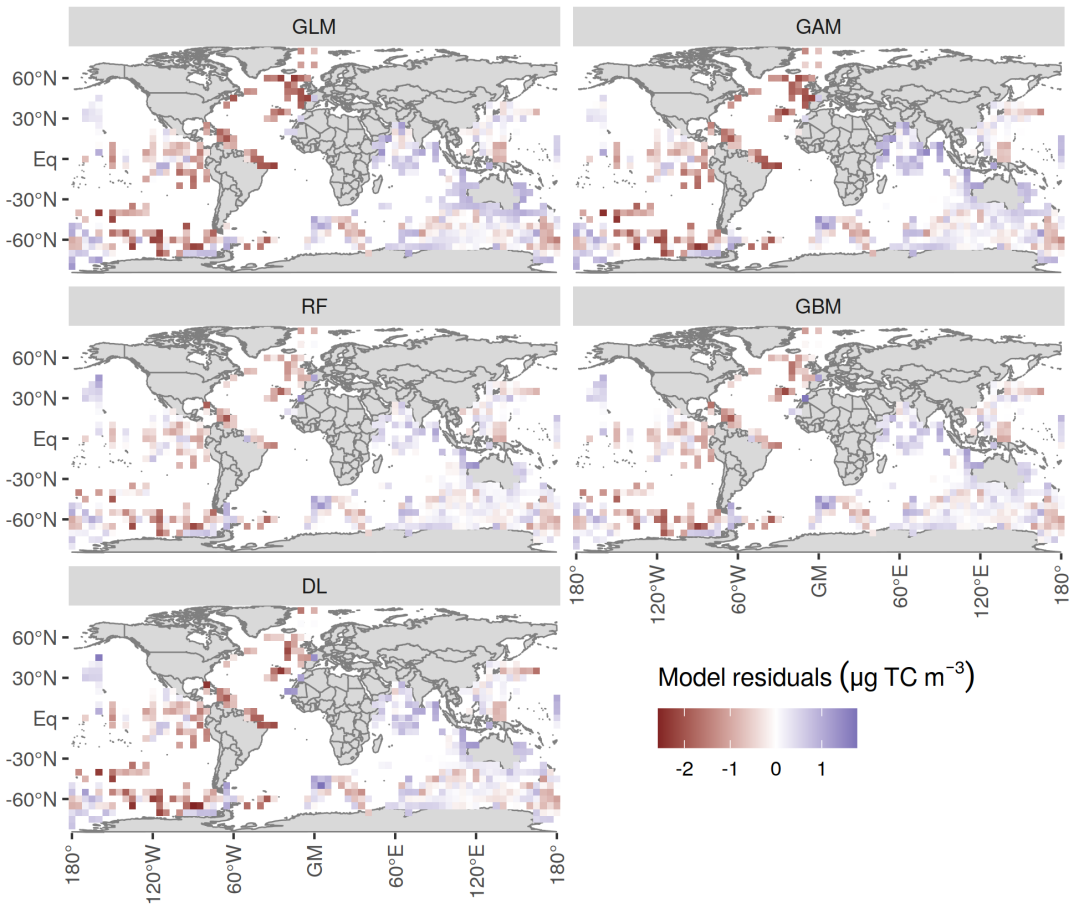

Figure S20. Foraminifer total carbon (TC) biomass prediction residuals, averaged over all months and 5° grid bins. The Random Forest model (RF) performs overall best, with lowest residual values everywhere, followed by the Boosted Regression Tree (GBM). The Generalized Linear Model (GLM) and Generalized Additive Model (GAM) strongly underestimate biomass concentrations in the highly productive regions of the North Atlantic, the equatorial region and the Southern Ocean between 180°W and 60°W. This trend is seen to a lesser extent in the Neural Network (DL) as well. In the GLM, GAM and DL, a slight overestimation of the true biomass values can be seen in the Indian Ocean and around Australia.

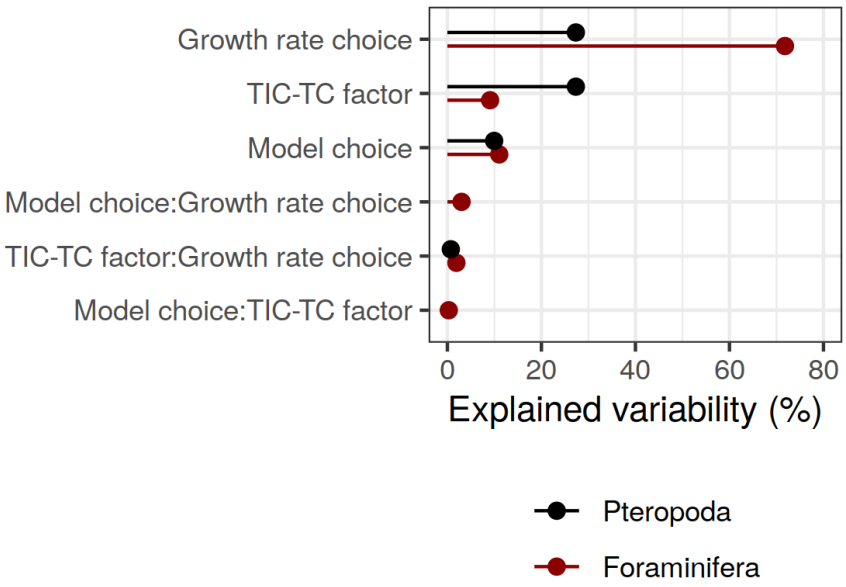

Figure S21. Percentage of variance in mean annual pteropod and foraminifer total inorganic carbon (TIC) export fluxes explained by different model setup choices as assessed with a multivariate Analysis of Variance (mANOVA).

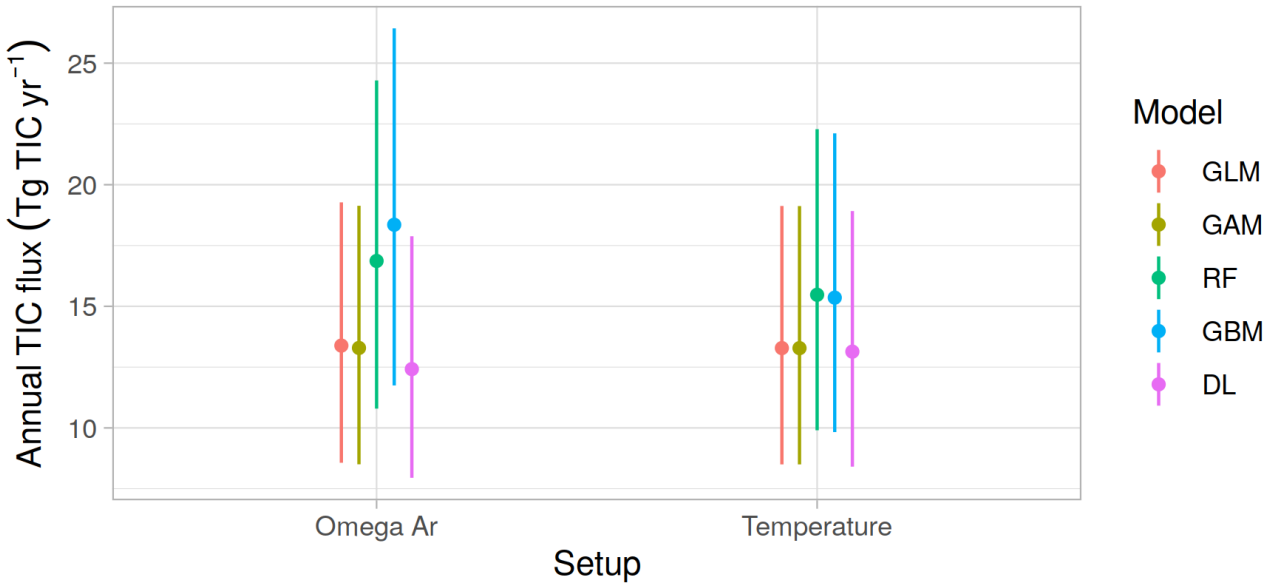

Figure S22. Global annual total inorganic carbon (TIC) fluxes for pteropods as calculated on the main predictor set including temperature averaged over the mixed layer and when replacing temperature by the aragonite saturation state (Ω_{Ar}) per SDM type. The range of values shown depicts the uncertainty range based on the TIC-TC conversion factor and the growth rate parametrization. For both plankton types, the difference in global annual TIC fluxes between the two setups is not statistically significant.

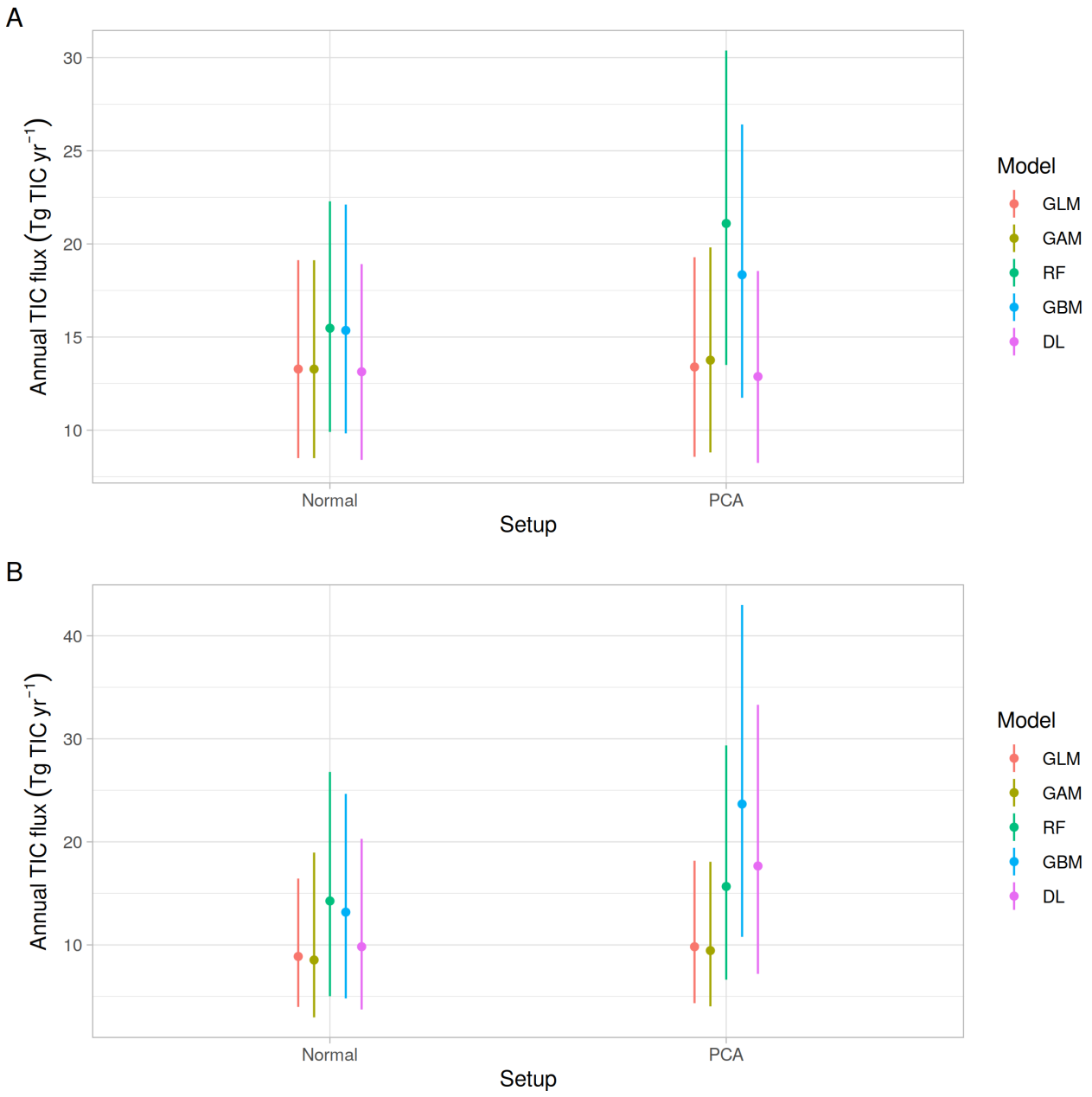

Figure S23. Global annual total inorganic carbon (TIC) fluxes for **A** pteropods and **B** foraminifers as calculated on the main predictor set and on a Principle Component Analysis (PCA) transformation of all environmental variables shown in table **??** per SDM type. The range of values shown depicts the uncertainty range based on the TIC-TC conversion factor and the growth rate parametrization. For both plankton types, the difference in global annual TIC fluxes between the regular setup and the PCA-setup is not statistically significant.

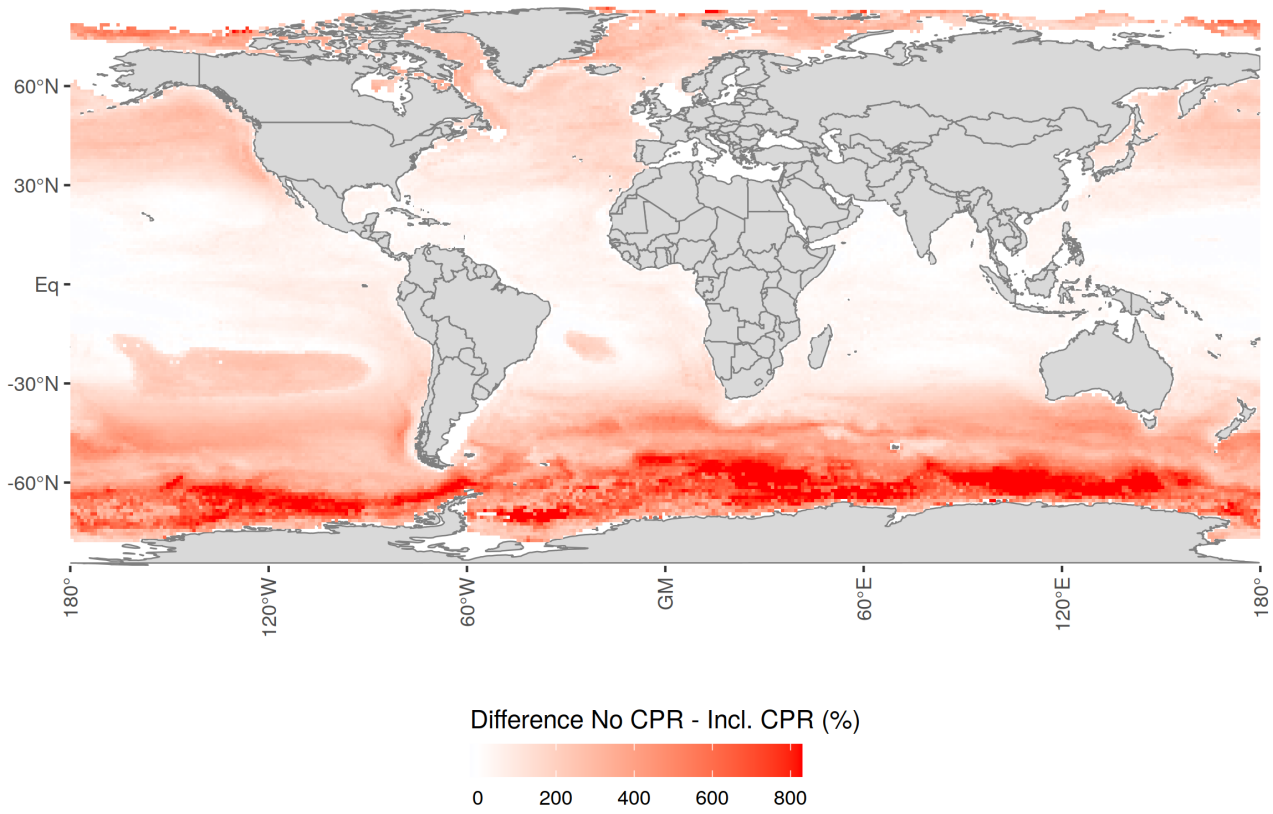

Figure S24. Relative change in pteropod biomass concentrations to baseline model when removing all CPR data.

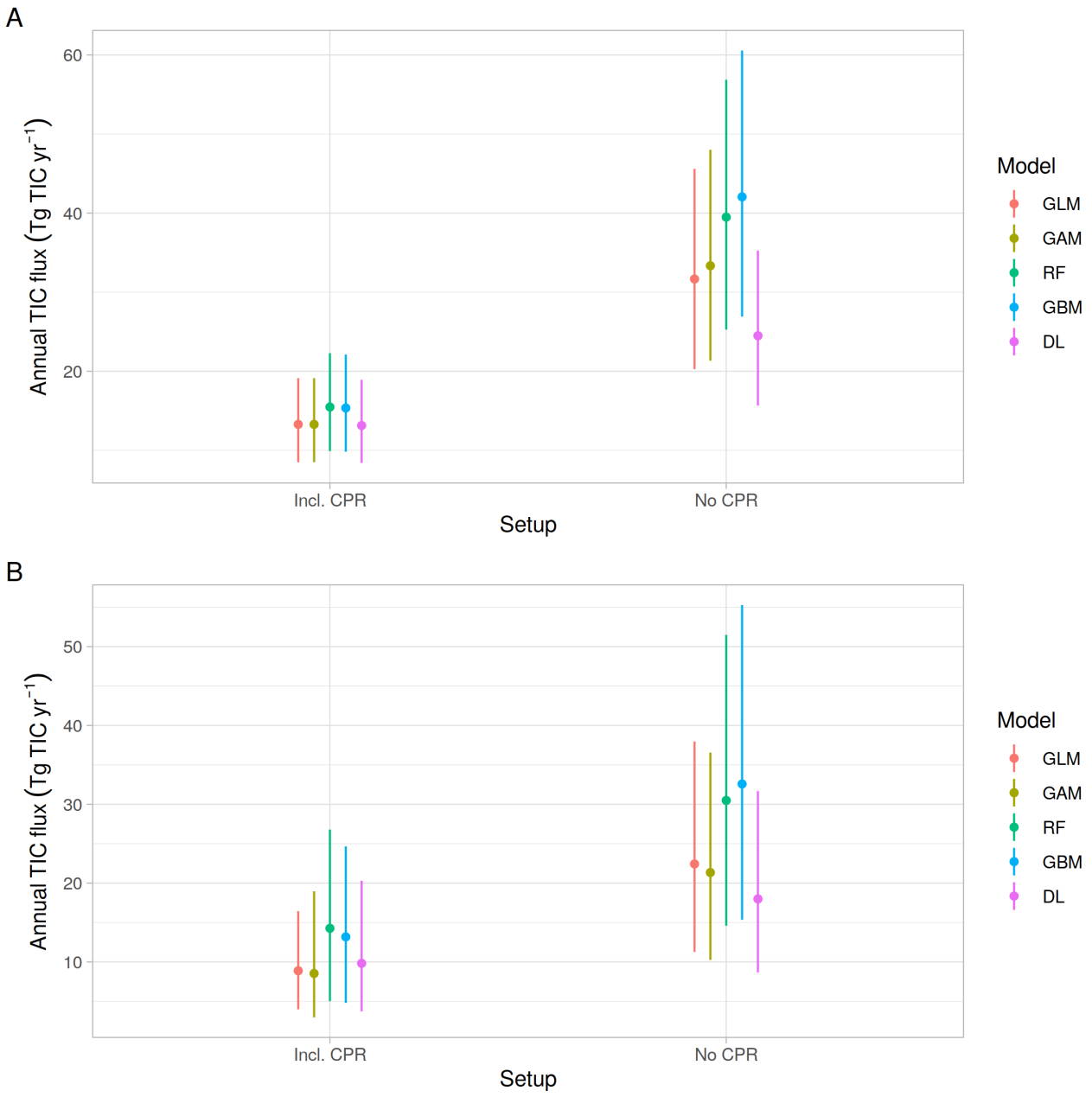

Figure S25. Global annual total inorganic carbon (TIC) fluxes for **A** pteropods and **B** foraminifers per SDM as calculated on the full dataset and only on non-CPR data, respectively. The range of values shown depicts the uncertainty range based on the TIC-TC conversion factor and the growth rate parametrization. For both plankton types, emitting all CPR values leads to a statistically significant increase in global annual TIC fluxes.

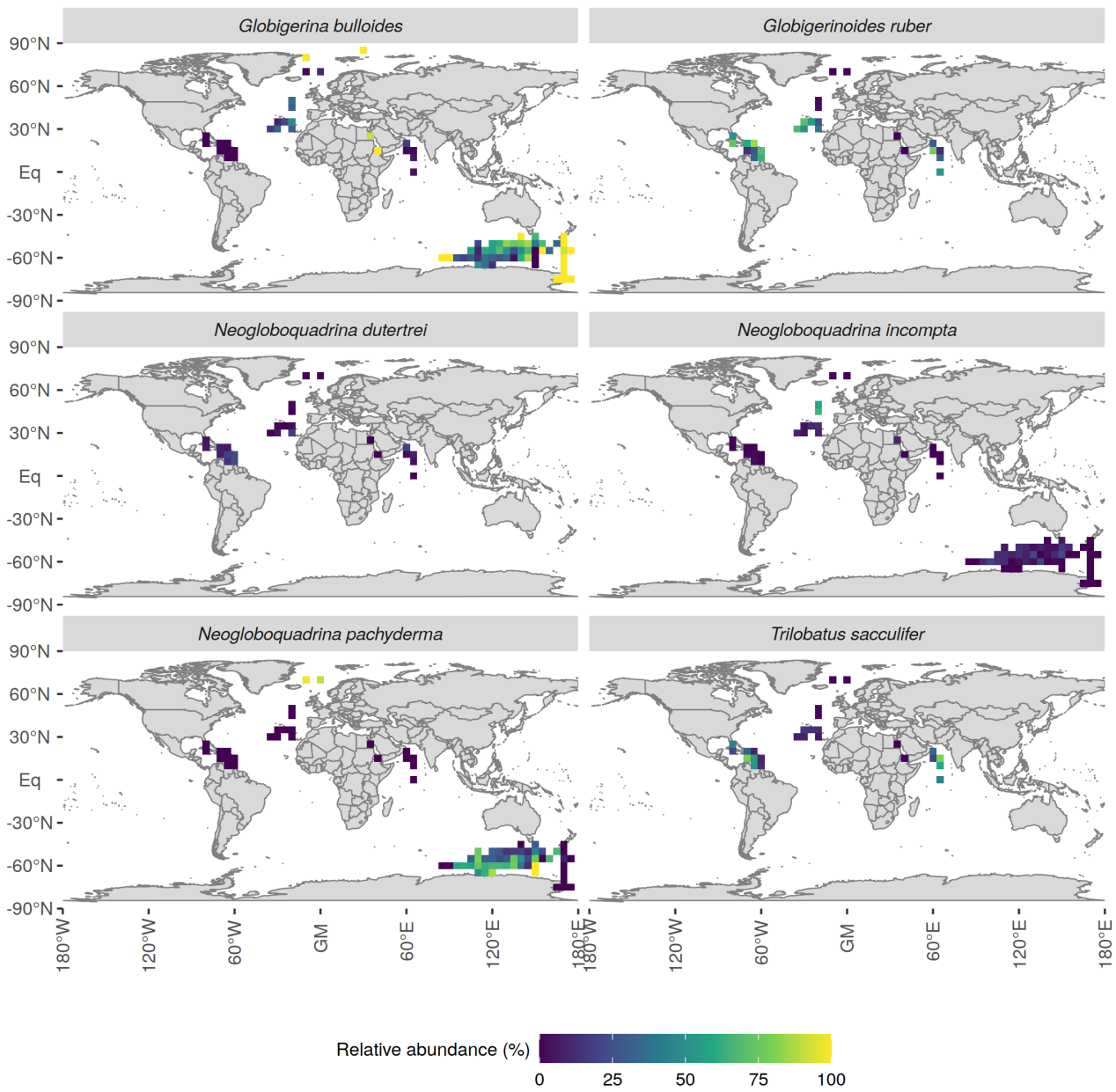

Figure S26. Relative species abundance in % of six common foraminifer species. The species-specific abundances were calculated by summing all unique counts of one species from a single tow and subsequently computing $5 \times 5°$ gridded annual means. The relative abundance values were then calculated as a species-specific fraction of the sum over the six species' abundances. The patterns agree reasonably well with those found in Kretschmer et al. (2018) and Lombard et al. (2011) with the exception of edge cases in the Antarctic.

Tables

Table S1. Pteropod biomass conversion equations to compute wet weight (WW) or dry weight (DW) in mg based on an organisms length L or diameter D (collection adapted from Bednaršek et al. (2012)). Equations are from [1] Bednaršek et al. (2012), [2] Little and Copley (2003) and [3] Davis and Wiebe (1985).

Species	Group	Source	Equation
Limacina helicina	Round/cylindrical/globular	[1]	$DW = 0.137 * D^{1.5005}$
Limacina spp.	Round/cylindrical/globular	[1]	$WW = 10^{(2.533*\log_{10}(L)-3.89095)} * 10^5$
Clione spp.	Barell/oval-shaped (naked)	[2]	$WW = \pi * L^{(3*3/25)}$
Hyalocylis spp.	Cone/needle/tube/bottle-shaped	[2]	$WW = \pi * L^{(3*3/25)}$
Styliola spp.	Cone/needle/tube/bottle-shaped	[2]	$WW = 10^{(2.533*\log_{10}(L)-3.89095)} * 10^5$
Spongiobranchaea spp.	Barell/oval-shaped (naked)	[2]	$WW = 10^{(2.533*\log_{10}(L)-3.89095)} * 10^5$
Pneumodermopsis spp.	Barell/oval-shaped (naked)	[2]	$WW = 10^{(2.533*\log_{10}(L)-3.89095)} * 10^5$
Paedocline spp.	Barell/oval-shaped (naked)	[2]	$WW = 10^{(2.533*\log_{10}(L)-3.89095)} * 10^5$
Cavolinia spp.	Triangular/pyramidal	[2]	$WW = 0.2152 * L^{2.293}$
Clio spp.	Triangular/pyramidal	[2]	$WW = 0.2152 * L^{2.293}$
Creseis spp.	Cone/needle/tube/bottle-shaped	[2]	$WW = \pi * L^{(3*3/25)}$
Cuvierina spp.	Cone/needle/tube/bottle-shaped	[2]	$WW = \pi * L^{(3*3/25)}$
Diacria spp.	Triangular/pyramidal	[2]	$WW = 0.2152 * L^{2.293}$
Euthecosomata	Shelled	[3]	$WW = 0.2152 * L^{2.293}$
Gymnosomata	Naked	[3]	$WW = 10^{(2.533*\log_{10}(L)-3.89095)} * 10^3$
Pteropoda	Shelled	[3]	$WW = 0.2152 * L^{2.293}$

Table S2: Pteropod average length values (mm; from Bednaršek et al. (2012)) for different taxa as used in the analysis. The third column indicates the number of data points corresponding to this taxon in the full quality controlled dataset, and the fourth one indicates the number of non-zero abundances. Where no length value was available in Bednaršek et al. (2012), the fifth column indicates the choices taken. Note that for Pseudothecosomata without a given length value, the average value for the entire pteropod taxon was used.

Taxon	Length (mm)	# Obs	#Obs (non-zero)	Comment for length value
Cavolinia gibbosa	6.2	62	2	Family value used
Cavolinia globulosa	6			
Cavolinia inflexa	7.7	247	50	Mean of subspecies
Cavolinia inflexa imitans	8			
Cavolinia inflexa inflexa	7			
Cavolinia inflexa labiata	8			
Cavolinia longirostris angulosa	3.9			
Cavolinia longirostris longirostris	6.2			
Cavolinia longirostris strangulata	4			
Cavolinia uncinata	6.3	62	3	Mean of subspecies
Cavolinia uncinata pulosatupsilla	6.1			
Cavolinia uncinata uncinata	6.5			
Cavolinia spp.	6.2	23849		
Clio convexa	8	3292	217	
Clio cuspidata	20	62	10	
Clio piatkowskii	13.5			

Table S2 continued from previous page

Taxon	Length (mm)	# Obs	#Obs (non-zero)	Comment for length value
Clio pyramidata	20	56077	645	
Clio pyramidata antarctica	17	31	3	
Clio pyramidata lanceolata	20			
Clio pyramidata martensi	17			
Clio pyramidata spp.	18.5			
Clio recurva	16.5	31	1	Family value used
Clio spp.	16.5	52136		
Clione limacina antarctica	40	51717		66
Clione limacina meridionalis	20			
Clione limacina larvae	0.3			
Clione limacina spp.	12	1589		
Clione spp.	14.57	51739		
Corolla	8.9	31	3	Pteropod value used
Creseis acicula acicula	33			
Creseis acicula clava	6			
Creseis acicula spp.	19.5	524		
Creseis clava	11.5	31	14	Family value used
Creseis conica	11.5	62	17	Family value used
Creseis spp.	11.5	11211		
Creseis virgula conica	7			
Creseis virgula constricta	3.5			
Creseis virgula spp.	5.5	557		
Creseis virgula virgula	6			

Table S2 continued from previous page

Taxon	Length (mm)	# Obs	#Obs (non-zero)	Comment for length value
Cuvierina atlantica	8.1	31	3	Thecosomata value used
Cuvierina columnella columnella	10			
Cuvierina spp.	8.1	62		Thecosomata value used
Desmopterus papilio	8.9	1	1	Pteropod value used
Diacavolinia spp.	8.1	62		Thecosomata value used
Diacria costata	2.3			
Diacria danae	1.7	31	14	
Diacria major	10.7	31	1	
Diacria quadridentata	3			
Diacria rampali	9.5			
Diacria trispinosa	8	277	56	Mean of subspecies
Diacria trispinosa trispinosa	8			
Diacria spp.	5.9	3708		
Gleba spp.	8.1	31		Thecosomata value used
Heliconoides inflatus	8.1	4755	2970	Thecosomata value used
Hyalocylis	8	162	9	Mean of subspecies
Hyalocylis striata	8	217	9	
Hydromylidae	12	7056	1	Gymnosomata value used
Limacina bulimoides	2	3732	466	
Limacina helicina antarctica	5	31	6	
Limacina helicina antarctica rangii	2			
Limacina helicina helicina	6	31	1	
Limacina helicina pacifica	5			

Table S2 continued from previous page

Taxon	Length (mm)	# Obs	#Obs (non-zero)	Comment for length value
Limacina helicina spp.	4.22	1538		
Limacina inflata	1.3	104	104	
Limacina lesueuri	0.8	1073		
Limacina rangii	2.98	62	7	Family value used
Limacina retroversa	2.5	9070	1422	
Limacina retroversa australis	2.5	62	3	Species value used
Limacina spp.	2.98	62618		
Limacina trochiformis	1	3741	1389	
Paedoclione doliiformis	1.5	3	3	
Peracle bispinosa	8.9	31	3	Pteropod value used
Peracle diversa	8.9	31	10	Pteropod value used
Peracle reticulata	8.9	524	133	Pteropod value used
Peracle valdiviae	8.9	31	5	Pteropod value used
Peracle spp.	8.9	4193		Pteropod value used
Pneumodermopsis	6.5	5	5	
Pneumodermopsis canephora	12			
Pneumodermopsis ciliata	15	1		
Pneumodermopsis macrochira	2			
Pneumodermopsis paucidens	5			
Pneumodermopsis polycotyla	5			
Pneumodermopsis pulex	8			
Pneumodermopsis simplex	5			
Pneumodermopsis spoeli	3			

Table S2 continued from previous page

Taxon	Length (mm)	# Obs	#Obs (non-zero)	Comment for length value
Pneumodermopsis teschi	9.1			
Spongiobranchaea australis	22	58773	103	
Spongiobranchaea australis larvae	10			
Spongiobranchaea spp.	15			
Styliola	13	8	8	Mean of subspecies
Styliola subula	13	66	29	
Telodiacria danae	8.1	62	11	Thecosomata value used
Telodiacria quadridentata	8.1	337	5	Thecosomata value used
Thielea helicoides	8.1	3184	119	Thecosomata value used
Euthecosomata	8.1	340250	43596	
Gymnosomata	12	2331	741	
Pteropoda	8.9	79613	14713	
Total		**841239**	**66978**	

Table S3. Foraminifer shape groups as defined for the following analysis. The images are exemplary for each shape type. Sources refer to the images.

Group	Species	Example	Source
1 Digitate type	*Beella digitata* *Globigerinella adamsi* *Hastigerinella digitata*	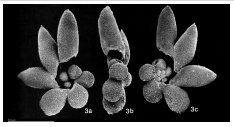	Saito, Thompson, and Breger (1976)
2 Low trochospiral type	*Berggrenia pumilia* *Dentigloborotalia anfracta* *Tenuitella fleisheri* *Tenuitella iota* *Tenuitella parkerae* *Globigerinita humilis* *Turborotalita quinqueloba* *Orcadia riedeli* *Globigerinita minuta* *Globigerinoides tenellus* *Globorotaloides hexagonus* *Neogloboquadrina dutertrei* *Neogloboquadrina incompta* *Neogloboquadrina pachyderma*	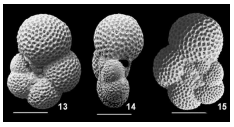	Coxall and Spezzaferri (2018)
3 Medium trochospiral type	*Candeina nitida* *Globigerina bulloides* *Globigerina falconensis* *Globigerinita glutinata* *Globigerinoides ruber* *Globoquadrina conglomerata* *Globoturborotalita rubescens* *Spaeroidinella dehiscens* *Trilobatus sacculifer*	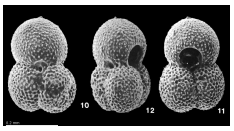	Loeblich and Tappan (1994)
4 Oblique planispiral type	*Hastigerina pelagica* *Globigerinella calida* *Globigerinella siphonifera*	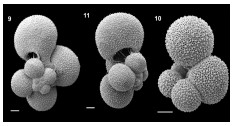	Weiner, Weinkauf, Kurasawa, Darling, and Kucera (2015)
5 Discoidal-pyramidal type	*Globorotalia scitula* *Globorotalia theyeri* *Globorotalia crassaformis* *Globorotalia hirsuta* *Globorotalia menardii* *Globorotalia tumida* *Globorotalia ungulata* *Globorotalia truncatulinoides* *Globorotalia inflata*	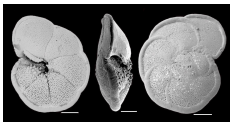	Lam and Leckie (2020)
6 Subsphaeroidal type	*Pulleniatina obliquiloculata* *Globigerinoides conglobatus* *Sphaeroidinella dehiscens* *Trilobatus sacculifer*	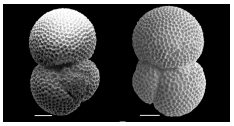	Lam and Leckie (2020)
7 Elongate type	*Globigerinita uvula* *Streptochilus globigerus*	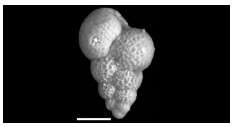	Miranda-Martínez, Carreño, and McDougall (2017)
8 Sphaeroidal type	*Orbulina universa*	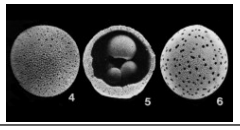	Srinivasan and Kennett (1983)

Table S4: Average length values (µm) for the different foraminifer taxa. Values for individual species were collected from the images in Schiebel and Hemleben (2017). The third column indicates the number of data points per taxon present in the full quality controlled dataset, while the fourth column shows the number of non-zero abundance observations. For higher taxonomic levels than the species level, the fifth column indicates the choices taken for the length calculation.

Taxon	Length (µm)	# Obs	#Obs (non-zero)	Comment for length value
Beella digitata	300	5650	4	
Berggrenia pumilio	100	5650	3	
Candeina nitida	250	5650	4	
Dentigloborotalia anfracta	100	5650	80	
Globigerina bulloides	250	57372	3445	
Globigerina falconensis	250	5650	141	
Globigerina spp.	250	11	11	Mean of species used
Globigerinella adamsi	400	5650	29	
Globigerinella calida	300	5650	194	
Globigerinella siphonifera	300	5650	1018	
Globigerinita glutinata	250	5650	1986	
Globigerinita minuta	100	5650	87	
Globigerinita uvula	150	57367	117	
Globigerinoides conglobatus	300	5650	34	
Globigerinoides ruber	250	11300	1971	
Globigerinoides tenellus	150	11300	498	

Table S4 continued from previous page

Taxon	Length (µm)	# Obs	#Obs (non-zero)	Comment for length value
Globoquadrina conglomerata	300	5650	11	
Globorotalia theyeri	300	5650	150	
Globorotalia crassaformis	250	5650	74	
Globorotalia hirsuta	250	5650	539	
Globorotalia inflata	250	57367	1212	
Globorotalia menardii	400	5650	273	
Globorotalia scitula	150	5650	990	
Globorotalia truncatulinoides	300	5650	757	
Globorotalia tumida	300	5650	31	
Globorotalia ungulata	300	5650	33	
Globorotalia spp.	278	65829	128	Mean of species used
Globorotaloides hexagonus	250	5650	185	
Globoturborotalita rubescens	150	5650	264	
Hastigerina pelagica	500	5650	169	
Hastigerinella digitata	500	5650	12	
Neogloboquadrina dutertrei	250	5650	630	
Neogloboquadrina incompta	200	57367	2001	
Neogloboquadrina pachyderma	200	57367	1235	
Orbulina universa	400	5650	242	
Orcadia riedeli	150	51717	2	
Pulleniatina obliquiloculata	250	5650	46	
Sphaeroidinella dehiscens	300	5650	23	
Tenuitella fleisheri	100	5650	15	

Table S4 continued from previous page

Taxon	Length (µm)	# Obs	#Obs (non-zero)	Comment for length value
Tenuitella iota	100	5650	54	
Tenuitella parkerae	100	5650	159	
Trilobatus sacculifer	300	11300	929	
Turborotalita humilis	125	5650	181	
Turborotalita quinqueloba	150	57367	1258	
Planktic foraminifers	242	344819	80782	Mean of all species used
Total		**1021283**	**102007**	

Table S5. Total carbon (TC) biomass conversion factors (BCF) for foraminifers. These factors are derived from length and test weight measurements from Schiebel and Hemleben (2000) and Takahashi and Bé (1984). The conversion factor for foraminifers in total is derived from Michaels et al. (1995). All conversion factors are converted to total carbon (TC) biomass, using equations (4) to (6) in the main document.

Taxon	Biomass conversion factor ($\mu g\,TC\,\mu m^{-3}$)
Species	
Globigerina bulloides	$1.1645 * 10^{-7}$
Globigerina falconensis	$1.9051 * 10^{-7}$
Globigerinella siphonifera	$0.7496 * 10^{-7}$
Globigerinita glutinata	$1.9304 * 10^{-7}$
Globorotalia hirsuta	$2.1544 * 10^{-7}$
Globorotalia scitula	$1.7367 * 10^{-7}$
Neogloboquadrina incompta	$2.1566 * 10^{-7}$
Turborotalita quinqueloba	$1.3571 * 10^{-7}$
Shape groups	
2 - Low trochospiral type	$1.7568 * 10^{-7}$
3 - Medium trochospiral type	$1.6667 * 10^{-7}$
4 - Oblique planispiral type	$0.7496 * 10^{-7}$
5 - Discoidal-pyramidal type	$1.9456 * 10^{-7}$
Foraminifers	$1.2109 * 10^{-7}$

Table S6. Hyperparameter options for the Random Forest (RF) model, the untuned parameter value and the final parameter choices for pteropods and foraminifers as determined via a grid search by assessing all hyperparameter options for those that would minimize the root mean squared error (RMSE). n_{tree} denotes the number of bootstrap samples created from the original dataset, using a fraction of r_{sample} of the entire data for each bootstrap. m_{try} refers to the number of predictors evaluated at each node for their ability to discriminate the data most clearly. min_{rows} describes the minimum number of observations in each terminal node and max_{depth} the maximum size of the tree. For an extensive description of the hyperparameters and their effects, refer to Boehmke and Greenwell (2019c).

Hyperparameter	Parameter values tested	Untuned parameter	Final value pteropods	Final value foraminifers
n_{tree}	30, 130, 230, 330, 430, 530, 630, 730, 830, 930	50	830	330
m_{try}	1, 2, 3	1	1	2
min_{rows}	1, 3, 5, 10	1	3	2
max_{depth}	10, 20, 30	20	30	10
r_{sample}	0.55, 0.632, 0.70, 0.80	0.632	0.80	0.632

Table S7. Hyperparameter options for the Gradient Boosting Machine (GBM) model, the untuned parameter value, and the final parameter choices for pteropods and foraminifers as determined via a grid search by assessing all hyperparameter options for those that would minimize the root mean squared error (RMSE). max_{depth} describes the maximum size of each individual tree and min_{rows} denotes the minimum number of observations in each terminal node. The model's learning rate is determined by r_{learn}. Each of the individual trees that together make up the GBM is trained on a a random fraction r_{sample} of the data, using a fraction $r_{samplecolumns}$ of the predictors. For an extensive description of the hyperparameters and their effects, refer to Boehmke and Greenwell (2019b).

Hyperparameter	Parameter values tested	Untuned parameter	Final parameter pteropods	Final parameter foraminifers
max_{depth}	1, 3, 5	6	5	5
min_{rows}	1, 5, 10 1		1	1
r_{learn}	0.01, 0.05, 0.1	0.3	0.01	0.01
r_{sample}	0.5, 0.75, 1	1	0.75	0.5
$r_{samplecolumns}$	$\frac{1}{3}$, $\frac{2}{3}$, 1	1	1	1

Table S8. Hyperparameter options for the Deep Learning (DL) model, the untuned parameter value, and the final parameter choices for pteropods and foraminifers as determined via a grid search by assessing all hyperparameter options for those that would minimize the root mean squared error (RMSE). The activation function describes the non-linear transformation applied at each neuron. The hidden layer structure determines the number of layers and the number of neurons per layer, e.g. (10, 10) denotes a network with two hidden layers of ten neurons each. λ_{L_1} and λ_{L_2} are weight parameters used for penalizing complexity. To avoid overfitting, L_1 (Lasso regression) or L_2 (Ridge regression) can be employed to add a penalty term based on the network weights. The strength of this penalizing factor is determined by the respective parameter λ. For an extensive description of all hyperparameters, refer to Boehmke and Greenwell (2019a).

Hyperparameter	Parameter values tested	Untuned parameter	Final parameter pteropods	Final parameter foraminifers
activation function	Rectifier, Rectifier with dropout, Tanh, Maxout, Maxout with dropout	Rectifier	Tanh	Tanh
hidden layer structure	(5, 5), (10, 10), (15, 15), (20, 20), (50, 50, 50)	(5) (20, 20)	(15, 15)	
λ_{L_1}	0, $1*10^{-3}$, $1*10^{-5}$	0	0	$1*10^{-3}$
λ_{L_2}	0, $1*10^{-3}$, $1*10^{-5}$	0	$1*10^{-3}$	$1*10^{-5}$

References

Bednaršek, N., Mozina, J., Vogt, M., O'Brien, C., & Tarling, G. A. (2012). The global distribution of pteropods and their contribution to carbonate and carbon biomass in the modern ocean. *Earth System Science Data*, *4*(1), 167–186. doi: 10.5194/essd-4-167-2012

Boehmke, B., & Greenwell, B. (2019a). Deep Learning. In *Hands-on machine learning with r* (1st ed., chap. 12). New York: Chapman and Hall/CRC. doi: https://doi.org/10.1201/9780367816377

Boehmke, B., & Greenwell, B. (2019b). Gradient Boosting. In *Hands-on machine learning with r* (1st ed., chap. 11). New York: Chapman and Hall/CRC. doi: https://doi.org/10.1201/9780367816377

Boehmke, B., & Greenwell, B. (2019c). Random Forests. In *Hands-on machine learning with r* (1st ed., chap. 11). New York: Chapman and Hall/CRC. doi: https://doi.org/10.1201/9780367816377

Coxall, H. K., & Spezzaferri, S. (2018). Taxonomy, biostratigraphy and phylogeny of Oligocene Catapsydrax, Globorotaloides and Protentelloides. *Cushman Found Foraminifer Res Spec Publ*, *46*, 79–124.

Davis, C. S., & Wiebe, P. H. (1985). Macrozooplankton biomass in a warm-core Gulf Stream ring: time series changes in size structure, taxonomic composition, and vertical distribution. *Journal of Geophysical Research*, *90*(C5), 8871–8884. doi: 10.1029/JC090iC05p08871

Kretschmer, K., Jonkers, L., Kucera, M., & Schulz, M. (2018). Modeling seasonal and vertical habitats of planktonic foraminifera on a global scale. *Biogeosciences*, *15*(14), 4405–4429. doi: 10.5194/bg-15-4405-2018

Lam, A. R., & Leckie, R. M. (2020, 7). Subtropical to temperate late Neogene to Quaternary

planktic foraminiferal biostratigraphy across the Kuroshio Current Extension, Shatsky Rise, northwest Pacific Ocean. *PLOS ONE*, *15*(7), e0234351. Retrieved from `https://doi.org/10.1371/journal.pone.0234351`

Little, W. S., & Copley, N. J. (2003). *WHOI silhouette DIGITIZER version 1.0 user's guide* (Tech. Rep. No. July). Woods Hole: Woods Hole Oceanographic Institute. doi: 10.1575/1912/62

Loeblich, A. R., & Tappan, H. (1994). *Foraminifera of the Sahul Shelf and Timor Sea* (Vol. 31). Cushman Foundation for Foraminiferal Research.

Lombard, F., Labeyrie, L., Michel, E., Bopp, L., Cortijo, E., Retailleau, S., ... Jorissen, F. (2011). Modelling planktic foraminifer growth and distribution using an ecophysiological multi-species approach. *Biogeosciences*, *8*(4), 853–873. doi: 10.5194/bg-8-853-2011

Michaels, A. F., Caron, D. A., Swanberg, N. R., & Howse, F. A. (1995). Primary productivity by symbiont-bearing planktonic sarcodines (Acantharia, Radiolaria, Foraminifera) in surface waters near Bermuda. *Journal of Plankton Research*, *17*(1), 103–129. doi: 10.1093/plankt/17.1.103

Miranda-Martínez, A. Y., Carreño, A. L., & McDougall, K. (2017). The Neogene genus Streptochilus (Brönnimann and Resig, 1971) from the Gulf of California. *Marine Micropaleontology*, *132*, 35–52.

Saito, T., Thompson, P. R., & Breger, D. (1976). Skeletal ultramicrostructure of some elongate-chambered planktonic foraminifera and related species. In Y. Takayanagi & T. Saito (Eds.), *Progress in micropaleontology: selected papers in honor of prof. kiyoshi asano, special publication* (pp. 278–304). New York: ARRAY(0x55981508b818). Retrieved from `https://oceanrep.geomar.de/id/eprint/33439/`

Schiebel, R., & Hemleben, C. (2000). Interannual variability of planktic foraminiferal populations and test flux in the eastern North Atlantic Ocean (JGOFS). *Deep-Sea Research Part II: Topical Studies in Oceanography*, *47*(9-11), 1809–1852. doi: 10.1016/S0967-0645(00)00008-4

Srinivasan, M. S., & Kennett, J. P. (1983). The oligocene-miocene boundary in the South Pacific. *Geological Society of America Bulletin*, *94*(6), 798–812.

Takahashi, K., & Bé, A. W. (1984). Planktonic foraminifera: factors controlling sinking speeds. *Deep Sea Research Part A, Oceanographic Research Papers*, *31*(12), 1477–1500. doi: 10.1016/0198-0149(84)90083-9

Weiner, A. K. M., Weinkauf, M. F. G., Kurasawa, A., Darling, K. F., & Kucera, M. (2015). Genetic and morphometric evidence for parallel evolution of the Globigerinella calida morphotype. *Marine Micropaleontology*, *114*, 19–35.